SHEDDING OF MULTIPLE SESSILE DROPLETS

AYSAN RAZZAGHI

A THESIS SUBMITTED TO
THE FACULTY OF GRADUATE STUDIES
IN PARTIAL FULFILLMENT OF THE REQUIREMENTS
FOR THE DEGREE OF
MASTER OF SCIENCE

GRADUATE PROGRAM IN MECHANICAL ENGINEERING
YORK UNIVERSITY
TORONTO, ONTARIO

JANUARY 2018

Abstract

A droplet which is placed on a surface and is exposed to an airflow, can be shed, if the drag force overcomes the droplet's adhesion force. Presence of other sessile droplets, in proximity, changes the drag force, so the minimum airflow velocity required to shed the droplets (U_{cr}) can vary. In this thesis, an experimental study on shedding of the multiple sessile droplets was performed on both hydrophilic and hydrophobic surfaces. The effects of the droplets' arrangement type, and the spacing on U_{cr} were elucidate. For a pair of sessile droplets, a model was proposed to predict the U_{cr} based on droplets' size, spacing, arrangement, and surface wettability. For three, or four sessile droplets arranged in triangle, square, reversed triangle, and diamond configurations, the effects of the droplets' interaction on variation of the U_{cr}, was clarified. A critical value for spacing was determined beyond which multiple sessile droplets shed independently.

Dedication

This thesis is dedicated to my parents,

Sousan and Davoud.

Acknowledgements

First of all, I am thoroughly grateful to my supervisor, Prof. Alidad Amirfazli, for his endless support and generous guidance. I consider myself a very lucky individual as I had a chance to work under his supervision where I learned how to think scientifically, and to make my thought accessible both verbally and in writing.

I would also like to thank my colleague Sayed A. Banitabaei for performing numerical simulations of this thesis. In addition, I am thankful to all my friends in the Surface Engineering and Instrumentation Lab for their help and support.

I would like to acknowledge NSERC, NATO, and ESA for their financial support.

Finally, I am grateful to my parents for their love, encouragement, and endless support.

Table of Contents

List of Tables

List of Figures

Chapter 1: Introduction

1.1 Background and Motivation

This thesis studies the interaction of the sessile droplets (droplets which sit on a surface) with a shearing airflow. For instance, consider the accumulation of the rain droplets on the body of an aircraft. If the droplets are not shed by the airflow, then in subzero temperatures, they can freeze, which affects the performance of the aircraft. It has been found that the ice accretion on the body of the aircrafts decreases the maximum lift coefficient, and increases the drag [1], so the fuel use by the aircraft increases. Other industrial applications of the droplets' shedding include enhanced oil recovery [2] where liquid droplets shed by a liquid shear flow. In Proton Exchange Membrane (PEM) fuel cells, the water droplets emerge through the gas diffusion layer, which results in the pressure drop inside the channel [3]. Removal of the droplets by the shearing airflow can enhance the fuel cell's efficiency. Droplets detachment (from a surface) by viscous flow also have biological applications; in the body, cell adhesion can be controlled by the mechanical forces such as viscous forces of the fluids, e.g. blood in micro-vessels [4].

Droplet shedding in an airflow is achieved by exposing a sessile droplet to an increasing airflow. As it is shown in Figure 1.1 two main forces which are co-interacting during the shedding, are aerodynamic drag and the adhesion force.

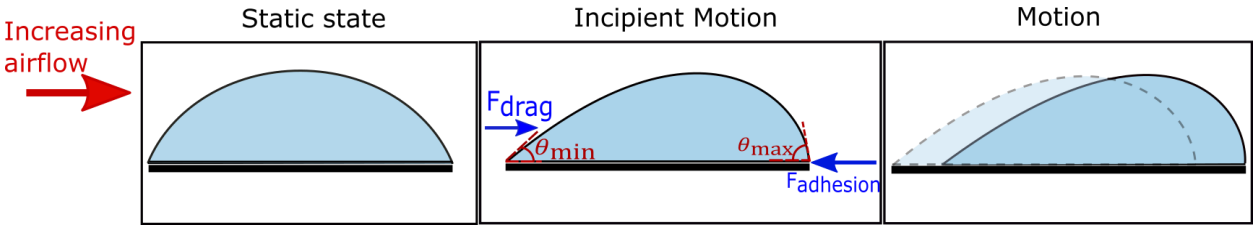

Figure 1.1: Schematic of a sessile droplet which is exposed to an increasing airflow at three different states, from static until the motion is achieved. At the incipient motion, Fadhesion ≤ Fdrag.

The drag force has a pressure drag component which is the integration of the pressure over the surface of the sessile droplet, and a shear stress components which depends on the airflow velocity magnitude [5]. Adhesion force is the summation of the surface tension force, distributed all around the contact line of the droplet [6]. As an airflow with increasing speed is introduced to a sessile droplet, the lateral adhesion force increases to resists the motion of the droplet baseline. As a result, the interface of the droplet deforms in an asymmetric form; i.e. the contact angle at the upstream decreases and it increases at the downstream (see Figure 1.1). At the incipient motion, the adhesion force cannot further increase, so the drag force overcomes the adhesion, which results in droplet shedding. The airflow velocity at the incipient motion is called critical air velocity (U_{cr}), and the upstream and downstream contact angles are called minimum (θ_{min}) and maximum (θ_{max}) contact angles, respectively.

There are many experimental and numerical studies on shedding of a single sessile droplet. Dussan [7] conducted an experimental study on a sessile droplet which is exposed to shearing airflow; they provided an expression for the critical airflow gradient based on the contact angle hysteresis (the difference between advancing and receding contact angles), and droplet volume (V). They pointed that the viscosity of the droplet has no significant effect on the critical air flow, and the critical airflow gradient is proportional to the $V^{-1/3}$. However, the model is valid only for the small contact angle hysteresis values. Fan et al. [8], experimentally studied the shedding of a sessile droplet for various droplet-surface systems (the static contact angles ranged from 50° to 90°). They showed that, depending on the droplet-surface system, by increasing the droplet volume from 13 to 40 μl, the U_{cr} decreases by maximum 27%. They also identified three main regimes for the shape of droplet during the motion on the surface. This includes the droplet which maintains its original shape while sliding on the surface, the droplet which has a short tail, and the droplet which has an extensive tail that breaks down during the motion. One may think that the shape of the droplet during the motion, also, significantly changes due to the contact angle.

However, the contact angles considered in [8] are limited to $\theta_s \leq 90°$. In an experimental-numerical study, Hao et al. [9], proposed a semi-empirical model to predict the critical air velocity for a single sessile droplet on a superhydrophobic surface. Their model is in good agreement with experimental results from Milne and Amirfazli [10]. However, the model is complicated due to the fact that it is a function of the force which is exerted to a similar droplet while it is sliding on a tilted surface. Mandal et al. [11], experimentally investigated the shedding of a single sessile droplet of various sizes (from 5 to 100μl) on hydrophilic, hydrophobic, and superhydrophobic surfaces in icing condition (-5℃). Their results show that in icing condition, particularly for drops larger than 50 μl, the critical air velocity increases compared to that of laboratory temperature. Also, the amount of the increase in critical air velocity is more pronounced for drops on hydrophilic surface. As a reminder, one application of droplet shedding is in decreasing the icing on the surfaces where multiple droplets are accumulated in subzero temperatures, e.g. airfoils. However, study in [11] is limited to a single sessile droplet.

Many studies can be found examining the sessile droplet shedding emerging into the gas diffusion membrane in fuel cells. Wu and Djilali [12] observed three different regimes in detachment of water droplet emerging through a pore inside a microchannel. The variable parameters in [12] are the airflow velocity and the rate of water injection into the pore. However, the pore size, and the pinning effects that it may have on the droplet's detachment, has not been clarified. Also, the observed regimes are limited to the hydrophobic substrate which were used in [12]; how the wettability of the substrate affects these regimes needs to be studied.

Mondal et al. [13] using Volume of Fluid method, simulated the movement of a single water droplet on the proton exchange membrane (PEM) in the fuel cell. They considered different contact angles (for hydrophilic surfaces), and airflow velocities (5 t0 12.5 m/s). They pointed that decreasing the contact angle of the membrane slows down the water droplet transportation inside the fuel cell. However, they only considered the effects of the contact angle variation on the drag force (due to the change of the droplet's shape). The effects of the contact angle on the adhesion

force were not implemented in the simulations. Golpaygan and Ashgriz [14], in a numerical study, showed that decreasing the droplet surface tension, or the wettability of the solid surface, has more significant effect on increasing the droplet mobility compared to increasing the airflow velocity. The study is limited to low Re number ($Re<250$).

Studies above indicate that the wettability of the substrate, size of the droplet, and properties of the liquid and flow are the main parameters in determining the minimum flow velocity for shedding. Most of the above mentioned studies, give a little attention to the adhesion force, or consider a single surface's wettability. Among all, [10] conducted a more systematic study in terms of defining a criteria for shedding, and considering the wide range of droplet's volume and surface wettabilities. In general, decreasing the wettability of the solid substrate results in reduction of the critical flow velocity. Also, critical flow velocity is a function of the inverse of the droplet's size. Still, all of the above studies consider shedding of a single droplet, which is not exactly the case of industrial, and biological applications where more than one droplet appear on the surface. As a conceptual example, consider the multiple droplets which condensate on the fin of a heat exchanger. Droplets which occupy the surface of the fin, result in reduction of the heat transfer rate, and reduce the efficiency of the heat exchanger. One possible way to remove these droplets is by airflow forces [15]. As such, the question is how the onset of the shedding for each droplet is influenced by the presence of the other one?

For a pair of sessile droplets placed in tandem, experimental and numerical studies exist [16-18]. In [16], results show that the critical air velocity of the downstream droplet increases (compared to that of a single droplet) when it is placed within the wake of the upstream droplet. The study was conducted for a single surface's wettability (static contact angles of 49.1°). Consequently, the effects of the drag force variation (due to the droplets' shape change), or adhesion force variation (due to the wettability) has not been considered. In [17] and [18] results indicate that as the airflow is introduced, the upstream droplet moves toward the downstream droplet while the downstream droplet moves, in the opposite direction of the flow, toward the upstream one. However, the effects

of the presence of the other droplet on onset of the motion is not studied in [17] and [18]. In fact, determining the onset of the motion is important due to the fact that it indicates the minimum airflow velocity required to have a droplet-free surface.

As per discussions above, studies for the shedding of multiple sessile droplets is only limited to two droplets in a tandem arrangement. To further understand how the drag force may be affected by presence of the other droplets in proximity, we refer to the findings for the drag force variation with arrangement and spacing, over the multiple suspended bodies to gain some basic understanding in analogy with sessile droplets.

Jadoon et al. [19] numerically investigated the drag coefficient on a pair of suspended solid spheres at different arrangements and spacing. According to [19] at Re=600, when the center to center distance ratio to a sphere's diameter is 1.5, for two spheres in tandem, the vortex shedding at the aft of the upstream sphere decreases due to the interference with the downstream sphere. Consequently, the drag coefficient on the upstream sphere reduces by 10 % (compared to a single sphere). At the constant spacing, as the relative position of the spheres changes from tandem to be side-by-side, drag coefficient increases on both spheres. For the side by side spheres, at the spacing of 1.5, drag coefficient of both spheres is 12% higher than that of a single sphere. Schouveiler et al. [20] numerically achieved the flow pattern over two side-by-side suspended spheres at Re of 300. In [20], when two spheres are very close to each other, they act as a single bluff body (i.e. a single recirculation wake forms at the aft of the spheres). As the spacing, ratio of center to center distance to a sphere's diameter, increases to 1.3, two separate, but strongly interactive wakes form (the wakes combined at the downstream). By further increase in the spacing to 3, two discrete streets of the wakes, which are still interacting, form at the aft of each sphere. Beyond the spacing of 3, the interaction of the spheres disappears. Chen et al. [21] numerically considered the drag force acting on the suspended spheres arranged in a cubical configuration at Re of 200. Their results show that as the spacing between the spheres decreases, the drag force which is exerted to each sphere, also decreases.

As it can be understood, when neighboring suspended bodies are exposed to an airflow, the interaction of the flow over the bodies leads to changing the drag force. For a pair of suspended bodies, there is a ~10 % increase in drag coefficient when they are placed side-by-side within small spacings. In tandem arrangement, both bodies generally experience a lower drag coefficient compared to that of a single body. For more than two suspended bodies, the variation of the drag force with arrangement, or spacing is even more complicated; as more bodies are interacting to change the flow pattern, and consequently the drag coefficient.

As it was mentioned earlier, drag force co-interacts with adhesion to shed the sessile droplets, so one expects that the U_{cr} for multiple sessile droplets vary (compared to that of a single droplet) with respect to arrangement and spacing of the sessile droplets (see Figure 1.2). However, shedding of multiple sessile droplets has not been studied yet for more than two droplets, or a pair of droplets in a side-by-side arrangement.

Also, it is shown in [22] and [23], that the change in shape of the neighboring bodies, affect the variation of the drag with arrangement/spacing. For sessile droplets, the wettability of the substrate changes the shape of the droplet, so the shedding of the multiple sessile droplets supposed to be affected by the wettability of the substrate.

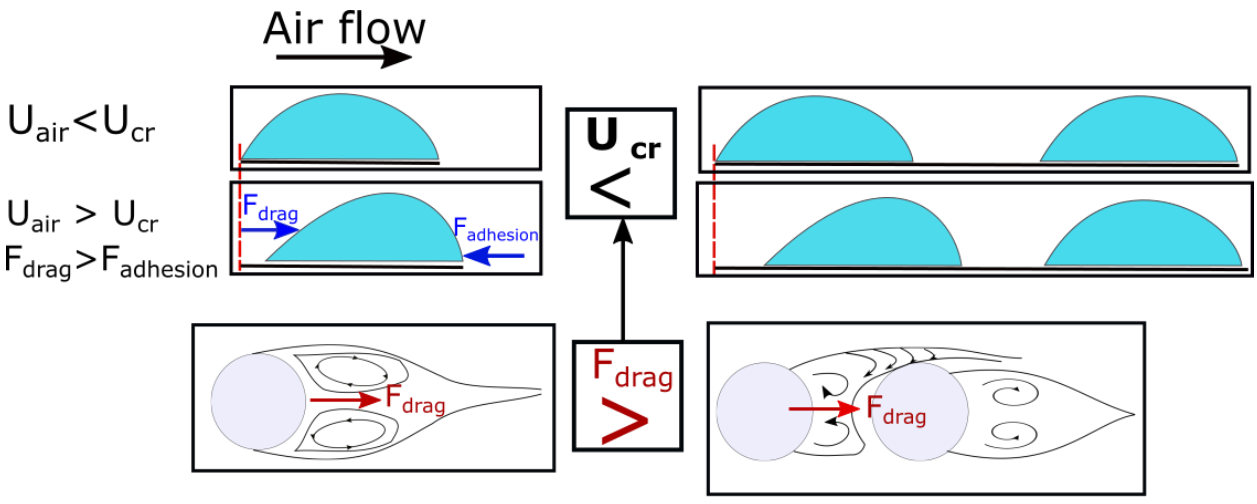

Figure 1.2: Schematic view of the shedding of a single sessile droplet, compared to the case of two droplets in a tandem arrangement.

1.2 Objectives of the Thesis

Considering the state of the current knowledge and the gaps mentioned above, this study is conducted to:

1) Understand how the critical airflow for a pair of sessile droplets in tandem and side-by-side arrangements, within different spacing, is different from that of a single droplet.
2) Investigate the effects of substrate wettability and the size of the droplets on shedding of a pair of sessile droplets.
3) Propose a model to predict the critical airflow velocity for shedding of a pair of sessile droplets at a given spacing, based on the droplets size and the wettability of the substrate.
4) Gain knowledge how the findings for shedding a pair of sessile droplets can be extended to shedding of three or four droplets within the arrangements such as square, triangle, diamond, etc.
5) Obtain the flow structure over the multiple sessile droplets through numerical simulation to better understand the role of drag force, and provide the theoretical explanation for experimental results.
6) Characterize the airflow to which the sessile droplets are exposed, and achieve the airflow velocity profiles at the position of the droplets.

1.3 Outline of Thesis

This thesis is organized based on the two papers which are either submitted, or in the process of submission to peer reviewed journals. Chapters 2 and 3 are made of these papers, so each chapter has its detailed literature review, and motivation. The numerical simulations in Chapter 3 is done in collaboration with Sayed A. Banitabaei.

Chapter 2 contains an investigation of the critical air velocity required for shedding a pair of sessile droplets in tandem and side-by-side arrangements within different spacing. Also, it

considered the effects of the surface wettability on the critical air velocity variation with spacing for the upstream droplet in tandem arrangement and the droplets in side-by-side arrangement. Furthermore, an empirical model is proposed in Chapter 2 which allows the estimation of critical air velocity for a pair of sessile droplets at any spacing, based on droplets volume and substrate wettability.

Chapter 3 presents the experimental results of the critical air velocity comparison for the upstream droplet/droplets in square, triangle, reversed triangle, and diamond arrangements. Also, it contains the numerical simulation results for the flow over the simulated droplets in mentioned arrangements. Finally, it investigates the spacing range beyond which droplets shed independently, regardless of the arrangement's configuration.

Chapter 4 summarizes the findings and remarks on conclusions of this thesis regarding the shedding of multiple sessile droplets on hydrophilic and hydrophobic surfaces. Also, it suggests possible future works.

Appendix provides further details for the experimental setup as well as the air velocity profiles of the wind tunnel which is used in the experiments. Also, complementary graphs to those presented in Chapters 2 and 3, but for additional size of droplets, or surfaces with different wettability, are shown.

Chapter 2: Shedding of a Pair of Sessile Droplets[1]

2.1 Introduction

Droplet shedding is particularly important to applications such as air frame icing [24], water management in fuel cells [25], enhanced oil recovery [2], wind turbine icing [26], and cleaning [27]. In many of the above applications, the goal is to clear the surface with a minimum airflow velocity. The minimum airflow velocity at which the incipient motion of a sessile droplet is achieved is called the critical air velocity (U_{cr}). Critical air velocity was found to be a function of air density, surface tension, droplet frontal area, droplet baseline length, contact angle hysteresis, and drag coefficient [10]. Other studies on droplet shedding in icing temperatures also exist with emphasis on the role of droplet size and the substrate wettability [28] as well as temperature variation in icing conditions [11].

Wettability of the substrate affects the contact angle, drag coefficient, droplet baseline length, and the frontal area for a given droplet volume. It has been found that the critical air velocity is lower on less wettable surfaces [28]. In icing temperatures (-1≥T≥-8℃) Mandal et al. [11] showed that for droplets larger than 50μl, the critical air velocity increases compared to the laboratory conditions. In a numerical study, Dimitrakopoulos and Higdon [29] showed that for low Re numbers, at small contact angles ($\theta \approx 10°$), the viscosity of the sessile droplet has no significant influence on the critical airflow velocity; however, at higher contact angles ($\theta \approx 80°$) increasing the viscosity by 10 times, decreases the critical airflow velocity. Zhu et al. [30] at the initial Re ≈ 47 (based on the freestream velocity and the initial droplet diameter) numerically studied the water droplet emergence and shedding in a PEM fuel cell. The study focused on the special case of gas diffusion layer (GDL) wettability. Hydrophilic GDL retards droplet formation and creates a water film which in turn results in higher critical air velocity, but a hydrophobic GDL results in droplet

[1] This chapter has been submitted to Physical Review Fluids. Authors: Aysan Razzaghi and Alidad Amirfazli

detachment. Carroll and Hidrovo [31] experimentally investigated the minimum Reynolds number needed to detach the droplet of a particular size which emerges through a pore. They showed that at lower Re numbers (Re ≈ 50) the detachment mainly occurs as a result of hydrodynamic pressure difference while as Re increases up to 100, the detachment process is controlled by inertial drag.

The above studies have examined the result of a change in the adhesion force (e.g. in case of changing surface wettability), or aerodynamic forces (e.g. change of droplet's shape due to its size or contact angle), for shedding of a single droplet

In many applications, droplets rarely appear solely on a surface. In fact, often there are many droplets on a surface. So, the question is, if the critical air velocity will be any different for multiple sessile droplets on a surface than that of a single droplet. Studies examining the shedding of multiple sessile droplets is very limited. Moghtadernejad et al. [17] conducted an experimental study on shedding of two tandem droplets on a hydrophilic surface. Although this study provides some information on the coalescence of two sessile droplets in tandem, it does not examine how the onset of the shedding for each of the droplets is affected by the presence of the other. Recently, Hooshanginejed and Lee [16] both experimentally and numerically studied the depinning of a sessile droplet in the wake of an upstream body (i.e., solid hemisphere or sessile droplet). They found that when a sessile droplet is placed in tandem and downstream of a solid hemisphere, beyond a critical distance, it sheds independently from the upstream body. The critical distance was found to be 2.4 times the droplet baseline length. They demonstrated that when the upstream body is also a sessile droplet, within the critical distance (which was the same as the critical distance for the solid hemisphere case), upstream droplet deppins before the downstream droplet. This means that within the critical distance, downstream droplet is interacting with the wake of the upstream droplet. However, it is not clear in [16] how this interaction affects the upstream droplet's shedding, or if the critical air velocity of the upstream droplet is any different from that of a single droplet.

A search of literature reveals that references [16] and [17] are the only works which studied the shedding of a pair of sessile droplets in a tandem arrangement, and there is no study investigating the shedding of the sessile droplets in a side-by-side or any other arrangement. However, studies on neighboring suspended bodies (e.g. spheres) which are exposed to airflow can be found [32-38]. One can use, as a departing point, the information for drag on the neighboring suspended bodies, and adopt it to understand the shedding of a pair of sessile droplets. However, it is important to keep in mind that the presence of a solid surface in case of sessile drops, will give rise to the adhesion force, and affect to a certain degree, the flow compared to suspended bodies. For the interaction between the neighboring suspended bodies in a flow, there are a number of studies which focus on the drag force. Tal et al. [32] numerically found the drag coefficient on two suspended solid spheres placed in tandem at Re=40. They pointed that the drag coefficient on both spheres is lower than that of a single sphere; also, drag coefficient on upstream sphere reduces even more by positioning the downstream sphere inside its recirculation wake. Chen and Wu [33] experimentally, and Yoon and Yang [34] numerically, investigated the drag coefficient on a pair of suspended solid spheres placed at different distances from each other. In [33], the Re number (based on freestream velocity and sphere diameter) was $Re<118$ which is below the critical range for vortex shedding. In [34], Re number was 300 which is within the range of laminar vortex shedding. However, the results of both studies indicated that in tandem position, and when the gap between two spheres is two times larger than the sphere diameter, the drag coefficient on the upstream spheres is 10% less than that of a single sphere. When spheres positioned side-by-side, the drag coefficient increased by $\sim$ 12% compared to that of a single sphere [34]. Liang et al. [35] experimentally and numerically studied the interaction of two tandem solid spheres inside a pipe in the presence of a flow. The Re number of the pipe (based on the flow velocity and pipe diameter) ranged from 180 to 636, and the Re number of the spheres, based on the sphere diameter, was $30<Re<106$. They focused on the effects of the distance of the spheres from the pipe's wall on the drag of the downstream sphere. Results in [35] indicate that both the presence

of a wall, and Re number enhancement, result in increasing the drag coefficient; however, the role of Re number was more significant. To address the effects of the neighboring bodies' geometry on the flow pattern, wake interaction, and the drag force, Kishore [36], numerically investigated the flow patterns and drag coefficient on tandem spheroid solid particles at Re=100 (based on the particles' polar diameter). It was shown that for prolate particles, even when the gap between them is 5 times larger than the diameter, still the downstream particle sits at the wake of the upstream one. However, as the shape of the particles change to be more oblate, they become independent at smaller gap ratio.

In the case of neighboring suspended liquid droplets, there are also some studies examining the flow patterns and drag force changes. Mulholland et al. [37] experimentally measured the drag coefficient on a stream of monodispersed suspended droplets at Re ranging from 90 to 290 (based on droplet diameter). The drag coefficient was found to be a function of droplets relative distance and the Re number. Raju and Sirignano [38] numerically investigated the interaction between two tandem suspended droplets in an airflow for $50 < Re < 200$ (based on the flow speed and the droplets diameter). They found that the drag coefficient for the upstream droplet approaches the value of a single droplet when the distance between the droplets is twice the droplet diameter. At this distance, for the case of solid spheres, however, the upstream sphere has a lower drag coefficient compared to the single sphere [34]. This difference can be due to either the deformability of the droplets, or the range of the Re numbers considered in the two studies. In [38], the Re number is below the onset of the recirculation wake instability [5], and probably the wake interference is not strong enough to affect the flow energy. Kim et al. [39] conducted a numerical study on the interaction of two side by side suspended droplets. Their results show that positioning of the two droplets besides each other at small spacing (when the ratio of center to center distance to drops diameter is 1.5), leads to an increase in the drag coefficient on both suspended droplets. As center to center distance between the two droplets reaches 6 times of the drop diameter, drag coefficient drops off and approaches the value of the

drag coefficient on a single suspended droplet. This is very similar to the case of side-by-side solid spheres [34] in terms of the spacing at which drag coefficient approaches the value of a single sphere.

Considering the above studies, one can understand that the drag coefficient of the neighboring bodies changes with the relative position and the distance between the bodies. In general, for a pair of suspended spheres, drag coefficient approaches the value for that of a single sphere at dimensionless distances (center to center distance to diameter ratio) larger than ~ 5; for tandem arrangement, the maximum decrease of drag coefficient for the upstream solid sphere, was found to be $\sim 35\%$ [32].

In the context of sessile droplets, [16] and [17] made some points in terms of drag force reduction on the downstream droplet in a tandem arrangement. However, there is no information on drag force of the upstream sessile droplet despite its importance in shedding. The upstream droplet is the one which sheds first, so it can hit the downstream droplet, grow larger, and hence continue to shed; as the results in [10] show, the larger drops shed more easily than a smaller one. So, considering the above sequence of events, the surface will be droplet free. For the side-by-side sessile droplets, there is lack of information in literature; also, it remains untouched how the drag force variation co-interacts with the adhesion force to compel a sessile droplet to shed. We do not expect droplet adhesion to a surface to substantially change, just due to presence of another droplet; the change in shedding behavior of a pair of sessile droplets, compared to that of a single sessile droplet, is most likely the result of changes in drag force. With such motivation, we study the critical air velocity variation for an upstream droplet in tandem arrangement, and two droplets in a side-by-side (SbS) arrangement. Also, the surface wettability changes the shape of the droplet which in turn leads to changes in drag, and the recirculation wake size. To address the effects of the surface wettability on the droplets wake interaction, both hydrophilic and hydrophobic surfaces are considered in this chapter.

2.2 Theoretical Background

Droplet shedding is mainly controlled by two counteracting forces; adhesion and drag. Adhesion force (F_{adh}) is a function of liquid surface tension (γ), contact angle (θ), and the baseline length of the droplet (L_b) [40]. As air flows over the droplet, the liquid-air interface of the drop deforms in a way that the contact angle at the upstream (θ_{min}) decreases, and the one at the downstream (θ_{max}) increases above the static contact angle. The adhesion force can be calculated with:

$$F_{adh} = KL_b\gamma(\cos\theta_{min} - \cos\theta_{max}) \qquad (2.1)$$

where K accounts for the droplet baseline variation from the circular shape and the local variation of contact angle along the contact line [40].

The drag force (F_{drag}) exerted on a droplet due to the airflow is:

$$F_{drag} = \frac{1}{2}C_D\rho U_{air}^2 A \qquad (2.2)$$

where ρ is the air density, U_{air} is the free stream velocity, A is frontal area of the deformed droplet, and C_D is the drag coefficient. In some works, where droplet is viewed from its side, the projected side area is used as a proxy for A [10]. Note that it is understood that droplet may be partially submersed in the boundary layer, but in this chapter the C_D will be defined with this understanding in mind.

In experiments where airflow is increased from zero over a sessile droplet, drag force increases; and the lateral adhesion force, as a resistance force to drag also increases from zero. With further increase of the airflow speed, drag and lateral adhesion forces are evolving in proportion to each other until the incipient motion. At the moment of incipient motion, the lateral adhesion force cannot further increase and the droplet sheds (see Eq. 2.3)

$$\begin{cases} KL_b\gamma(\cos\theta_{min} - \cos\theta_{max}) \propto \frac{1}{2}C_D\rho U_{air}^2 A & Up\ to\ the\ incipient\ motion \\ KL_b\gamma(\cos\theta_{min} - \cos\theta_{max}) \leq \frac{1}{2}C_D\rho U_{cr}^2 A & At\ the\ incipient\ motion \end{cases} \qquad (2.3)$$

When multiple sessile droplets are placed at the vicinity of each other, the adhesion force parameters (i.e. baseline length and contact angles) are not directly subjected to change due to the presence of the other droplet. However, if the aerodynamic drag force is affected by the presence of the other droplet, the lateral adhesion force may indirectly be affected as described above (i.e. reaction of the lateral adhesion force to drag force as air velocity changes).

As there is no information for flow variation with respect to sessile droplets' distance and arrangement, below, we refer to flow variation over the suspended solid spheres, as a departing point for discussions later.

Figure 2.1 schematically illustrates how the flow pattern and the wakes' interaction can change over a pair of suspended solid spheres due to their arrangement and spacing. For two tandem spheres, when the spacing is small (Figure 2.1a), the shear layer of upstream sphere also envelopes the downstream sphere. As a result, the recirculation wake forms at the rear of the downstream sphere and two spheres act as a single bluff body.

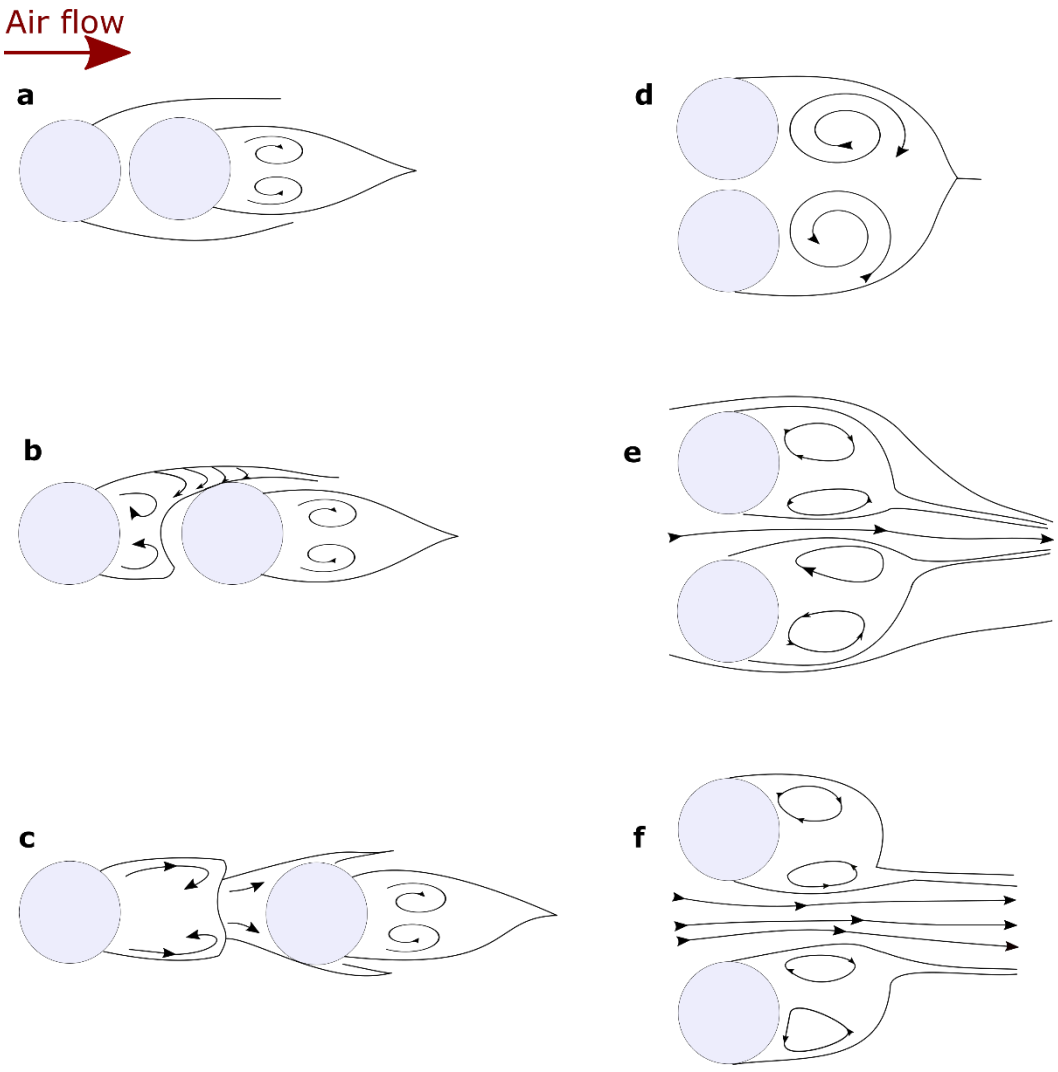

Figure 2.1: Flow patterns for two suspended solid spheres at different center to center spacings. (a-c) Tandem arrangement at Re= 220 (based on the sphere diameter); the Figure is redrawn from [41]. (d-f) Side-by-Side suspended spheres at Re= 5×105 (based on the sphere diameter); the figure is redrawn from [42].

As the center to center spacing between the spheres increases (Figure 2.1b), the flow over the upstream sphere cannot envelop downstream sphere and vortices form at the rear of the upstream sphere. When two spheres are sufficiently far from each other (Figure 2.1c) the vortex formation and vortex shedding occurs from the aft of both spheres independently. The described flow pattern is consistent with the drag coefficient variation in Yoon and Yang [34] and Mulholland et al. [37], i.e. at small spacings, the drag coefficient for the upstream sphere is at 90% of the drag

coefficient for a single sphere. As the spacing increases and flow coupling decreases, the drag coefficient reaches the value of a single sphere.

For side-by-side (SbS) spheres, at small spacings (Figure 2.1d), a single recirculation wake with two counter-rotating vortices forms at the rear; and the spheres act as a single bluff body. With an increase of spacing (Figure 2.1e), two separate wakes form at the aft of each sphere. These wakes are interacting strongly due to the shear layer instability. As the spacing between the spheres further increases (Figure 2.1f), two separate and low-interacting wakes form at the aft of each sphere.

2.3 Experimental Methods

The experiments were conducted inside a closed loop wind tunnel. The test section width, height, and length is 10.4, 6.4, and 30.5 cm, respectively. The speed of the airflow was controlled using a regulator to vary the fan speed. The flow inside the tunnel and in the position of the droplets is laminar. Details of the wind tunnel setup, and its velocity profiles in the test section is provided in the Appendix A. The Re number which is defined based on the critical air velocity and the sessile droplet's height ($Re = {}^{\rho U_{cr} H}/_{\mu}$) was in the range of 580 to 975 depending on the size of the droplet. The velocity and temperature of the airflow were measured using a EE75 hot-film anemometer (E+E Electronics, accuracy 0.1m/s). Two Phantom high speed cameras were operating synchronously at 450 frames/second to capture the side and top views during the sessile droplets shedding process. Shedding experiments were conducted for two volumes of 5 and 10 μl droplets. The arrangement of droplets is shown in Figure 2.2; both droplets had the same size for each arrangement.

Spacing (S), the dimensionless parameter to describe the space between droplets, is the ratio of center to center distance between two sessile droplets to the baseline length of a sessile droplet.

DI water droplets were placed by a syringe on 25 mm × 75 mm hydrophilic and hydrophobic surfaces.

Hydrophilic surfaces were made of an aluminum substrate which were spin coated (at 800 RPM for 70 seconds) by a PMMA solution [2% (w/w) PMMA in Toluene]. The advancing and receding contact angles of the PMMA coated substrate were 74° and 58 °, respectively. Hydrophobic surfaces were Teflon [5:1 (v/v) FC-75, 3-M / Teflon AF] coated aluminum (spin coated with the same method as the hydrophilic surface) with advancing and receding contact angles of 122° and 107°, respectively. Note that apparent texture of the substrate which is seen in Figure 2.2, did not have a notable effect on the conclusions, considering ~ 1.3% error in the critical air velocity when the surfaces were turned 90°.

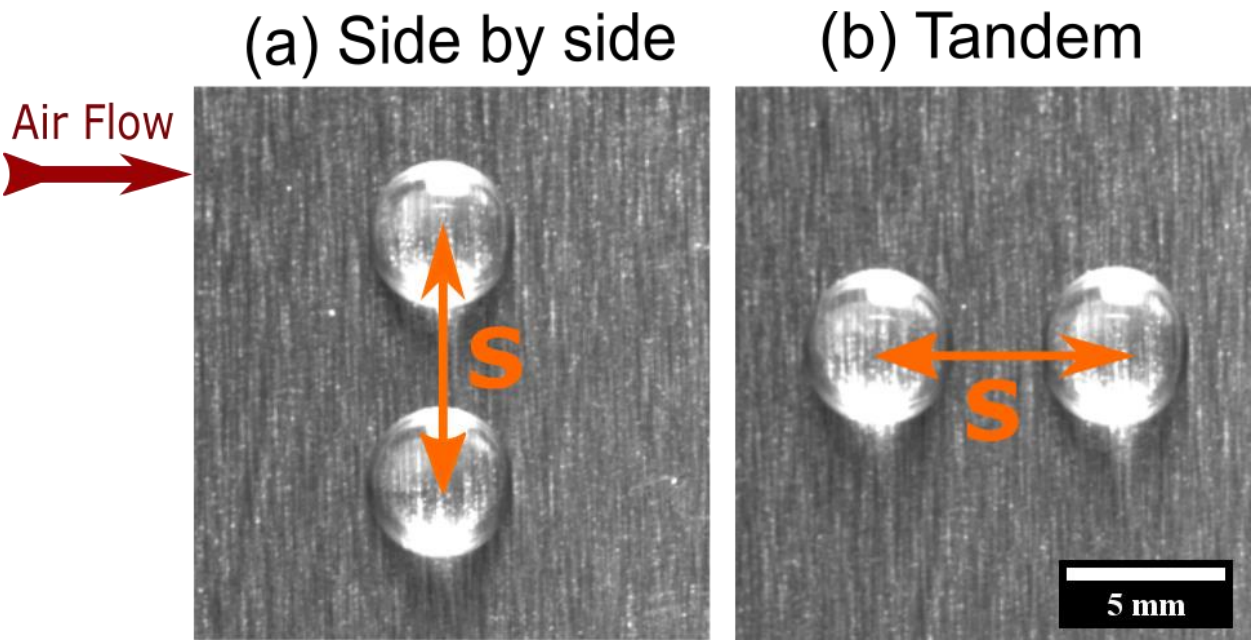

Figure 2.2: Two 10 μl droplets in tandem and side-by-side arrangements on a hydrophilic surface. Droplets were identical for each arrangement, and airflow direction is shown by an arrow.

Experiments began by triggering the high-speed cameras and the fan at the same time. The speed of the airflow was increased at a constant rate of ~1 m/s^2. The air velocity that resulted in a 5 pixel (which is equivalent to 220 μm- pixel density: 22.7 pixel/mm) movement of the baseline

of the upstream droplet/droplets, was considered as the critical air velocity (U_{cr}). This procedure was similar to earlier studies [10] [11]. The recorded videos of experiments were processed via Image-J software. Experiments were repeated three times and the standard deviation of the three data sets is reported as the error bars.

2.4 Results and Discussions

Shedding of Droplets in the Tandem Arrangement

Figure 2.3 shows the critical air velocity ratio as a function of spacing for the upstream droplet in a tandem arrangement. The drops of 5 and 10 μl were placed on a hydrophilic surface (a similar plot for hydrophobic surface is provided in the Appendix A). In this study, we focused on the shedding of the upstream droplet(s). As it is mentioned in [16], for two tandem droplets, when the downstream droplet is shielded in the wake of the upstream droplet, the upstream droplet sheds before the downstream droplet. In this case, upstream droplet can coalesce with the downstream one and shed as a single droplet. As such, studying the shedding of the upstream droplet is of primarily importance. As it is shown in Figure 2.3, the critical air velocity at S ≈ 1.4 is higher than that of a single droplet. As spacing increases, U_{cr} / $(U_{cr})_{single}$ decreases up to S ≈ 5.5 where it approaches the U_{cr} of a single droplet (U_{cr} / $(U_{cr})_{single}$≈1). For both droplet sizes, the critical air velocity ratio to that of a single droplet, shows the same trend with spacing.

When a sessile droplet is exposed to an airflow, recirculation wake forms at its aft (similar to our discussion earlier for spheres); the interaction of such wakes when two droplets are present can change the drag on each of the droplets. In this experimental study, the drag force has not been measured independently; however, as the drag and the lateral adhesion forces are evolving proportionally throughout the shedding process, the adhesion force is also an indication of how drag changes by presence of the downstream droplet.

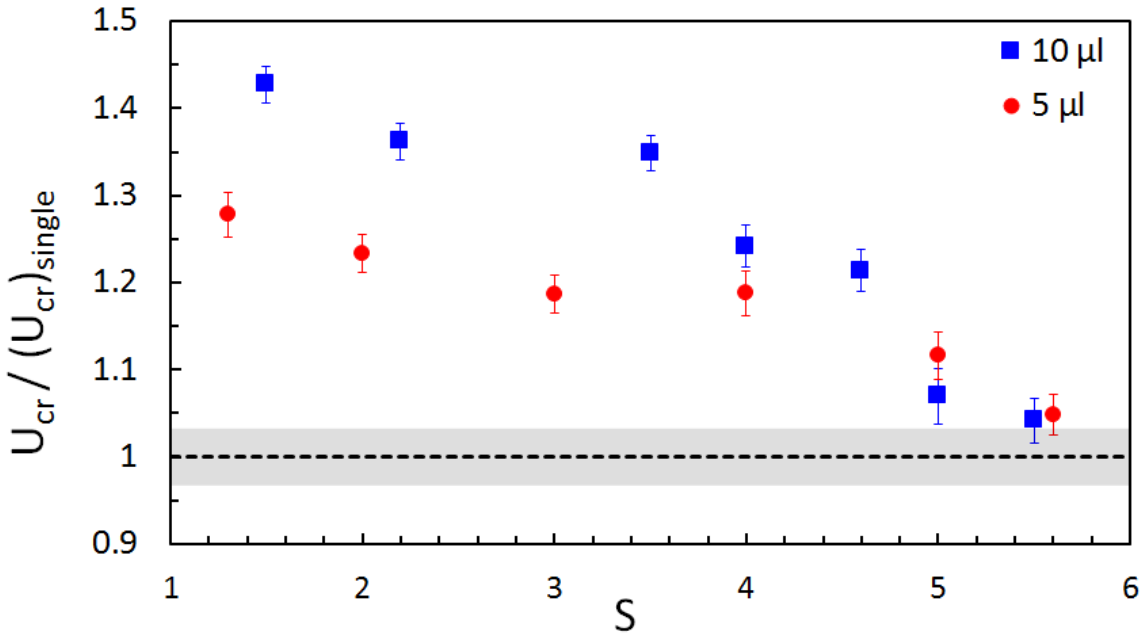

Figure 2.3: The ratio of the critical air velocity for tandem arrangement to that of a single droplet as a function of spacings. Data shown are for the upstream droplet, on a hydrophilic surface. The error limits for a single droplet is shown by the shaded band.

Considering the parameters involved in the adhesion force, one can understand that the baseline length of the upstream droplet does not change by the presence of the downstream droplet. As such, the adhesion force trend is proportional to the "$\cos\theta_{min} - \cos\theta_{max}$" trend (see Eq. 2.1). Figure 2.4 shows the "$\cos\theta_{min} - \cos\theta_{max}$" as a function of airflow velocity. From Figure 2.4, one can understand that at any air velocity (e.g. U_{air}= 4.54 m/s), "$\cos\theta_{min} - \cos\theta_{max}$" has a larger value for higher spacing of the droplets. The inset of Figure 2.4 (which is plotted at U_{air}= 4.54 m/s) shows that with increasing the spacing between the droplets in tandem, the value of the "$\cos\theta_{min} - \cos\theta_{max}$", and consequently the lateral adhesion force, increases. As adhesion and drag forces are proportional at a constant air velocity, up to the moment of droplet's incipient motion (see Eq. 2.3), therefore, drag force is also lower for the smaller spacing of the droplets. Considering the Eq. 2.2 for the drag force, droplet frontal area (A) and drag coefficient (C_D) are the only parameters which may be changed by the presence of the downstream droplet at a given

air velocity. As the size of the droplet is of the order of the capillary length, the frontal area of the sessile droplet can be approximated by a spherical cap [28] as:

$$A = \frac{(6V_d)^{2/3}\left(\sin\frac{\theta_s}{2}\right)^{4/3}}{(2\pi + \pi\cos\theta_s)^{2/3}} \frac{\theta_s - \sin\theta_s\cos\theta_s}{(1-\cos\theta_s)^2} \qquad (2.4)$$

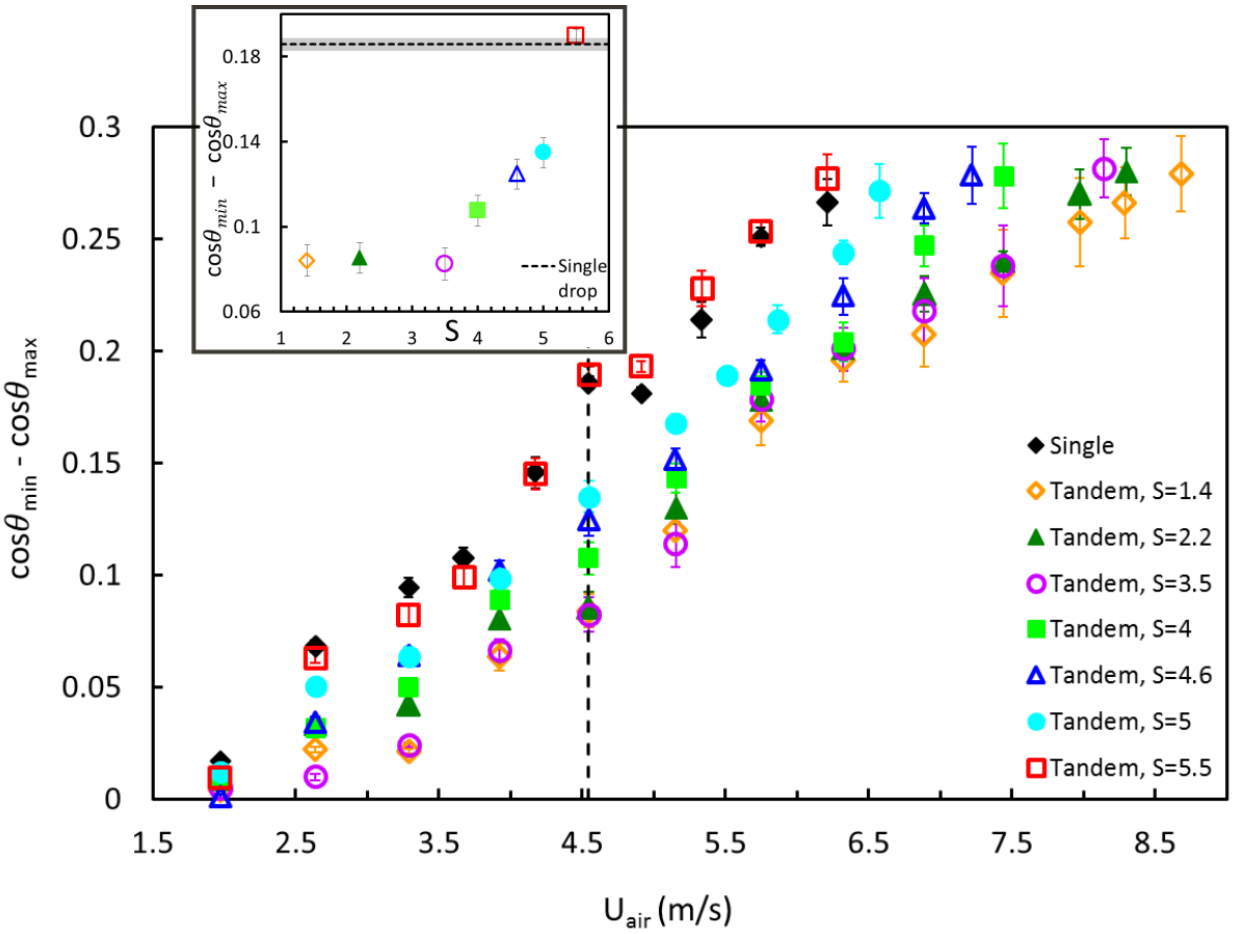

Figure 2.4: The trend of $cos\,\theta_{min} - cos\,\theta_{max}$ at different spacings, as a function of air velocity for the upstream droplet in a tandem arrangement. The data are for 10 μl droplet on a hydrophilic surface. The air velocity is changing from its minimum value up to the critical air velocity (Uair=Ucr). The inset shows the trend of $cos\,\theta_{min} - cos\,\theta_{max}$ as a function of spacing at Uair=4.54 m/s; the shaded band represents the error limits for a single droplet data.

where V_d is the volume of the droplet and θ_s is the average of θ_{min} and θ_{max}. Using Eq. 2.4, at a particular air velocity, the frontal area of the upstream droplet was found to change by a maximum of 1.5% compared to that of a single droplet. This change in frontal area is not large enough to

increase the U_{cr}, so C_D is the main parameter in Eq. 2.2 which is affected by the presence of another droplet. When the downstream droplet is placed sufficiently close to the upstream droplet, it interacts with the wake of the upstream droplet. In fact, for the unsteady laminar flow which is the case of this study (considering the droplets Re number), the downstream droplet reduces the drag by suppressing the vortex shedding at the aft of the upstream droplet. This condition is analogous to the mechanism of drag reduction seen for an upstream body by placing a downstream body at its wake [43]. As the spacing between sessile droplets increases, downstream droplet interacts less with the upstream wake, and drag coefficient approaches to that of a single droplet. This is similar to the study in [34] for suspended tandem spheres in an unsteady laminar flow, where the drag coefficient of the upstream sphere increases with spacing until it approaches the value of a single sphere at S>5. Two sessile droplets placed in tandem in [16], shed independently at S=2.4; although the substrate is more wettable in [16] compared to our case, the following discussion will show that the wettability of the substrate cannot be the reason for such a difference between [16] and our results.

At S≈1.4, C_D of the upstream sessile droplet should be lower than that of a single droplet, as higher U_{cr} is required to overcome the maximum adhesion force. As it is shown in Figure 2.3, for $S \leq 3.5$ - 4 the reduction in critical air velocity with spacing is not as sharp as it is for $3.5 - 4 < S < 5.5$. The sharper reduction of U_{cr} (i.e. lower $U_{cr} / (U_{cr})_{single}$) may occur due to the positioning of the downstream droplet, partially or fully, outside of the wake. In this study, the deformation of the sessile droplets along with the increasing Re number (due to the increasing U_{air}) constantly alters the size of the wake or the rate of the vortex shedding. As such, even if the downstream droplet initially is positioned outside of the upstream droplet's wake, it may later get trapped inside the wake, which again results in reduction of drag on the upstream droplet. Eventually at $S \approx 5.5$, U_{cr} of the upstream droplet approaches the value of a single droplet ($U_{cr} / (U_{cr})_{single} \approx 1$), and two

tandem sessile droplets shed independently as they are not aerodynamically coupled anymore. Note that for all of the S < 5.5, the upstream droplet sheds first.

Also, in Figure 2.3, the ratio of the upstream droplet's critical air velocity to that of a single droplet, especially within small spacing, is greater for the larger volume of droplet. It has been shown in [10] that U_{cr} as a function of adhesion force has a steeper slope as the size of a sessile droplet decreases. It means that for a large droplet size, shedding becomes less dependent on the lateral adhesion force, so the relative importance of the drag force in controlling the shedding increases. As such, the larger a sessile droplet, the more significant is the aerodynamic force effects, and the more influential is the role of the downstream droplet in changing the drag on the upstream droplet. In the Appendix A, the data similar to Figure 2.4, but for 5 μl droplets is shown; essentially, one can see similar results for both droplet sizes.

Shedding of droplets in a Side-by-Side (SbS) Arrangement

The ratio of critical air velocity for SbS droplets to that of a single droplet as a function of spacing is shown in Figure 2.5. For side-by-side arrangement, two droplets shed simultaneously and identically. When S is smaller than 1.4, the critical air velocity of SbS droplets is similar to that of a single droplet of the same size. From S≈ 1.5 to 2.6, U_{cr} increases; however, from S≈ 2.6 to 4.2, the U_{cr} fluctuates within an 8% band. For S values larger than 4.2, U_{cr} decreases, and at S≈5.5, two SbS droplets shed independently with U_{cr} of a single droplet, considering the error bars. The S value to recover the single droplet behavior is similar to the case for upstream droplet of the tandem arrangement. Note that the double pick trend which is observed for 5 μl droplets, and not for 10 μl droplets, can be attributed to the frequency of the droplets oscillation which is higher for smaller droplets, although oscillation is beyond the scope of this study.

Similar to the tandem arrangement, for SbS droplets, the " $\cos\theta_{min} - \cos\theta_{max}$ " variation with U_{air} is plotted in Figure 2.6.

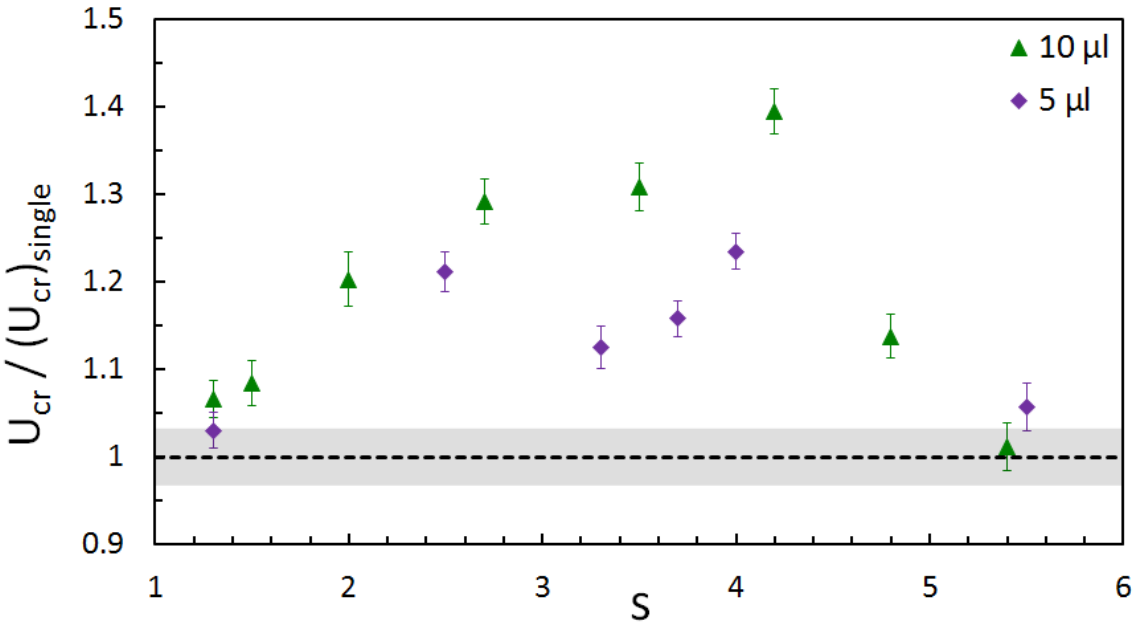

Figure 2.5: The ratio of the critical air velocity for the droplets in a side-by-side arrangement to that of a single droplet as a function of spacings. Data shown are for hydrophilic surfaces. The error limits for a single droplet is shown by the shaded band.

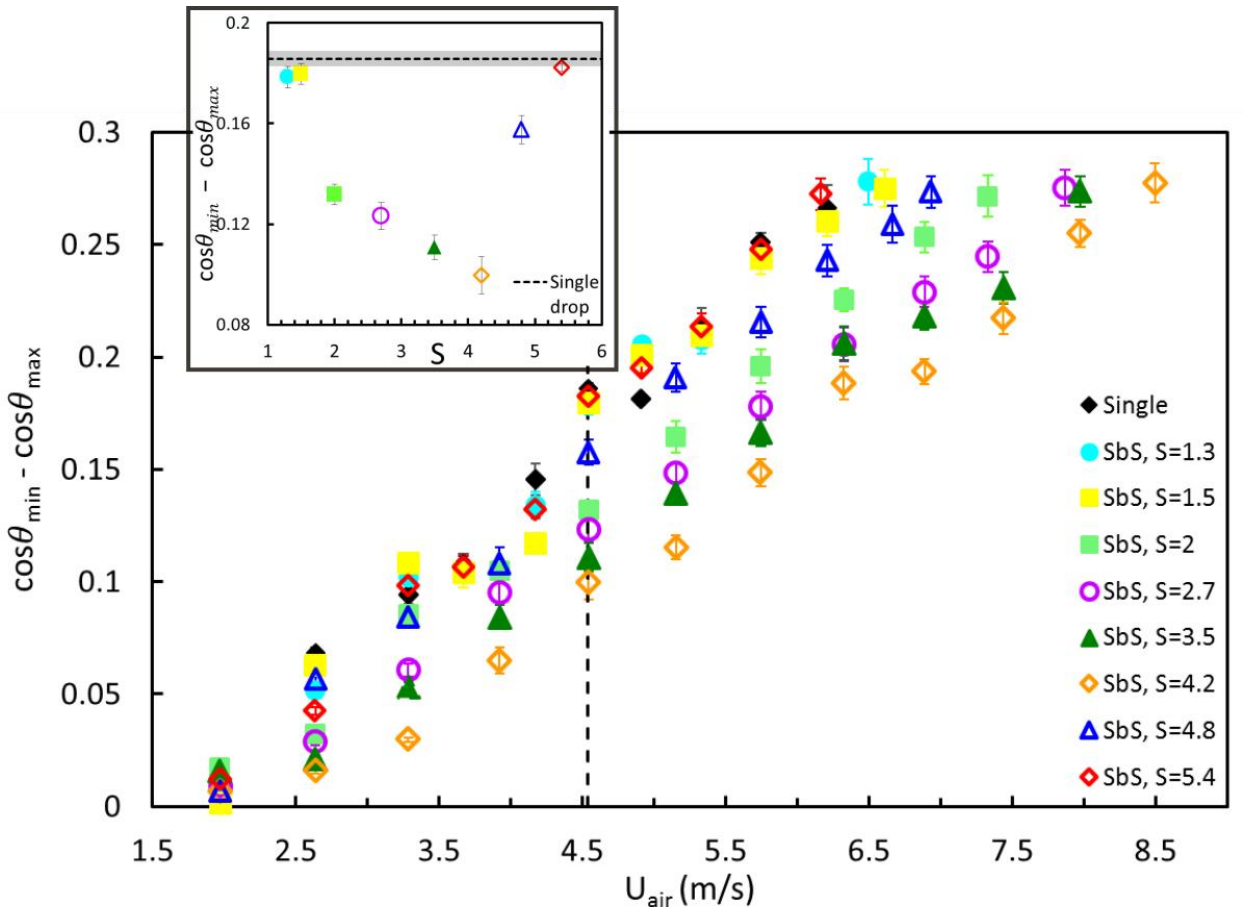

Figure 2.6: The trend of $cos\ \theta_{min} - cos\ \theta_{max}$ at different spacings, as a function of air velocity for droplets in a side-by-side arrangement. The data are for 10 μl droplets on a hydrophilic surface. The air velocity is changing from its minimum value up to the critical air velocity (Uair=Ucr). The inset shows the trend of $cos\ \theta_{min} - cos\ \theta_{max}$ as a function of spacing at Uair=4.54 m/s.

It can be understood from Figure 2.6 that the lateral adhesion force, and consequently the drag (see the discussion made for tandem droplets) has similar values for a single droplet and the two SbS droplets at small spacing (S≈1.4). This behavior is different from that is observed for SbS suspended bodies in [34], [38], and [44], where the drag coefficient on SbS suspended solid spheres or droplets at S≈1.4, increases by ~12% compared to that of a single sphere. Such difference can be due to the presence of the solid surface which can affect the flow pattern and recirculation wake formation over the SbS sessile droplets compared to that of suspended bodies. As the S increases, two strongly interacting wakes [42] (conceptually similar to that of Figure 2.1e)

form at the aft of the SbS sessile droplets. The interaction of two wakes may result in the reduction of the drag on the droplets. This is a similar condition to the study performed on two SbS cylinders at Re=3500 [45]; where at the intermediate spacing (S = 1.7), drag coefficient decreases below the value for that of a single cylinder due to the flow energy cancelation, which resulted from interaction of recirculation wakes. As drag decreases on each of the sessile droplets, U_{cr} needs to increase above the value of a single sessile droplet to overcome the maximum adhesion force. For S ≥ 4.2, as S increases, droplets' wakes should interact less (see figure 2.1f), and the drag reduction effects become less pronounced. As such, U_{cr} of both SbS sessile droplets decreases and reaches the value for that of a single droplet at S ≈5.5. This is similar to the value of spacing at which SbS suspended bodies experience the same drag as the single suspended body does in [34], and [38]. Data similar to Figure 2.6, but for 5 μl droplets is provided in the Appendix A.

Wettability Effect

Figure 2.7 shows the critical air velocity as a function of spacing for upstream droplet/droplets on both hydrophilic and hydrophobic surfaces. The general trend of U_{cr} with spacing is similar for both surface wettabilities. However, on a hydrophobic surface, the range of spacing within which U_{cr} deviates from the value for a single droplet is narrower compared to a hydrophilic one. This means that as the wettability of the surface decreases, the effects of the neighboring sessile droplets on each other also decreases. One reason for such a behavior is the adhesion of the sessile droplets to the surface; sessile droplet adheres strongly to a hydrophilic surface compared to that of a hydrophobic surface. Baseline length, and "$\cos\theta_{min} - \cos\theta_{max}$" for a 10 μl droplet, are 1.64, and 1.4 times larger, respectively, on hydrophilic surface (Eq. 2.1) compared to the hydrophobic surface in this study. On the other hand, for a given droplet volume, the frontal area of a sessile droplet is larger on the hydrophobic surface than on a hydrophilic one. Using Eq. 2.4, the frontal area for a 10 μl droplet is 4.94 mm^2 on hydrophobic surface, and is 3.83 mm^2 on a

hydrophilic surface. In fact, higher adhesion along with a lower drag (due to the smaller frontal area and the more aerodynamic shape) leads to a higher critical air velocity for droplet on a hydrophilic surface. Droplets on a hydrophobic surface have a shape closer to a sphere, and sit higher on the surface; as it is reported in [36], for the bodies which sit higher (larger polar diameter) the spacing within which wakes interact, is wider. However, one should note that larger air velocity on a hydrophilic surface may increase the wake instability and vortex shedding, which in turn promotes the interaction between droplets on a hydrophilic surface. Also, sessile droplets on a hydrophilic surface undergo stronger oscillations compared to those on a hydrophobic surface. Oscillation of a droplet increases the vortex shedding, which in turn reinforce the oscillation; this phenomenon which is known as the aeroelastic coupling [5] increases the wake instability at the aft of a sessile droplet. Accordingly, on a hydrophilic surface, compared to a hydrophobic one, the neighboring sessile droplets are exposed to a more unstable wake, and their effect on drag reduction is more significant. The stronger interaction of the droplets on a hydrophilic surface leads to droplets independently shedding, in a relatively wider spacing. Wettability of the substrate has the same effects for both sizes of droplets (a figure similar to Figure 2.7, but for 5 μl droplets, has been provided in the Appendix A).

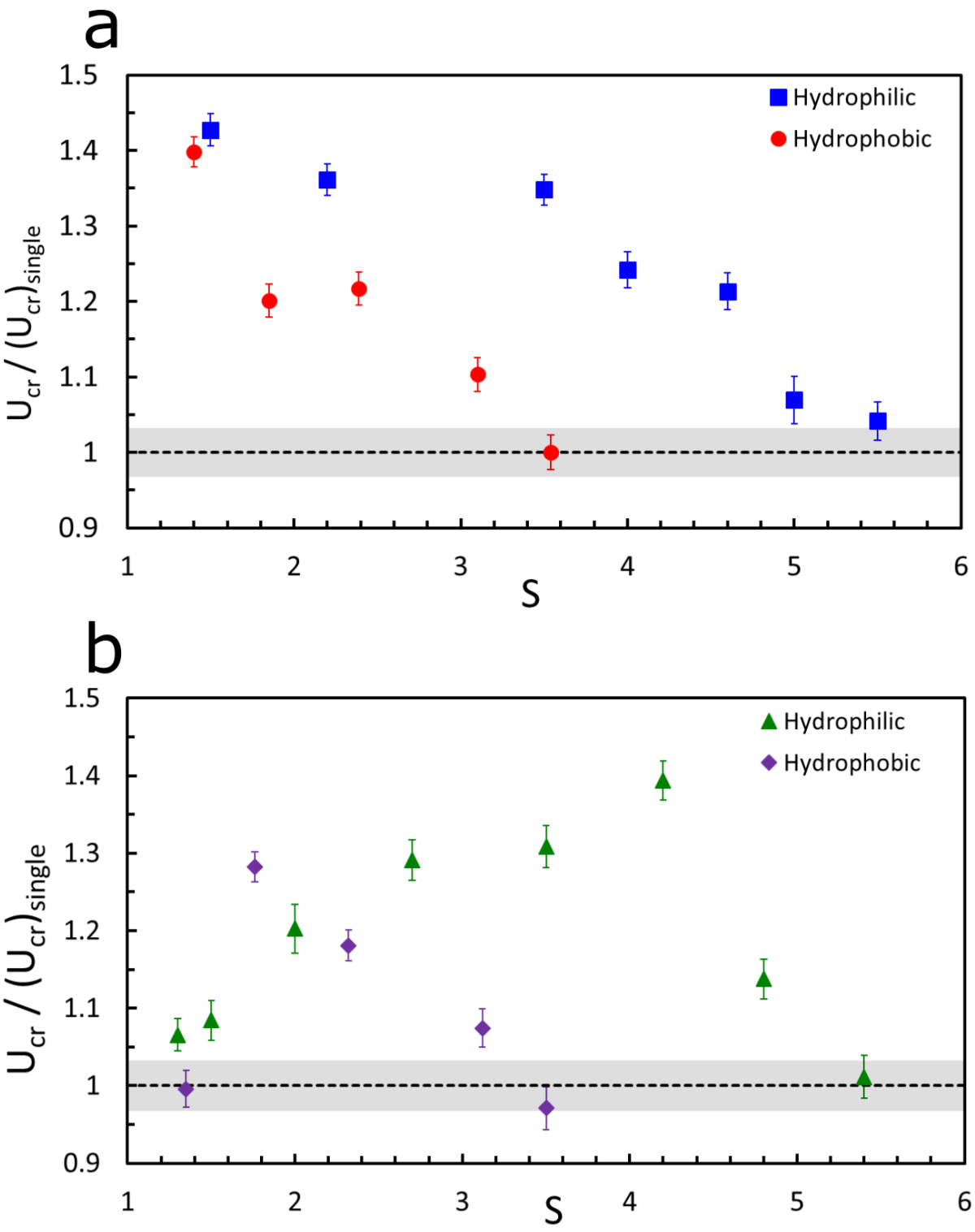

Figure 2.7: The ratio of the critical air velocity a) the upstream droplet in tandem arrangement, and b) droplets in the side-by-side arrangement, to that of a single droplet. Data shown are for 10 μl droplets. The error limits for a single droplet is shown by the shaded bands.

Critical Air Velocity Estimation

In an attempt to relate the critical air velocity and the spacing, an empirical expression is proposed for tandem and side-by-side droplets. Considering Eq. 2.1 and Eq. 2.2, the ratio of drag to adhesion force is:

$$\frac{F_{drag}}{F_{adh}} = \frac{C_D}{2K} \cdot \frac{\rho A U_{air}^2}{\gamma L_b(\cos\theta_{min} - \cos\theta_{max})} \qquad (2.5)$$

If we define β as a non-dimensional number to describe the relative strength of drag to the adhesion force, at the incipient motion, one has:

$$\beta = \frac{\rho A U_{cr}^2}{\gamma L_b(\cos\theta_{min} - \cos\theta_{max})} \qquad (2.6)$$

Since at the incipient motion $\frac{F_{drag}}{F_{adh}} \approx 1$, then considering Eq. 2.5:

$$\beta = \frac{2K}{C_D} \qquad (2.7)$$

β is changing with spacing, as C_D will change as per discussions above.

Considering the spherical cap approximation, the relation between the sessile droplet's frontal area (A), and baseline (L_b) is (for details see the Appendix A):

$$A = \frac{L_b^2}{4} \cdot \frac{2\theta_s - \sin 2\theta_s}{1 - \cos 2\theta_s} \qquad (2.8)$$

Substituting Eq. 2.8 in Eq. 2.6:

$$\beta = \frac{(2\theta_s - \sin 2\theta_s)}{4(1 - \cos 2\theta_s)} \cdot \frac{\rho L_b U_{cr}^2}{\gamma(\cos\theta_{min} - \cos\theta_{max})} \qquad (2.9)$$

θ_s is 62° for hydrophilic surface in this study, and it is 115° for the hydrophobic surface.

For 0° < θ_s <120°, $\frac{2\theta_s - \sin 2\theta_s}{1 - \cos 2\theta_s} \propto \theta_s$ (for details see Appendix A). As such:

$$\beta = \frac{\theta_s}{(\cos\theta_{min} - \cos\theta_{max})} \cdot Weber_{cr} \qquad (2.10)$$

where $Weber_{cr} = \frac{\rho L_b U_{cr}^2}{\gamma}$, and θ_s is an indicator of surface's wettability.

Applying Eq. 2.10 to our experimental data, β is found for the upstream droplet(s) in the tandem, and SbS arrangements at different spacings, as it is shown in Figures 2.8 and 2.9. As the S increases beyond 5.5 (for hydrophilic surfaces) and beyond 3.5 (for hydrophobic surfaces), the β fluctuates around the value of β for a single droplet; this range of spacing is defined as "Far Regime" (see Figures 2.8 and 2.9). In "Far Regime", there is no, or very limited interaction between the droplets. On the other hand, in the "Near Regime" (S<5.5 for hydrophilic surface, and S<3.5 for hydrophobic surface), the value of β strongly changes with the spacing. For the upstream droplet in the tandem arrangement, the slope of the β is steeper at the intermediate spacing (3.5<S<5.5) compared to the small spacing. The reason is that the upstream droplet experiences more changes in drag when the downstream droplet is positioned partially or fully outside of its wake.

Considering above discussion, a curve is fitted to the experimental data using Eq. 2.11 that captures the described behavior in mathematical form for the upstream droplet(s) in the tandem, and SbS arrangements (Figures 2.8 and 2.9).

$$\beta = a\frac{b + c(S-d)^4}{1 + c(S-d)^4} \qquad (2.11)$$

The fitting coefficients of Eq. 2.11 are given in Table 2.1 for Tandem, and SbS arrangements for both types of surfaces.

Table 2.1: The values of coefficients for Eq. 2.11 for both tandem and SbS arrangements.

Arrangement	Wettability	a	b	c	d
Tandem	Hydrophilic	11	1.78	0.011	1
	Hydrophobic	4.4	1.78	0.78	1
Side-by-side	Hydrophilic	11	1.54	0.21	3.4
	Hydrophobic	4.4	1.54	25.85	2

In Eq. 2.11, a represents the value of β for a single droplet (β_{single} is 11 for a hydrophilic surface, and is 4.4 for a hydrophobic surface); b is a multiplier for β_{single} to determine the maximum value of β (e.g. the maximum value of β, and consequently U_{cr}, for the upstream droplet in the tandem arrangement is higher than that of SbS arrangement). c indicates the change in the intensity of the droplets' interaction with spacing (the slope of the curves in Figure 2.8 and 2.9), and d shows the spacing for maximum U_{cr}. Droplets in tandem arrangement have the maximum interaction when they are within the minimum spacing; however, SbS droplets has the most interaction at an intermediate spacing.

One application of Eq. 2.11 is to determine the drag coefficient (C_D) for sessile droplets in the tandem and the SbS arrangements at different spacings. As seen in Eq. 2.7, β is proportional to the inverse of the drag coefficient (C_D). Parameter K is found to be on the order of ~1 for a sessile droplet (e.g. on an inclined surface) [46]. Using the equation proposed in [46], in our study, K is found to be 1.17 for a sessile droplet at the incipient motion.

Also, if controlling the position of the droplets on the surface is of the interest (e.g. by surface patterning), then using Eq. 2.10 and Eq. 2.11, one can estimate the optimum spacing at which specific droplets shed at a given airflow velocity.

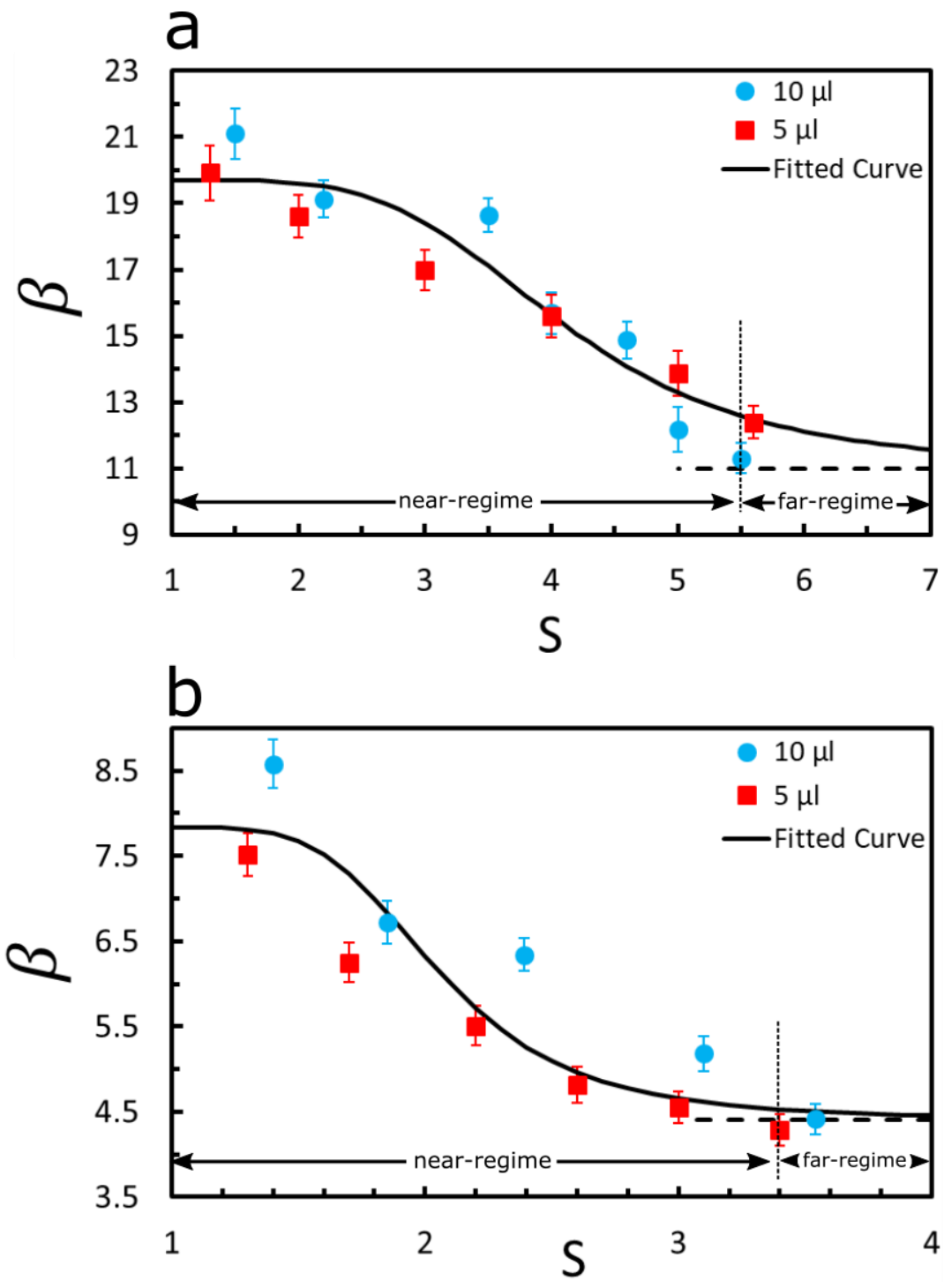

Figure 2.8: Relationship between β and spacing for the upstream droplet in a tandem arrangement on a) hydrophilic, and b) hydrophobic surfaces.

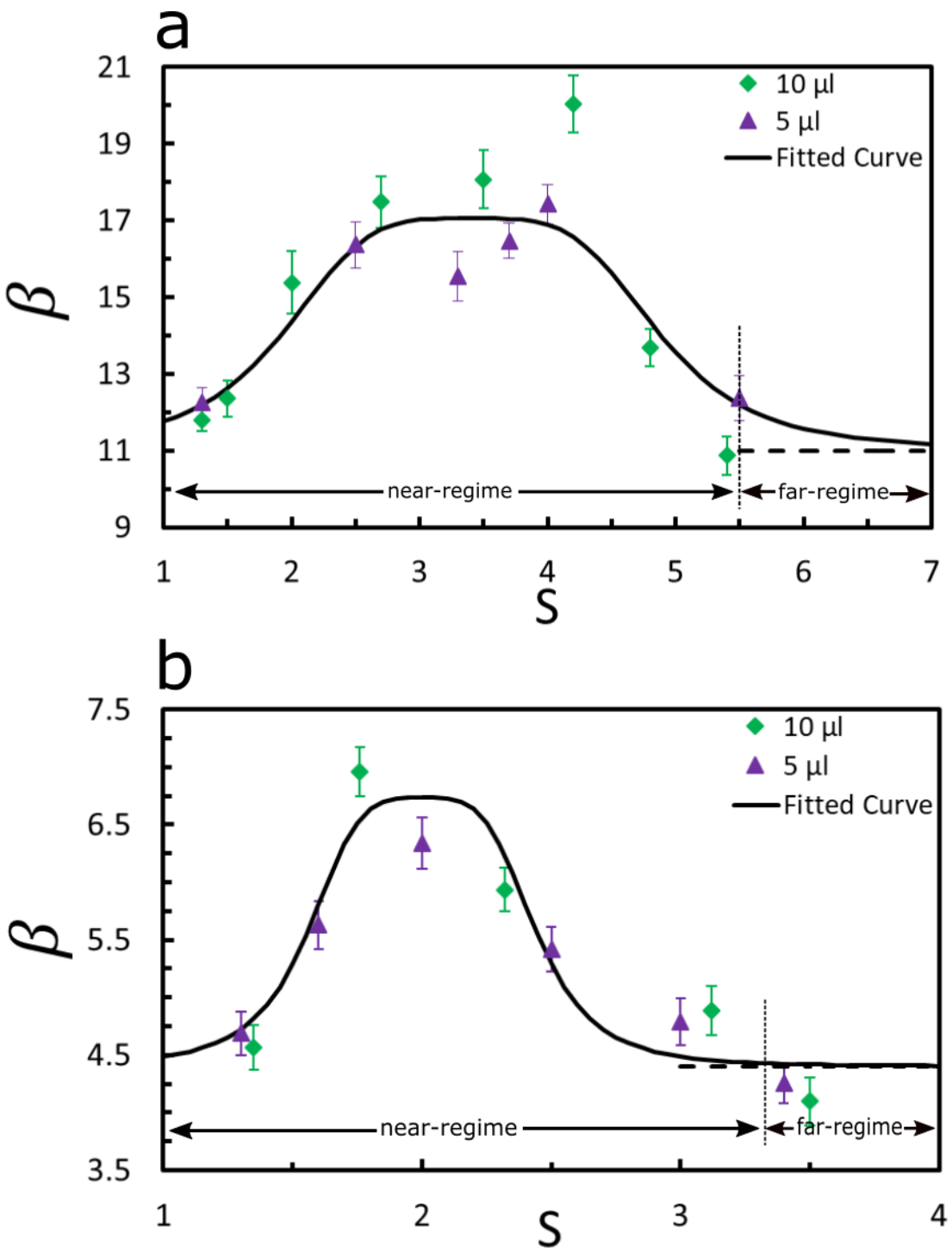

Figure 2.9: Relationship between β and spacing for the side-by-side droplets on a) hydrophilic, and b) hydrophobic surfaces.

Chapter 3: Role of Drag Force in Shedding of Multiple Sessile Droplets[2]

3.1 Introduction

Shedding of sessile droplets due to a shearing airflow is of particular interest due to its applications in spray coating [47], distillation [48], condensation [15], and biological application [49]. A droplet which is placed on the surface and is exposed to an airflow, can shed, if the aerodynamic drag force overcomes the droplet's adhesion to the surface. The minimum airflow velocity which leads to a sessile droplet shedding, is called the critical air velocity (U_{cr}). Shedding of a single sessile droplet has been studied widely [8][10][50]. However, often more than one droplet appears on a surface in the above applications. While shedding of a pair of sessile droplets has been investigated through a limited number of experimental and numerical studies such as [18] and Chapter 2, shedding of multiple sessile droplets remains untouched. Moghtadernejad et al. [18] used the VOF coupling with LES turbulence to simulate the shedding and coalescence of two sessile droplets placed in tandem on a superhydrophobic surface at 1000<Re<13000 (based on diameter of a sessile droplet). In [18] the initial center to center distance ratio to a droplet's baseline length was 1.88; as the air with a constant velocity flows over the droplets, they moved towards each other, and coalesced. The flow pattern and the drag force variation with time is presented in [18] for both droplets; however, it is not clear how the interaction of the droplets' wakes changes the shedding behavior compared to a single sessile droplet. In Chapter 2, we experimentally studied the shedding of a pair of tandem and side-by-side sessile droplets on hydrophilic and hydrophobic surfaces. Our results indicate that the critical air velocity (U_{cr}) can increase by 42% (compared to a single droplet) depending on the droplet pair's arrangement, spacing, and substrate wettability. Also, we determined the range of the spacing within which a

[2] This chapter is to be submitted for publication soon. Authors: A. Razzaghi, S. A. Banitabaei, A. Amirfazli

pair of droplets are interacting; beyond this range, sessile droplets shed independently and at the U_{cr} of a single droplet.

In the literature, shedding of multiple sessile droplets in the presence of an airflow has not been studied. Drag and adhesion are the two forces that co-interact during shedding of sessile drops. To form a basis, due to a lack of information for sessile drops, we first review the drag force variation with arrangement, and spacing for multiple suspended bodies. Tsuji et al. [51] experimentally studied the turbulent flow (Reynolds of ~40000 inside a tube) over a group of solid spheres arranged in the form of a repeating square and hexagonal grids, while the center to center distance between any two spheres was twice as the diameter of each sphere. They reported that regardless of the type of the arrangement, all spheres within a repeating grid showed a lower drag coefficient compared to a single sphere. As the number of repeating cells increased, the drag coefficient for each sphere decreased; also, the spheres in hexagonal arrangement showed a larger drag coefficient compared to those in a square arrangement. At a similar spacing of spheres (ratio of the center to center distance to the diameter of a sphere) to that of [51], Liang et al. [35] studied the drag coefficient for suspended solid spheres in hexagonal, and cubical arrangements at $Re \leq 100$. Their results indicate that in contrast to [51], a sphere in both arrangements, experienced a higher drag coefficient compared to that of a single sphere. This could be due to difference in flow regimes, i.e. turbulent in [51] and laminar in [35]. Still, both [51] and [35] agree that in a hexagonal arrangement, spheres show a higher drag coefficient value compared to that of a cubical arrangement. In [35], as spacing was increased (from 2 to 2.5), the drag coefficient decreased by 5%. Zhu et al. [52] also emphasized the significance of the spheres' spacing on the drag coefficient which is experienced by a solid sphere placed at the center of cubically arranged spheres at Re of 23. In [52] there is a maximum 38% increase in drag coefficient at spacing of 2.5. However, the amount of changes in drag coefficient, with respect to spacing, can vary significantly from one study to another. Ozgoren [53] experimentally obtained the flow pattern over three suspended spheres (using particle image velocimetry technique) arranged in an

equilateral triangular configuration; in [53] the spacing ranged from 1 to 2.5 and the Re number of the spheres was 5000. Their results show that the flow pattern is changing with the spacing, and the interaction of the two downstream spheres, results in fluctuation of the whole flow field.

You et al. [54] numerically simulated the flow over multiple spheres in a cubical arrangement at Re<100. Their results show that similar to [35], by reducing the spacing between the spheres, the drag coefficient increases. For three suspended solid spheres arranged in a linear array, Maheshwari et al. [55] numerically obtained the flow pattern and the drag coefficient values. They found that when the spacing is equal to 2, the drag coefficient on all spheres is less than that of a single sphere; the lowest drag coefficient was for the middle sphere. As the spacing increased to 4, the drag coefficient on the upstream sphere increased beyond the value for a single sphere. Considering the above literature, for multiple suspended spheres, compared to a single sphere, drag coefficient is significantly affected due to the interaction of the flow over the neighboring spheres. The type of the arrangement can alter the value of the drag coefficient; typically, spheres in a hexagonal arrangement have a higher drag coefficient compared to those in a cubical arrangement [51] [35]. The change in drag force was also affected by the flow regime. The above studies also show that for the suspended solid spheres, the effect of the spacing and arrangement on the drag force variation can be different for a pair of spheres than that of multiple spheres. For instance, in [53], increasing the spacing of suspended spheres results in increasing the drag coefficient on a pair of spheres arranged in tandem, but decreasing the drag for multiple spheres arranged cubically. As such, one can expect that the shedding of multiple sessile droplets will also be influenced by the arrangement types and the spacing of sessile droplets, but the question is how?

The study in this chapter is carried to investigate the critical air velocity for shedding of the upstream droplet(s) in various arrangements such as, equilateral triangle, square, reversed equilateral triangle, and diamond. Also, how the findings for shedding of a pair of sessile droplets

can be extended to the case of multiple sessile droplets within the above arrangements, is addressed in this chapter.

3.2 Methods

Experimental Methods

Figure 3.1 shows the schematic of the experimental setup. The experiments were performed inside a closed-loop wind tunnel; the height, width and the length of the test section is 6.4, 10.2 and 30.5 cm, respectively. Maximum airflow of 12 m/s is generated by the EBM-Papst fan, and to control the speed of the airflow, a regulator was used to vary the speed of the fan. At the maximum airflow velocity, the flow inside the test section is laminar; for details see Appendix A. The speed of the airflow was measured using an EE75 hot film anemometer. The experiments were conducted for droplets' Re number ranging from 573 to 1088 ($Re = {\rho U_{cr} H}/{\mu}$, where U_{cr} is the air velocity at the incipient motion of upstream droplets, and H is the height of sessile droplet).

Figure 3.2 shows the arrangements for sessile droplets. These arrangements can be considered as a repeating unit cell in a population of droplets (e.g. seen in dropwise condensation). All droplets within an arrangement had the same size, and experiments were conducted with 5 and 10 μl DI water sessile droplets. Droplets were placed on hydrophilic and hydrophobic surfaces by a syringe; Image J software was used to ensure that the desired spacing between the droplets is achieved (error for the spacing was ~4%). Hydrophilic surface was aluminum substrate, spin coated using a PMMA solution [2% (w/w) PMMA in Toluene] with advancing and receding contact angles of 74° and 58°, respectively. Hydrophobic surface was aluminum substrate, spin coated using a Teflon [5:1 (v/v) FC-75, 3-M / Teflon AF] with advancing and receding contact angles of 122° and 107°.

Dimensionless spacing (S) is defined as the droplets' center to center distance divided by a droplet's baseline length. In Chapter 2 for a hydrophilic surface, the upstream droplet in a tandem

arrangement showed a maximum ~42% increase in U_{cr} (compared to that of a single droplet) at S≈1.5. For two droplets in side-by-side arrangement, the maximum increase in U_{cr} (~30% compared to that of a single droplet) was observed at S≈3.5. For a hydrophobic surface, these values of spacing are 1.5 and 2.5, respectively. For the arrangements mentioned in this chapter, which are mostly formed by combining the tandem and the side-by-side arrangements, these two spacings are considered to observe the most changes in the U_{cr}.

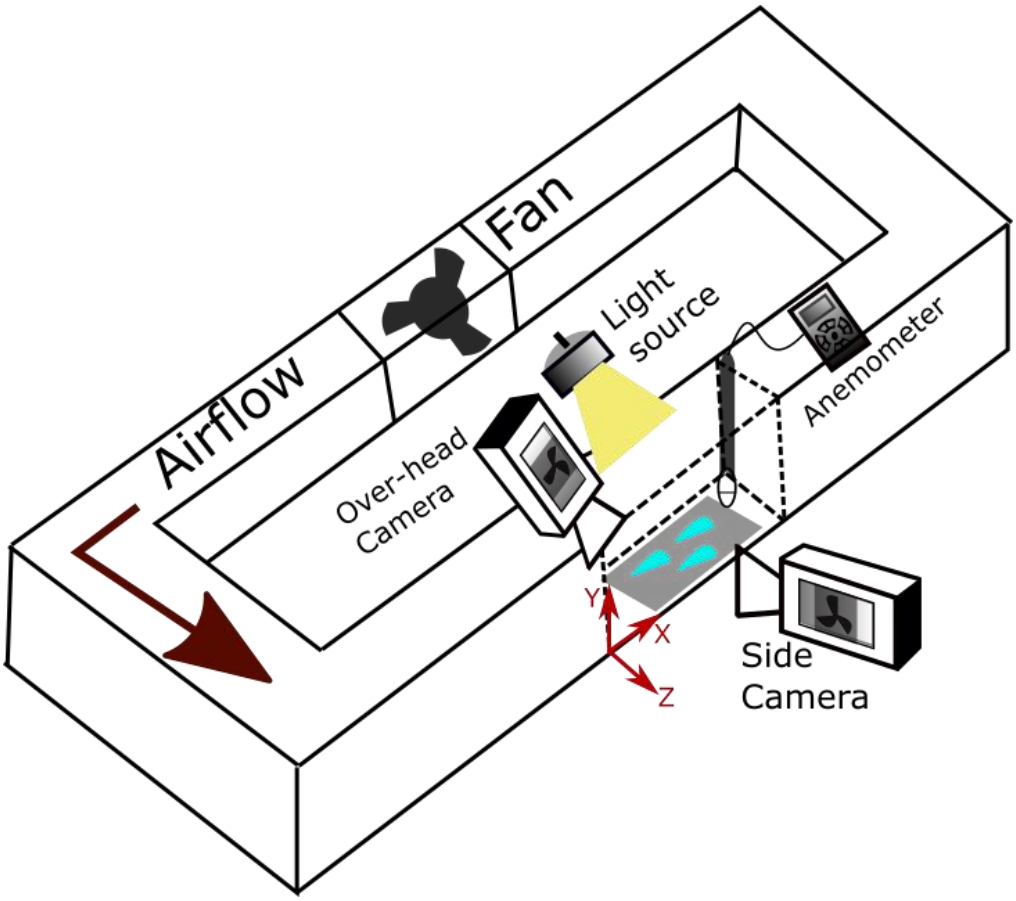

Figure 3.1: Schematic view of the experimental setup; the closed loop wind tunnel, high speed cameras, light source, and anemometer are shown.

To track the shedding of the sessile droplets, two Phantom high speed cameras (one for side, and one for overhead view) were operating synchronously capturing images at 450 frames per second. The incipient motion is defined as the moment when the contact line of the upstream droplet(s) moved 5 pixels (220 μm) on the surface in accordance to our past practice [10]. The air

velocity at the incipient motion is the so called critical air velocity (U_{cr}). Experiments were repeated three times and the standard deviation of the dataset is reported as the error.

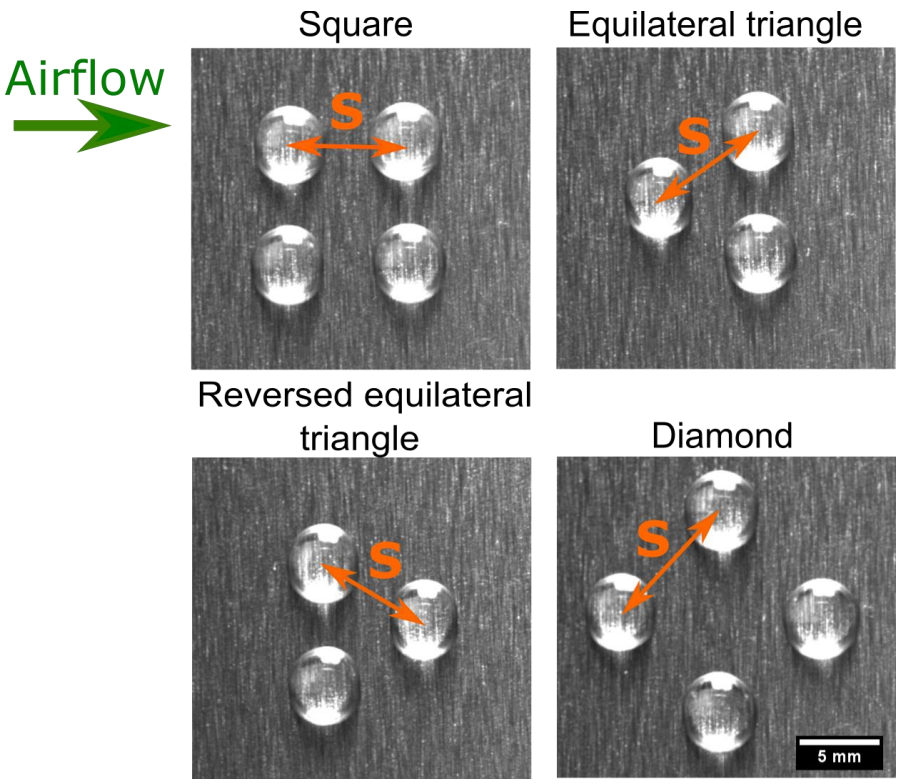

Figure 3.2: Sessile droplets in various arrangements on a hydrophilic surface. Droplets were identical for each arrangement. The apparent texture of the solid substrate has no notable effect on the results as there was a 1.3% error in the U_{cr} when surface was turned 90°.

Numerical Methods

To enhance our understanding of the flow interaction with the droplets at the moment of the incipient motion, a 3D numerical simulation was performed. We considered a steady state simulation rather than a transient one, since flow interaction with the droplets at the moment of incipient motion was of interest in this chapter. For simplicity, we considered droplets as solid objects; the geometry of the solid objects were fashioned after the shape of sessile droplets at the incipient motion. The details regarding the geometry of the objects, representing the sessile droplets at the moment of incipient motion, is provided in the Appendix B. ANSYS Fluent 18

software was used for the numerical simulations; the governing equations of continuity and momentum are:

$$\nabla \cdot U = 0 \qquad (3.1)$$

$$\rho \frac{DU}{Dt} = -\nabla p + \mu \nabla^2 U \qquad (3.2)$$

Where μ is the dynamic viscosity, and ρ is the density of air.

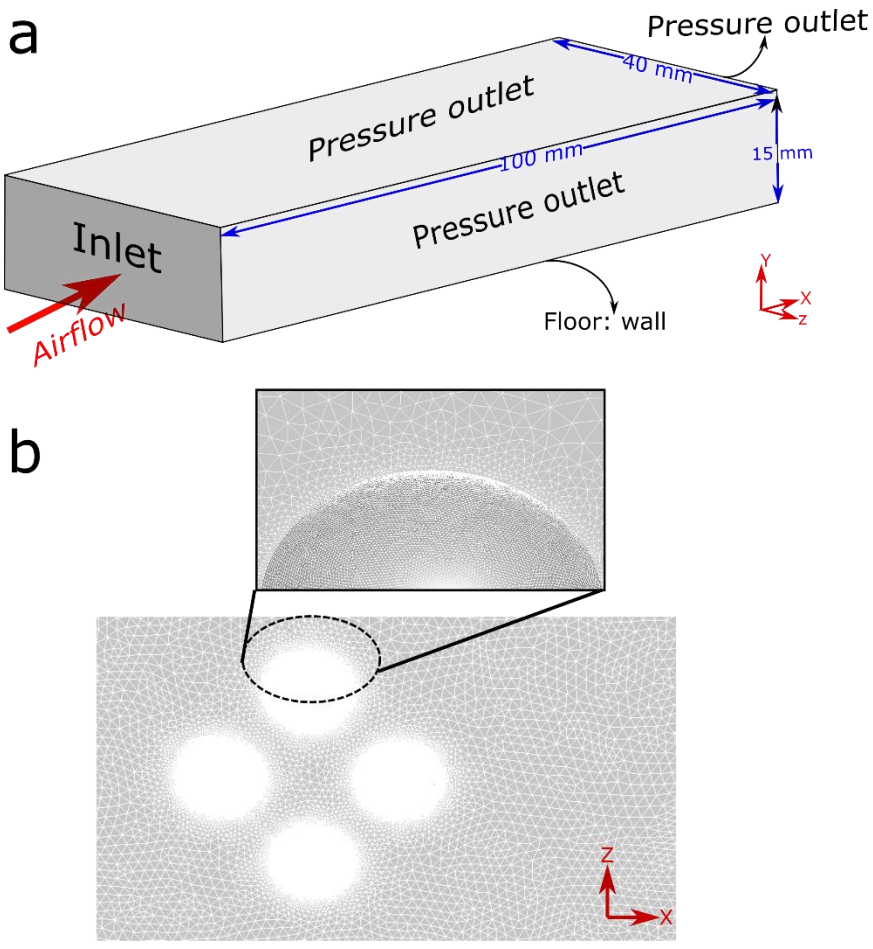

Figure 3.3: (a) Computational domain and the boundary conditions; (b) Mesh on the X-Z, Y=0 plane for diamond arrangement of 10μl simulated droplets at S=1.5. The inset shows the mesh density around the surface of the simulated droplets.

The computational domain, and the position of the simulated droplets is shown in Figure 3.3 for $10\mu l$ droplets. At the inlet, uniform airflow velocity which has the same magnitude as the experimentally observed U_{cr}, for each case, was implemented. The “pressure outlet” walls of the domain were at the atmospheric pressure, and had the same velocity magnitude as the inlet. On the floor, there was “no slipping” condition.

SIMPLE solution with a second order pressure and a second order upwind momentum for incompressible flow, were used.

The size of the meshes inside the boundary layer and around the simulated droplets is 0.01mm, and it is 0.5mm in the rest of the domain. To ensure the grid independency, the mesh size was reduced down to a quarter of the current size. However, no notable changes in the results were observed, while the computational time was significantly increased.

3.3 Results and Discussions

Figure 3.4 shows the $U_{cr}/(U_{cr})_{single}$ for the upstream droplet(s) in various arrangements on a hydrophilic surface. In all arrangements, the upstream droplet(s) shed first; at the smaller spacing (S=1.5), the common behavior is that the upstream droplet(s) hit the downstream droplet(s), and shed as a larger unit. So, our focus in this chapter is on comparison of shedding, and more specifically, the U_{cr} for the upstream droplets, in various arrangements. A figure similar to Figure 3.4, but for 5 μl droplets is provided in the Appendix B. The amount of change in $U_{cr}/(U_{cr})_{single}$ with respect to type of arrangement and spacing, is very similar for both droplets’ size.

The velocity field and the streamline pattern for each arrangement is examined through the numerical simulations. Due to the no-slip boundary condition on the solid substrate, the simulation plots at the X-Z, Y=0 plane is not interesting to observe. As such, unless to detect additional details, the plots are at the X-Z, Y=0.5 H plane. H is the simulated droplet’s height, which is 1.4

mm for a 10 μl simulated droplet on a hydrophilic surface. Plots at the X-Z, Y=0.75 H plane are provided in the Appendix B for interested readers.

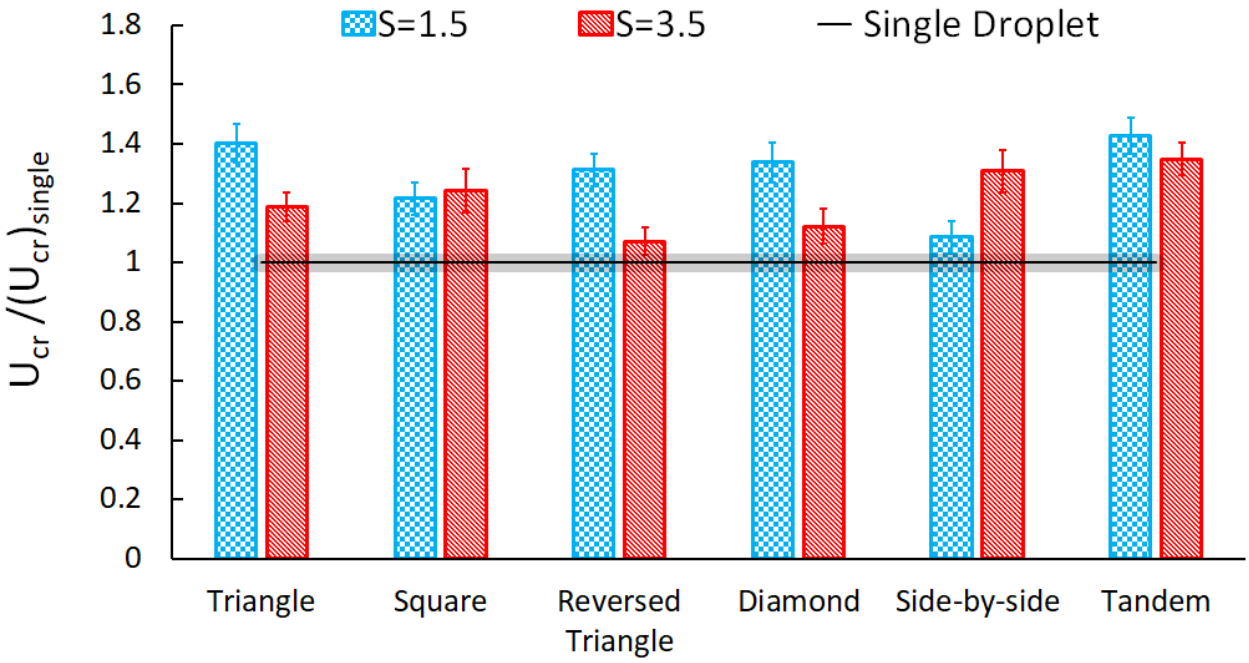

Figure 3.4: Critical air velocity for the upstream droplet(s) in different arrangements at two spacing (S) values. The data shown is for 10 μl droplets on a hydrophilic surface. The error of the U_{cr} for the single sessile droplet is denoted by the shaded band.

To determine the interaction intensity of simulated droplets, in each arrangement, the length and form of the ring-like vortices from numerical simulations was used. The vortex length was measured from the simulated droplet surface to the point where streamlines converge together. Note that as simulations were conducted at the airflow velocity of U_{cr}, aside from droplets' interaction, the change in the airflow velocity from case to case may also lead to variation of the size and form of the vortex ring. To elucidate this point, Figure 3.5 shows the velocity field, streamline pattern, and velocity vector for a single droplet (10μl) on a hydrophilic surface at two different airflow velocities: 6.1 m/s, and 8 m/s. The former velocity is the U_{cr} for a single sessile droplet and the latter is the average U_{cr} for the upstream droplet(s) in the triangle, square, reversed triangle, and diamond arrangements, at S=1.5. By increasing the airflow velocity (from

6.1 to 8, i.e. by 31 %), the ring-like vortex deforms and compresses by 27%, see Figure 3.5a and 3.5c. The length of the recirculation wake (measured from the droplet surface to the point where there is no backward vector), does not seem to decrease significantly (~10%).

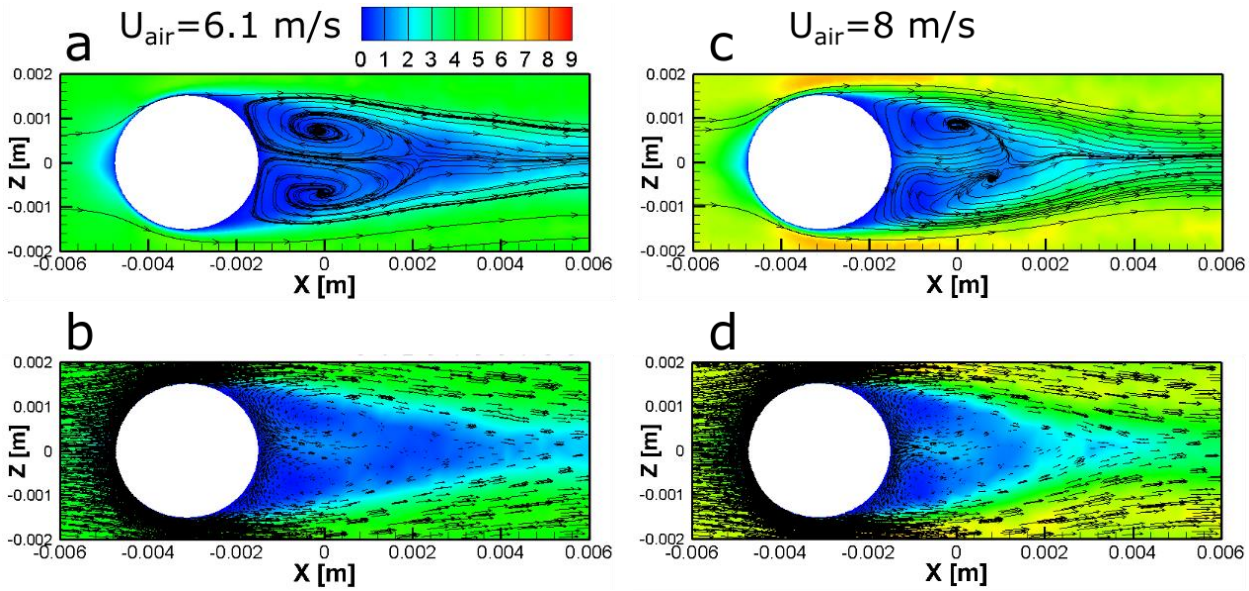

Figure 3.5: Streamlines (a & c), and Velocity vectors (b & d) for a single simulated droplet at two airflow velocities of 6.1 m/s (on the left) and 8 m/s (on the right). At 6.1 m/s the ring-like vortex, and recirculation wake length are 3.7 and 3 mm, respectively. At 8 m/s, both vortex ring and recirculation wake's length is 2.7 mm. Plots are for a 10 μl simulated droplet on a hydrophilic surface at X-Z, Y=0.5 H plane. Color plots online.

Equilateral Triangle Arrangement

As it is seen in Figure 3.4, the upstream droplet in an equilateral triangle arrangement shows a 40% increase in U_{cr} (compared to that of a single sessile droplet) at S=1.5. As spacing increases to 3.5, U_{cr} decreases; but it is still 18.6% higher than the value for a single droplet. Figure 3.6 shows the velocity field and streamlines for droplets arranged in an equilateral triangle configuration at the X-Z, Y=0.5 H plane. At S=1.5 (Figure 3.6a), the vortices at the rear of the upstream droplet shrink in length, with respect to that of a single droplet, by 73%. Considering the effect of the airflow velocity on the vortex length (Figure 3.5), the observed reduction in Figure 3.6a cannot be solely due to a higher airflow velocity. The suppression of the flow at the rear of

the upstream droplet (due to the presence of the downstream droplets) may decrease the drag, so a higher air velocity is required to overcome the adhesion force.

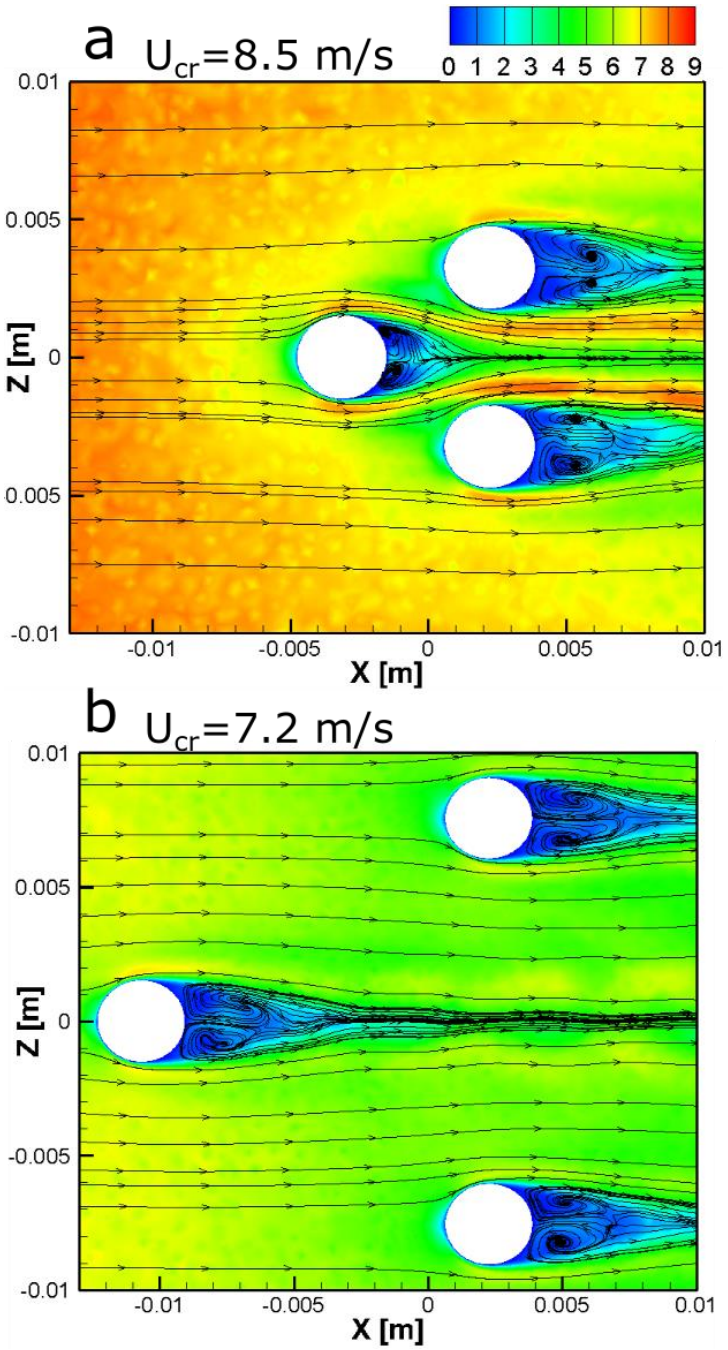

Figure 3.6: Velocity fields and streamline patterns for a) Three simulated droplets in an equilateral triangle arrangement at S=1.5, and b) Three simulated droplets in an equilateral triangle arrangement at S=3.5. Plots are for 10 μl simulated droplets on a hydrophilic surface at the X-Z, Y=0.5 H plane. Color plots online.

Similar results in terms of the interaction of the three suspended spheres in an equilateral triangle arrangement at S=1.5, and Re of 5000, was obtained in [53].

At the spacing of 3.5 (Figure 3.6b), the upstream droplet's vortex shows a 19% compression compared to that of a single droplet. Considering the above discussions, the compression is most likely due to a higher airflow velocity for triangle arrangement at S=3.5, and not due to the interaction of the simulated droplets. The increase in U_{cr} which were observed in experiments, however, implies that still exists a degree of interaction between the droplets at S=3.5. In fact, assumptions made to simplify the simulations, e.g. steady-state solution, and using simulated droplets, limits the exact observation of the interaction between droplets. Still, both experimental, and simulation results indicate that the interaction between the droplets decreases with spacing, and the U_{cr} approaches the value for that of a single droplet.

Square Arrangement

Square arrangement of four droplets is formed by two pairs of tandem droplets placed side-by-side; the $U_{cr}/(U_{cr})_{single}$ for the upstream droplets in a square arrangement is shown in Figure 3.4. For comparison the $U_{cr}/(U_{cr})_{single}$ of the upstream droplet in a tandem arrangement, and two droplets in a side-by-side arrangement, see Chapter 2, is also shown in Figure 3.4. At the spacing of 1.5, the upstream droplets in a square arrangement show a U_{cr} higher than that of a pair of side-by-side droplets, but lower than that of the upstream droplet in a tandem arrangement. By increasing the spacing to 3.5, no significant change in U_{cr} is observed for the upstream droplets in a square arrangement.

The velocity fields and streamline patterns for tandem, side-by-side, and square arrangements at S=1.5, at the X-Z, Y=0.5 H plane, is shown in Figure 3.7. In both tandem and square arrangements (Figure 3.7a and Figure 3.7c), the ring-like vortices fill the entire space between the upstream and downstream droplets. This is similar to the streamlines pattern which is obtained

by Tsuji et al. [44] over two suspended spherical particles placed in tandem at S=1.5 for Re of 200. As a result of flow suppression at the gap between the upstream and downstream droplets, the drag coefficient reduces (compared to that of a single droplet) in both tandem and square arrangements. So, a higher U_{cr} is required to overcome the adhesion of the upstream droplets to the surface (see Figure 3.4).

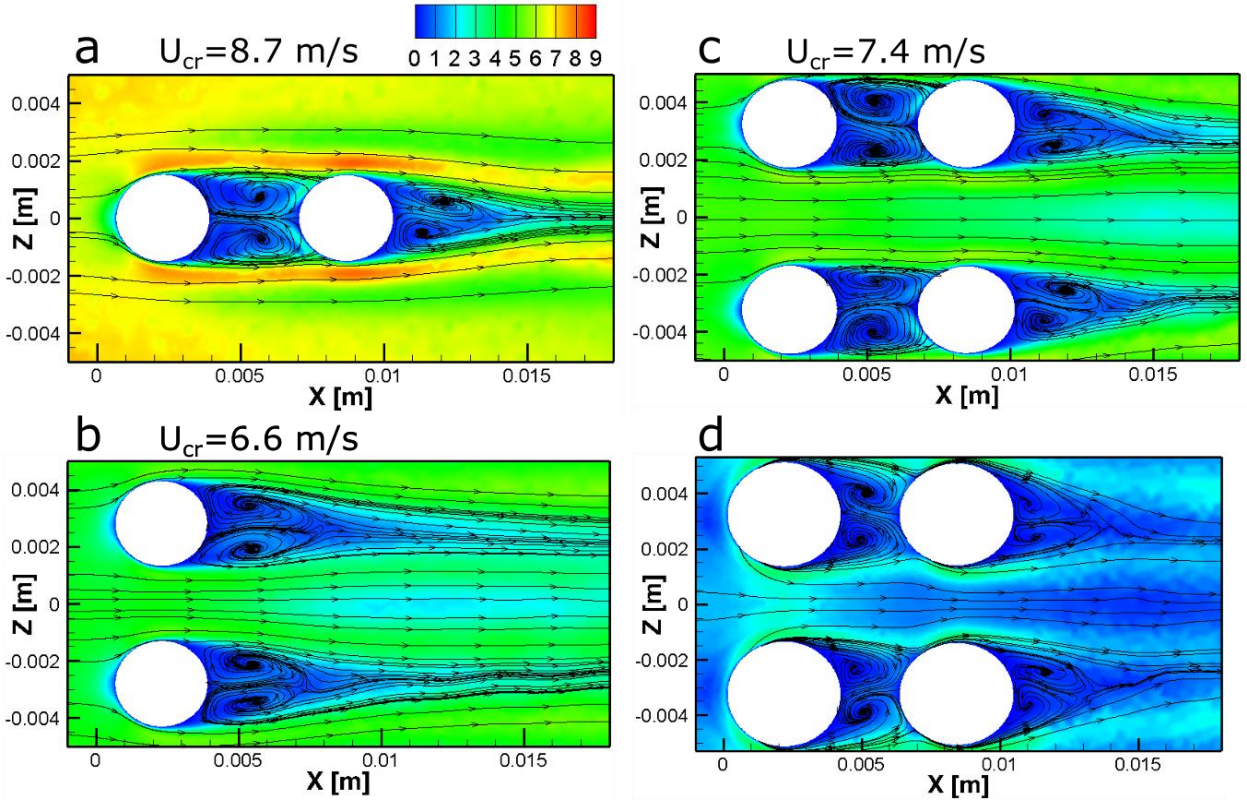

Figure 3.7: Velocity fields and streamlines for a) Tandem, b) Side-by-side, c) Square arrangements of simulated droplets all at the X-Z, Y=0.5 H plane, and d) Square arrangement of simulated droplets at the X-Z, Y=0.14 H plane. Plots are for 10 μl simulated droplets on a hydrophilic surface at S= 1.5. Color plots online.

Still, at S=1.5, the U_{cr} of the upstream droplets in a square arrangement is lower than that of a tandem arrangement. The possible explanation can be the acceleration of the airflow at the gap between the upstream, side-by-side droplets. Due to the shape of a sessile droplet on a hydrophilic surface, i.e. curvature of the interface, such an acceleration was not detected at the X-Z, Y=0.5H plane (Figure 3.7b). So, the velocity field for square arrangement is also examined

at the X-Z, Y=0.14 H, where droplets are closer together due to drop curvature (see Figure 3.7d). The flow acceleration at the gap between the side-by-side bodies was found to increase the drag coefficient [44]. The inverse effects of the tandem and side-by-side arrangements on drag coefficient variation, results in upstream droplets of square arrangement showing a U_{cr} between those of the tandem and side-by-side droplets.

From Figure 3.4 it can be understood that as spacing increases to 3.5, the U_{cr} decreases for the upstream droplet of tandem arrangement, and it increases for the side-by-side droplets. Accordingly, U_{cr} of the upstream droplets in the square arrangement, which is the combination of tandem and side-by-side arrangements, does not change significantly. The most possible reason for the increase of the U_{cr} of the side-by-side droplets at spacing of 3.5 is the continuous interaction of the droplets' recirculation wakes and vortices, due to the oscillation of the sessile droplets. It has been reported by Zhou et al. [45] that the oscillation of the side-by-side bodies results in the drag coefficient reduction (from the value for that of a single body) at an intermediate spacing. However, such an interaction of wakes and vortices cannot be detected in our simulation results due to the simplifications mentioned earlier.

Reversed Triangle and Diamond Arrangements

The upstream droplets in a reversed triangle arrangement show the same U_{cr} as the upstream droplet in a diamond arrangement, at both spacings of 1.5 and 3.5, considering the error bars (see Figure 3.4). The velocity field and the streamline patterns for droplets in a reversed triangle, and diamond arrangements, is shown in Figure 3.8 at the X-Z, Y=0.5 H plane. For reversed triangle, at S=1.5 (Figure 3.8a), the upstream vortices are compressed by ~26%, compared to that of a single simulated droplet at the same airflow velocity of 8 m/s (see Figure 3.5c). For diamond arrangement, the amount of the compression of the upstream vortices is even more; about 37% (Figure 3.8c). This implies that the suppression of the flow due to the interaction of the

nearby droplets should decrease the drag coefficient, since U_{cr} increases above the value for that of a single droplet.

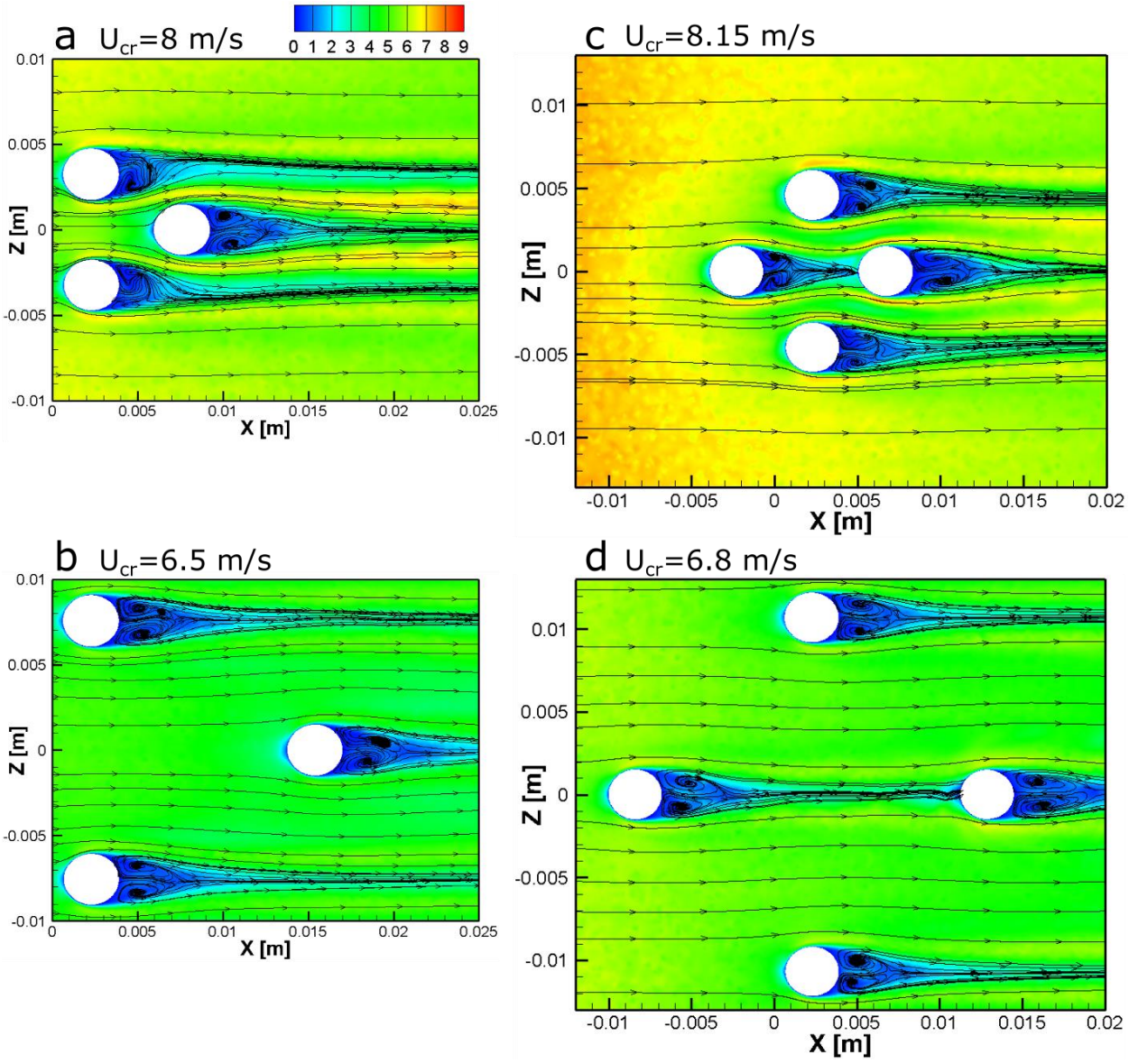

Figure 3.8: Velocity fields and streamline patterns for simulated droplets in reversed triangle arrangement a) at S=1.5, b) at S=3.5, and diamond arrangement c) at S=1.5, d) at S=3.5; at the X-Z, Y=0.5 H plane. Plots are for 10 μl simulated droplets on a hydrophilic surface. Color plots online.

As spacing increases to 3.5, Figures 3.8b and 3.8d show that the interaction of the droplets almost diminishes; as the ring-like vortices have a similar size to that of a single simulated droplet (see Figure 3.5a).

Effects of Surface Wettability

The wettability of the solid surface changes the shape of a sessile droplet, so the flow pattern and wake interactions will be changed. On a hydrophilic surface, compared to a hydrophobic surface, sessile droplets have a flatter shape and present a larger baseline length. Since the spacing is the ratio of droplets center to center distance to the baseline length; at a constant spacing, droplets are closer to each other on a hydrophobic surface, due to the smaller baseline length. Figure 3.9a-3.9d shows the flow fields and streamlines for simulated droplets in triangle and square arrangements at S=1.5 on a hydrophobic (3.9a and 3.9c) and a hydrophilic (3.9b and 3.9d) surfaces. Figure 3.9 is plotted at the X-Z, Y=0.5 H plane; where H is 2mm for the simulated droplets on a hydrophobic surface, and that is 1.4mm on a hydrophilic surface. For the square arrangement on a hydrophobic surface (Figure 3.9a) the streamlines between the upstream side-by-side simulated droplets are more squeezed compared to that of a hydrophilic surface (Figure 3.9b). Also, the suppression of the upstream vortices is more pronounced on a hydrophobic surface. For the triangle arrangement, the vortices formed at the rear of the upstream droplet, are more compressed on the hydrophobic surface (3.9c) compared to that of the hydrophilic surface (3.9d). In fact, the comparison of the flow fields indicates that the interaction of the simulated droplets is more intense on the hydrophobic surface than that of ones on hydrophilic surface. This is not surprising since at a constant spacing, droplets are closer to each other on the hydrophobic surface. Also, a more spherical shape of the droplets on the hydrophobic surface, leads to a higher intensity of interaction, compared to a flatter shape of them on the hydrophilic surface [23][36].

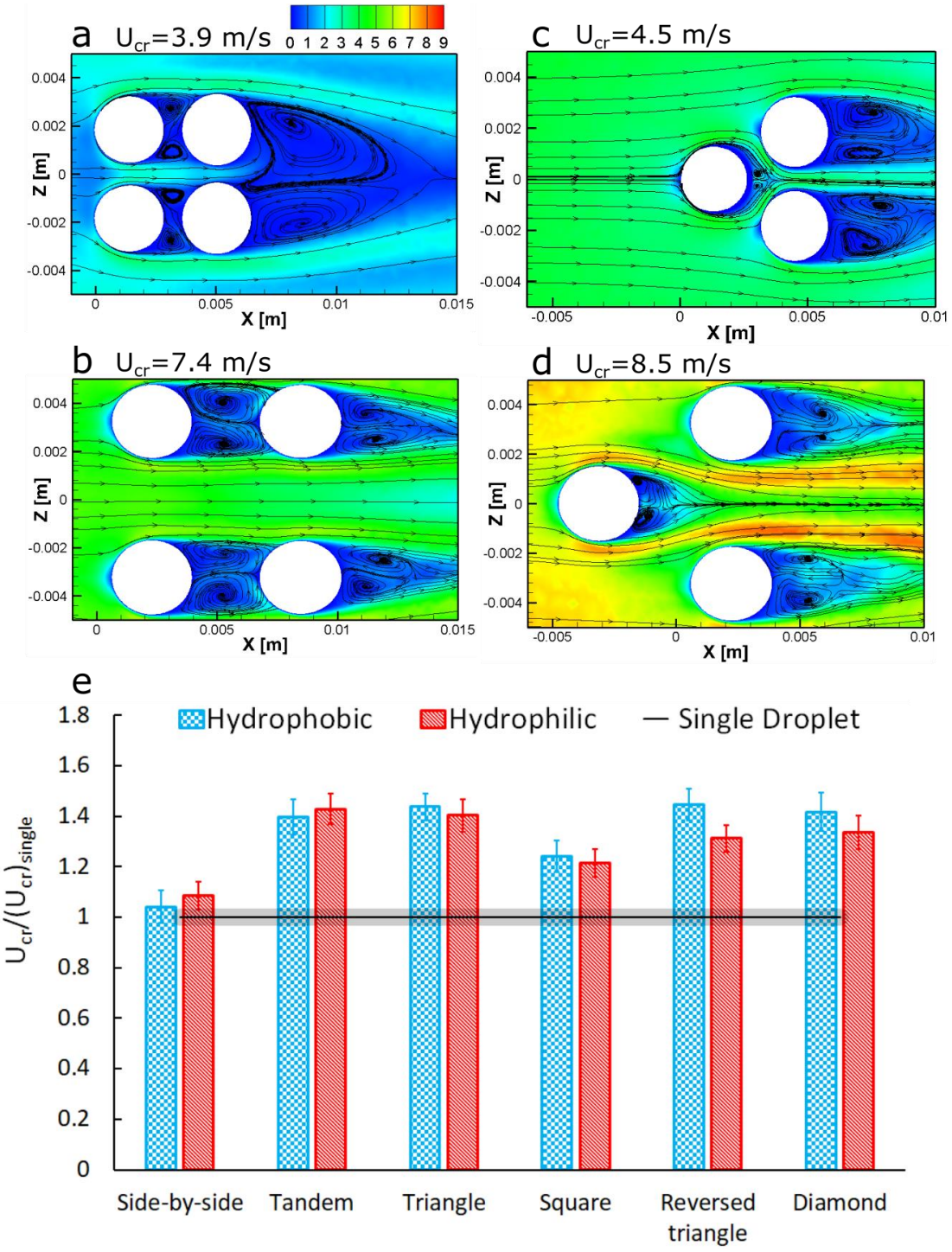

Figure 3.9: Velocity fields and streamlines for the simulated droplets in a) Square arrangement on a hydrophobic surface, b) Square arrangement on a hydrophilic surface, c) Triangle arrangement on a hydrophobic surface, d) Triangle arrangement on a hydrophilic surface, and e) U_{cr} comparison for the upstream droplet(s) in various arrangements on hydrophobic and hydrophilic surfaces. Plots are for 10 μl droplets at S=1.5.

Despite the higher interaction of neighboring droplets on a hydrophobic surface, Figure 3.9e shows the similar amount of increase in the U_{cr} for both surface wettabilities. On average, there is a maximum 40% increase for triangle, and a minimum 20% increase for square arrangement. Only, the upstream droplets in a reversed triangle arrangement have a ~13 % larger amount of increase in the U_{cr} on a hydrophobic surface than the hydrophilic one. Similar results in terms of the U_{cr} variation with substrate wettability is observed for 5 μl droplets; data are provided in the Appendix B. In Chapter 2, we showed that the drag and the adhesion forces evolve proportionally during the shedding process. The experimental results indicate that even if the change in drag force (due to the interaction of the droplets) is more intense on a hydrophobic surface, the adhesion and drag forces will be balanced in a way that the amount of change in U_{cr} remains the same for both surface types.

In addition, the oscillation of the sessile droplets found to be more intense on a hydrophilic surface compared to a hydrophobic surface. Milne et al. [56] showed that the frequency of the lateral oscillation for a 13 μl droplet on a hydrophilic surface is ~ 35% higher than that of a hydrophobic surface. Effects of the droplets' oscillation were not considered in the numerical simulations in this study. On the other hand, it has been found that the oscillation can significantly alter the vortex shedding, and the size of the recirculation wake for the bluff bodies [57][58]. Generally, higher frequency of oscillation is associated with a wider recirculation wake [58]. As such, the current flow fields represent the intensity of the interaction for multiple sessile droplets with limitations.

Comparison of the Arrangements

As it is seen in Figure 3.4, for a fix number of sessile droplets, the type of the droplets' arrangement affects the U_{cr}. For three sessile droplets, within a small spacing, the upstream droplet in a triangle arrangement shows a higher U_{cr} compared to the upstream side-by-side droplets in a reversed triangle arrangement. Similarly, for four droplets, the upstream droplet in a

diamond arrangement, presents a higher U_{cr} compared to the upstream droplets in a square arrangement.

As it was discussed before, two side-by-side sessile droplets, at an intermediate spacing, have the maximum U_{cr}; probably due to the aforementioned oscillations of sessile droplets, which increase the interaction between them. However, by presence of one droplet (like reversed triangle arrangement), or two droplets (like square arrangement) at the downstream of the side-by-side droplets, U_{cr} decreases. As such, at S=3.5, the upstream droplets in the reversed triangle, and square arrangements, have 22% and 5% lower U_{cr} compared to that of a pair of side-by-side droplets, respectively.

In general, there is a maximum ~40% increase in U_{cr} for the upstream droplet in tandem and triangle arrangement at S=1.5 on both hydrophilic and hydrophobic surfaces. As the spacing increases to 3.5, U_{cr} decreases for the upstream droplets in triangle, reversed triangle, and diamond arrangements; whereas in square arrangement the spacing does not affect the U_{cr}.

Independent Shedding of Multiple Sessile Droplets

As the effects of the droplets arrangement, and spacing on U_{cr} is identified, the next question to ask is when will droplets shed independent from each other at the U_{cr} of a single droplet, regardless of the type of arrangement.

To answer this question, we start from our findings in Chapter 2 for shedding of a pair of sessile droplets; we observed that when two droplets are at S≥ 5.5 on a hydrophilic surface, and at S≥ 3.5 on a hydrophobic surface, they shed independently, at the U_{cr} of a single droplet. This was true for both tandem and side-by-side arrangements. For side-by-side arrangement, both droplets also shed at the U_{cr} of a single droplet for S≤1.5 on both surface wettabilities. To see if the “no interaction” spacings hold for shedding of three or four sessile droplets, the following arrangements were considered: triangle at S=5.5, and rectangle at $S_{side\text{-}by\text{-}side} \times S_{tandem} = 1.5 \times 5.5$.

One may hypothesis that the “no interaction” spacing can be the same for both triangle and tandem arrangement. Also, rectangle arrangement of four droplets consists of two pairs of side-by-side and tandem droplets, both within no “interaction” spacings. As it is shown in Figure 3.10, droplets shed independently and at the U_{cr} of a single droplet. This means that as long as the droplets placed within the “no interaction” spacing, they will shed independently, regardless of the type of the arrangement configuration.

It can be understood from above discussions that there exists a critical value for spacing which is dependent to the surface wettability. For the spacings smaller than the critical value, both the arrangement type, and value of spacing affect the U_{cr} of the upstream droplets. Beyond the critical spacing, regardless of the type of arrangement, all droplets shed independently with the U_{cr} of a single sessile droplet.

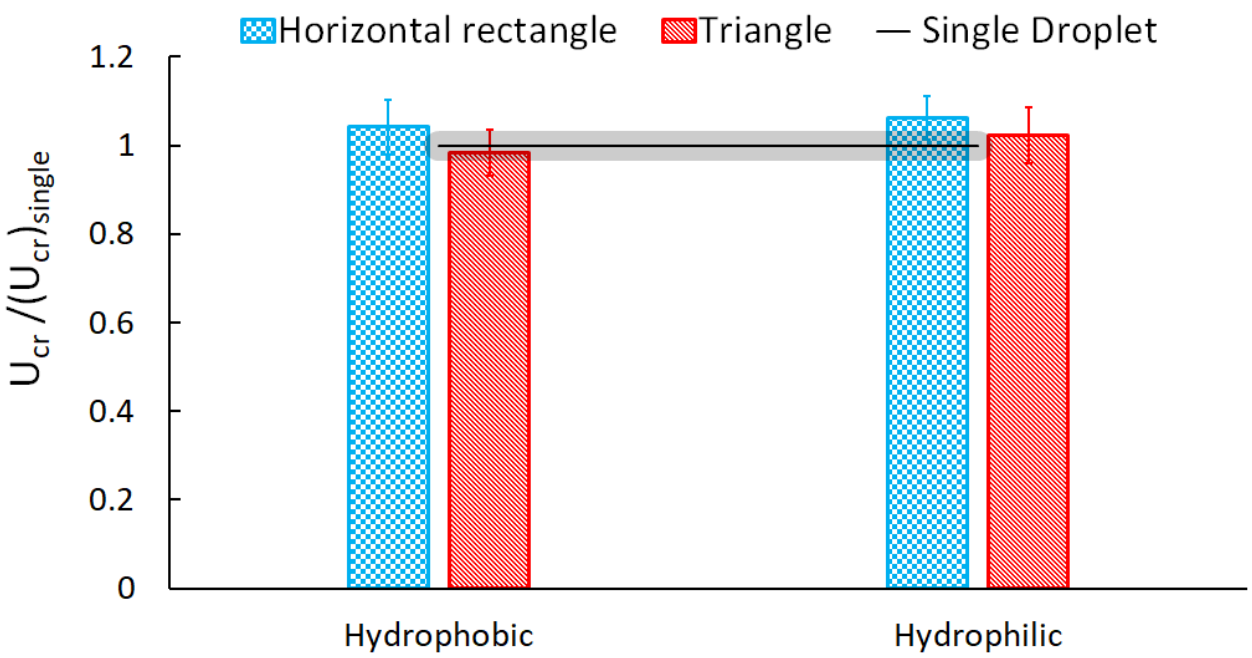

Figure 3.10: Critical air velocity ratio to that of a single droplet for the upstream droplets in a rectangle arrangement, and the upstream droplet in a triangle arrangement on both hydrophobic, and hydrophilic surfaces for 10 μl droplets. The value of spacing for the rectangle arrangement is $S_{side\text{-}by\text{-}side} \times S_{tandem}$ =1.5×3.5 on a hydrophobic surface, and is $S_{side\text{-}by\text{-}side} \times S_{tandem}$ =1.5×5.5 on a hydrophilic surface. For triangle arrangement, S is 3.5 for hydrophobic surface, and it is 5.5 for a hydrophilic surface. The error of the U_{cr} for the single sessile droplet is shown by the shaded band.

Chapter 4: Conclusions and Future Work

The conclusions of this thesis will be presented in this chapter. Also, the potential future work will be discussed considering the knowledge gained in this thesis.

4.1 Conclusions

For objectives 1, 2, and 3 which are mentioned in Chapter 1, an experimental study on shedding of a pair of sessile droplets was performed. Two droplets of the same size were placed either in tandem or in the side-by-side arrangements at different spacings. It was found that when two sessile droplets were placed in tandem, and within a very small spacing from each other, the critical air velocity of the upstream droplet increases by at most ~ 40%. However, U_{cr} decreases by increasing the spacing up to the point when two droplets shed independently. Two droplets which are placed side-by-side shed simultaneously, but the U_{cr} is significantly affected by the spacing; there exists an intermediate spacing at which two side-by-side droplets need about 30% higher U_{cr} compared to that of a single droplet to shed. Also, the increase in the critical air velocity, and the range of spacing within which two sessile droplets interact, is affected by the wettability of the substrate. On a hydrophobic surface, droplets are interacting within a smaller range of spacing compared to a hydrophilic surface. An empirical relationship is proposed to predict the critical air velocity for a pair of sessile droplets at any spacing, based on the sessile droplet baseline length, the surface wettability, and the arrangement of droplets (Eq. 2.11).

To investigate objectives 4 and 5, shedding of three and four sessile droplets, in proximity, within different arrangements, i.e. triangle, square, reversed triangle, and diamond were investigated. It was found that the interaction of multiple sessile droplets in an airflow alters the drag force in a way that U_{cr}, changes. It is also shown that the findings for shedding of a pair of sessile droplets in tandem and side-by-side arrangements can be extended to the case of three and four droplets.

Upstream droplets in all arrangements show a higher U_{cr} compared to that of a single droplet; with the highest value observed for triangle arrangement at S=1.5 (~40% higher), and the lowest for reversed triangle arrangement at S=3.5 (same as the single droplet). Similar results were found for both surface wettabilities. Increasing the spacing for triangle, reversed triangle, and diamond arrangement leads to a decrease in U_{cr}; for square arrangement, however, increasing the spacing does not change the U_{cr}. For three droplets, triangle arrangement with one droplet at the upstream, shows a higher U_{cr} compared to the upstream droplets in a reversed triangle arrangement, at both spacing. In a similar way, the upstream droplet in diamond arrangement has a higher U_{cr} compared to the upstream droplets in square arrangement. Finally, it was shown when the droplets placed far enough from each other (S≈5.5 for hydrophilic and S≈3.5 for hydrophobic surface), the configuration of the arrangement has no effect on the U_{cr}.

4.2 Possible Future Studies

Based on the insights gained through this experimental study on shedding of multiple sessile droplets, some future works can be proposed as following.

For a sessile droplet, it is important to understand how exactly the recirculation wake, and vortex shedding evolve, during the shedding process. Both increasing drag force (due to increasing the airflow velocity), and changing the shape of the liquid droplet (due to the increase in lateral adhesion force which leads to deformation of sessile droplet) instantaneously affect the flow field. For multiple sessile droplets, interaction of the wakes and vortices makes the condition even more complicated. Being able to achieve the transient flow filed, during the shedding process, is of the fundamental importance. This can be achieved either by numerical simulations (by implementation of transient solution), or by using Particle Image Velocimetry (PIV) technique. In current study, numerical simulations were conducted, but the solution was steady state without

considering the deformation, or oscillation of droplets. As such neither the increasing airflow velocity, nor the deformation of the sessile droplets, were not considered.

As a first step toward understanding the shedding of multiple droplets, we considered droplets in the particular arrangements. However, in reality it is more likely for droplets to be placed randomly; so another potential study would be looking at the shedding of droplets arranged randomly.

Moreover, it has been shown in both Chapters 2 and 3 that the wettability of the substrate affects the shedding of multiple sessile droplets. In the current study, hydrophilic (θ_s of 62°) and hydrophobic (θ_s of 115°) surfaces were examined. It would be interesting to vary the static contact angle (θ_s), even more, to find a clearer picture for variation of the spacing with θ_s. It was shown that hydrophobicity of the solid surface limits the range of the spacing within which droplets are interacting. As such, one may think that superhydrophobic surface, narrows the range of the spacing (within which droplets are interacting) even more. It is already known that one particular advantage of superhydrophobic is that it reduces the U_{cr} [11]. A study on shedding of multiple sessile droplet on a superhydrophobic surface may reveal another advantage of it on inducing independent shedding of multiple sessile droplets at smaller (compared to that of hydrophilic and hydrophobic surfaces) spacing.

Study of the shedding of multiple sessile droplets in icing condition ($T < 0$°C) is also practically important. For a single droplet, it was found in [11] that the icing temperature promotes the adhesion of the sessile droplets to the solid surface. Both size of a droplet, and wettability of the surface affect the U_{cr} in icing condition [11]. On the other hand, in this study it was found that the presence of sessile droplets in proximity, changes the drag force. Accordingly for multiple sessile droplets in icing condition, both drag and adhesion forces will be affected. It is required to conduct a study to understand if the amount of the change in U_{cr} is directly proportional to the amount of increase in the adhesion force, or the co-interaction of the drag and adhesion forces change the U_{cr} in a different way.

Finally, for the surface CAH ($\theta_{advancing} - \theta_{receding}$) considered in this study, a sessile droplet slides on the surface when it is exposed to an airflow. However, for very large CAH, the droplet's baseline elongates on the surface rather than slides. In this case, the lateral adhesion of the droplet will be different than that of the sliding droplet. A study can be conducted on the effects of the very large CAH on the observed S and U_{cr}.

Bibliography

[1] Holl, M.; Patek, Z.; Smrcek, L. Wind tunnel testing of performance degradation of ice contaminated airfoils. ICAS Technical Paper 3.1.1, 2000.

[2] Madani, S.; Amirfazli, A. Oil drop shedding from solid substrates by a shearing liquid. Colloids Surf. **2014**, 441, 796-806.

[3] Minor, G. Experimental Study of Water Droplet Flows in a Model PEM Fuel Cell Gas Microchannel. MASc, University of Victoria, 2007.

[4] Hodges, S. R.; Jensen, O. E. Spreading and peeling dynamics in a model of cell adhesion. J. Fluid Mech. **2002**, 460, 381-409.

[5] Clift, R.; Grace, J. R.; Weber, M. E. Bubbles, drops, and particles (Dover Publications: Mineola N.Y. USA, **2005**, 103).

[6] Milne, A. J. B. Shedding and Oscillation of Sessile Drops by Cross Flowing Air. PhD, University of Alberta, 2013.

[7] Dussan V, E. B. On the ability of drops to stick to surfaces of solids. Part 3. The influences of the motion of the surrounding fluid on dislodging drops. J. Fluid Mech. **1987**, 174, 381-397.

[8] Fan, J.; Wilson, M. C. T.; Kapur, N. Displacement of liquid droplets on a surface by a shearing air flow. J. Colloid Interface Sci, **2011**, 356, 286-292.

[9] Hao, P.; Lv, C.; Yao, Z. Droplet detachment by air flow for microstructured superhydrophobic surfaces. Langmuir. **2013**, 29, 5160-5166.

[10] Milne, A. J. B.; Amirfazli, A. Drop shedding by shear flow for hydrophilic to superhydrophobic surfaces. Langmuir. **2009**, 25, 14155-14164.

[11] Mandal, D. K.; Criscione, A.; Tropea, C.; Amirfazli, A. Shedding of water drops from a surface under icing conditions. Langmuir. **2015**, 31, 9340-9347.

[12] Wu, T. C.; Djilali, N. Experimental investigation of water droplet emergence in a model polymer electrolyte membrane fuel cell microchannel. J. Power Sources. **2012**, 208, 248-256.

[13] Mondal, B.; Jiao, K.; Li, X. Three-dimensional simulation of water droplet movement in PEM fuel cell flow channels with hydrophilic surfaces. Int. J. Energy Res. **2011**, 35, 1200-1212.

[14] Golpaygan, A.; Ashgriz, N. Effects of oxidant fluid properties on the mobility of water droplets in the channels of PEM fuel cell. Int. J. Energy Res. **2005**, 29, 1027-1040.

[15] Sommers, A. D.; Ying, J.; Eid, K. F. Predicting the onset of condensate droplet departure from a vertical surface due to air flow—Applications to topographically-modified, micro-grooved surfaces. Exp. Therm. Fluid Sci. **2012**, 40, 38-49.

[16] Hooshanginejad, A.; Lee, S. Droplet depinning in a wake. Phys. Rev. Fluids. **2017**, 2, 031601.

[17] Moghtadernejad, S.; Jadidi, M.; Esmail, N.; Dolatabadi, A. Shear-driven droplet coalescence and rivulet formation. Proc. Inst. Mech. Eng. C: J. Mech. Eng. Sci. **2016**, 230, 793-803.

[18] Moghtadernejad, S.; Tembely, M.; Jadidi, M.; Esmail, N.; Dolatabadi, A. Shear driven droplet shedding and coalescence on a superhydrophobic surface. Phys. Fluids. **2015**, 27, 032106.

[19] Jadoon, A.; Prahl, L.; Revstedt, J. Dynamic interaction of fixed dual spheres for several configurations and inflow conditions. Eur. J. Mech. B, Fluids. **2010**, 29, 43-52.

[20] Schouveiler, L.; Brydon, A.; Leweke, T.; Thompson, M. C. Interactions of the wakes of two spheres placed side by side. Eur. J. Mech. B, Fluids. **2004**, 23, 137-145.

[21] Chen, Y.; Third, J. R.; Müller, C. R. A drag force correlation for approximately cubic particles constructed from identical spheres. Chem. Eng. Sci. **2015**,123, 146-154.

[22] Rathore, A. S.; Chaitanya, P.; Kishore, N. Drag of tandem spheroids in power-law fluids at moderate Reynolds numbers. Ind. Eng. Chem. Res. **2013**, 52, 11773-11778.

[23] Kishore, N. Numerical investigation of interaction between spheroid particles in tandem arrangement at moderate Reynolds numbers. Ind. Eng. Chem. Res. **2012**, 51, 10265-10273.

[24] Cebeci, T.; Kafyeke, F. Aircraft icing. Annu. Rev. Fluid Mech. **2003**, 35, 11-21.

[25] Zhang, F. Y.; Yang, X. G.; Wang, C.Y. Liquid water removal from a polymer electrolyte fuel cell. J. Electrochem. Soc. **2006**, 153, A225-A232.

[26] White, E. B.; Schmucker, J. A. A runback criterion for water drops in a turbulent accelerated boundary layer. J. Fluids Eng. **2008**, 130, 061302-1.

[27] Thoreau, V.; Malki, B.; Berthome, G.; Boulange-Petermann, L.; Joud, J. C. Physico-chemical and dynamic study of oil-drop removal from bare and coated stainless-steel surfaces. J. Adhes. Sci. Technol. **2006**, 20, 1819-1831.

[28] Roisman, I. V.; Criscione, A.; Tropea, C.; Mandal, D. K.; Amirfazli, A. Dislodging a sessile drop by a high-Reynolds-number shear flow at subfreezing temperatures. Phys. Rev. E. **2015**, 92, 023007.

[29] Dimitrakopoulos, P.; Higdon, J. J. Displacement of fluid droplets from solid surfaces in low-Reynolds-number shear flows. J. Fluid Mech. **1997**, 336, 351-378.

[30] Zhu, X.; Sui, P.C.; Djilali, N. Numerical simulation of emergence of a water droplet from a pore into a microchannel gas stream. Microfluid. Nanofluid. **2008**, 4, 543-555.

[31] Carroll, B.; Hidrovo, C. Droplet detachment mechanism in a high-speed gaseous microflow. J. Fluids Eng. **2013**, 135, 071206.

[32] Tal, R.; Lee, D. N.; Sirignano, W. A. Heat and momentum transfer around a pair of spheres in viscous flow. Int. J. Heat Mass Transfer. **1984**, 27, 1953-1962.

[33] Chen, R. C.; Wu, J. L. The flow characteristics between two interactive spheres. Chem. Eng. Sci. **2000**, 55, 1143-1158.

[34] Yoon, D. H.; Yang, K. S. Flow-induced forces on two nearby spheres. Phys. Fluids. **2007**, 19, 098103.

[35] Liang, S. C.; Hong, T.; Fan, L. S. Effects of particle arrangements on the drag force of a particle in the intermediate flow regime. Int. J. Multiphase Flow. **1996**, 22, 285-306.

[36] Kishore, N. Flow and drag phenomena of tandem spheroid particles at finite Reynolds numbers. Ind. Eng. Chem. Res. **2012**, 51, 3186-3196.

[37] Mulholland, J. A.; Srivastava, R. K.; Wendt, J. O. Influence of droplet spacing on drag coefficient in nonevaporating, monodisperse streams. AIAA J. **1988**, 26, 1231-1237.

[38] Raju, M. S.; Sirignano, W. A. Interaction between two vaporizing droplets in an intermediate Reynolds number flow. Phys. Fluids A. **1990**, 2, 1780-1796.

[39] Kim, I.; Elghobashi, S.; Sirignano, W. A. Three-dimensional flow over two spheres placed side by side. J. Fluid Mech. **1993**, 246, 465-488.

[40] Antonini, C.; Carmona, F. J.; Pierce, E.; Marengo, M.; Amirfazli, A. General methodology for evaluating the adhesion force of drops and bubbles on solid surfaces. Langmuir. **2009**, 25, 6143-6154.

[41] Tsuji, Y.; Morikawa, Y.; Terashima, K. Fluid-dynamic interaction between two spheres. Int. J. Multiphase Flow. **1982**, 8, 71-82.

[42] Pinar, E.; Sahin, B.; Ozgoren, M.; Akilli, H. Experimental study of flow structures around side-by-side spheres. Ind. Eng. Chem. Res. **2013**, 52, 14492-14503.

[43] Hwang, J. Y.; Yang, K. S.; Sun, S. H. Reduction of flow-induced forces on a circular cylinder using a detached splitter plate. Phys. Fluids. **2003**, 15, 2433-2436.

[44] Tsuji, T.; Narutomi, R.; Yokomine, T.; Ebara, S.; Shimizu, A. Unsteady three-dimensional simulation of interactions between flow and two particles. Int. J. Multiphase Flow. **2003**, 29, 1431-1450.

[45] Zhou, Y.; Wang, Z. J.; So, R. M.; Xu, S. J.; Jin, W. Free vibrations of two side-by-side cylinders in a cross-flow. J. Fluid Mech. **2001**, 443, 197-229.

[46] Extrand, C. W.; Kumagai, Y. Liquid drops on an inclined plane: the relation between contact angles, drop shape, and retentive force. J. Colloid Interface Sci. **1995**, 170, 515-521

[47] Dimitrakopoulos, P.; Higdon, J. J. L. On the displacement of three-dimensional fluid droplets from solid surfaces in low-Reynolds-number shear flows. J. Fluid Mech. **1998**, 377, 189-222.

[48] White, Edward B.; Schmucker. A. J. A runback criterion for water drops in a turbulent accelerated boundary layer. J. Fluids Eng. **2008**, 130, 061302.

[49] Ding, H.; Spelt, P. D. Onset of motion of a three-dimensional droplet on a wall in shear flow at moderate Reynolds numbers. J. Fluid Mech. **2008**, 599, 341-362.

[50] Ding, H.; Gilani, M. N.; Spelt, P. D. Sliding, pinch-off and detachment of a droplet on a wall in shear flow. J. Fluid Mech. **2010**, 644, 217-244.

[51] Tsuji, Y.; Morikawa, Y.; Fujiwara, Y. Pipe flow with solid particles fixed in space. Int. J. Multiphase Flow. **1985**, 11, 177-188.

[52] Zhu, C.; Lam, K.; Chu, H. H.; Tang, X. D.; Liu, G. Drag forces of interacting spheres in power-law fluids. Mech. Res. Commun. **2003**, 30, 651-662.

[53] Ozgoren, M. Flow structures around an equilateral triangle arrangement of three spheres. Int. J. Multiphase Flow. **2013**, 53, 54-64.

[54] You, C.; Qi, H.; Xu, X. Drag force in dense gas-particle two-phase flow. ACTA Mech. Sin. **2003**, 19, 228.

[55] Maheshwari, A.; Chhabra, R. P.; Biswas, G. Effect of blockage on drag and heat transfer from a single sphere and an in-line array of three spheres. Powder Tech. **2006**, 168, 74-83.

[56] Milne, A. J. B.; Defez, B.; Cabrerizo-Vílchez, M.; Amirfazli, A. Understanding (sessile/constrained) bubble and drop oscillations. Adv. Colloid Interface Sci. **2014**, 203, 22-36.

[57] Bearman, P. W. Vortex shedding from oscillating bluff bodies. Annu. Rev. Fluid Mech. **1984**, 16, 195-222.

[58] Blackburn, H. M.; Henderson, R. D. A study of two-dimensional flow past an oscillating cylinder. J. Fluid Mech. **1999**, 385, 255-286.

Appendix A: Supporting Information for Chapter 2

A.1 Experimental Setup

Figure A.1 shows the experimental setup used in this study.

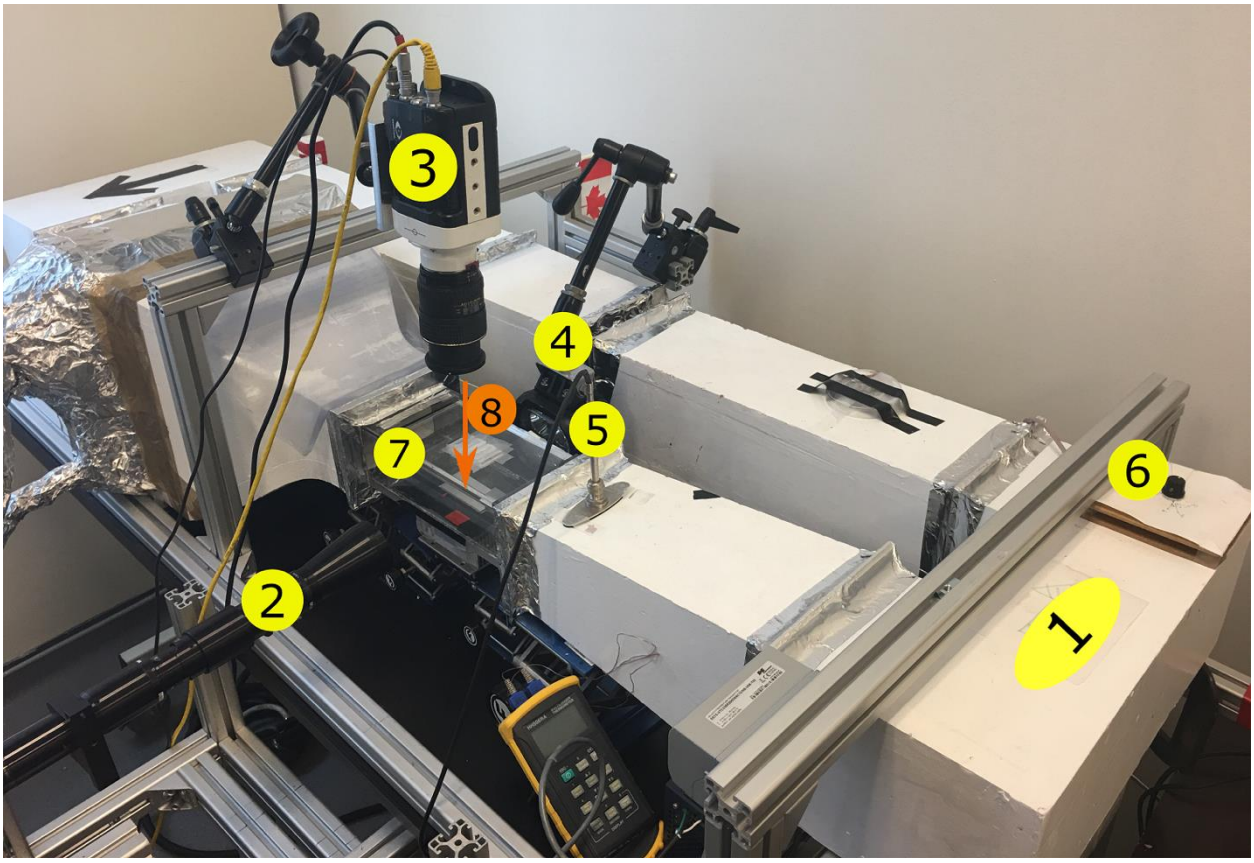

Figure A.1: Experimental setup used in sessile droplets shedding experiments. 1) Closed-loop wind tunnel, 2) Side camera lens, 3) Over-head camera, 4) Light source, 5) EE 75 Hot-film anemometer, 6) Regulator to vary the fan speed, 7) Test section, 8) Position of TSI, T-1.5 hot wire anemometer.

A.2 Supplemental Plots for Section 2.4

Figure A.2 shows the critical air velocity (U_{cr}) ratio, as a function of spacing for a pair of sessile droplets on a hydrophobic surface for both 5 and 10 μl droplets.

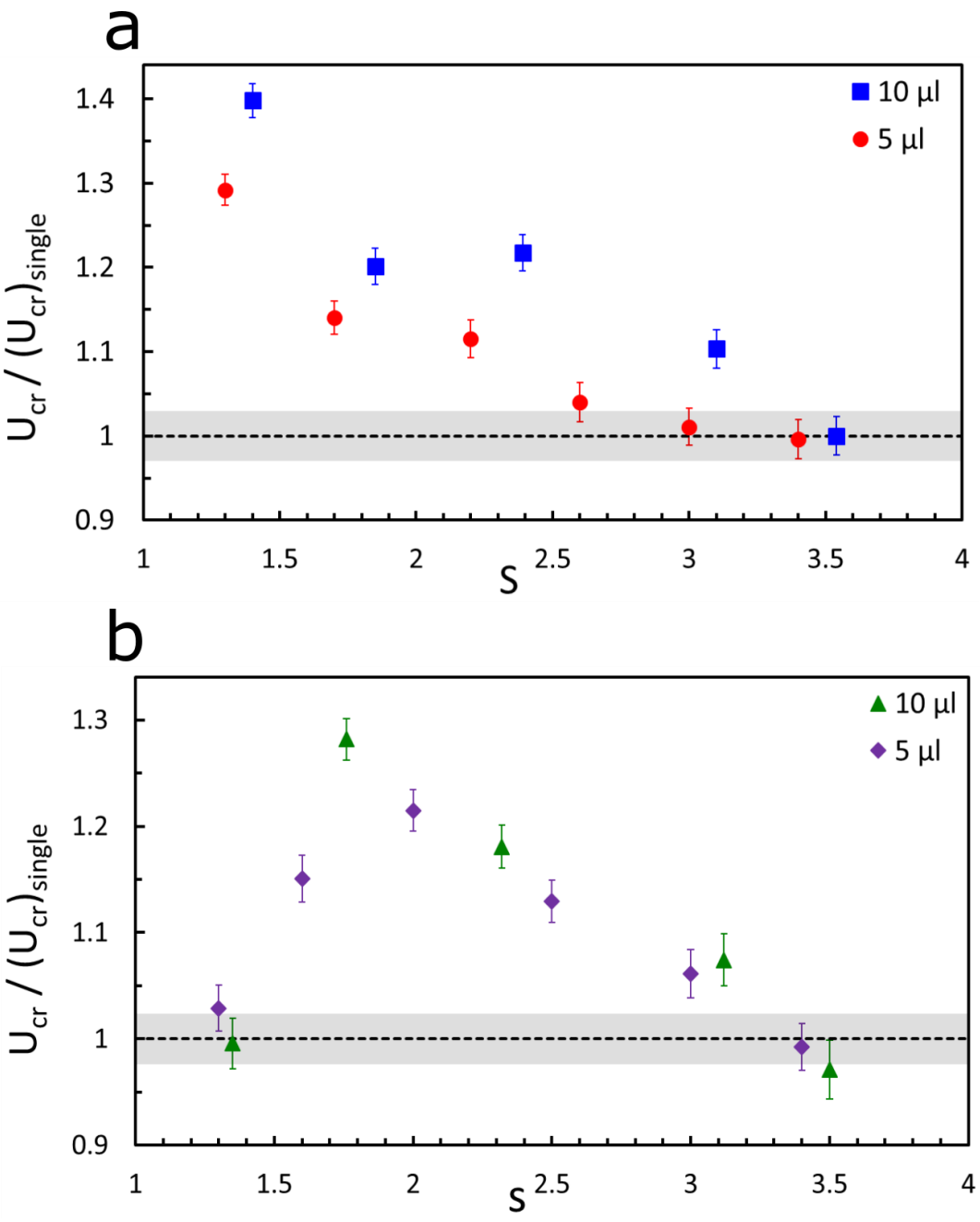

Figure A.2: The ratio of the critical air velocity for a) the upstream droplet in tandem arrangement; and b) droplets in the side-by-side arrangement, to that of a single droplet as a function of spacings. Data shown are for droplets on a hydrophobic surface. The error limits for a single droplet is shown by the shaded bands.

Figure A.3 shows the effects of wettability on shedding of a pair of 5 μl sessile droplets.

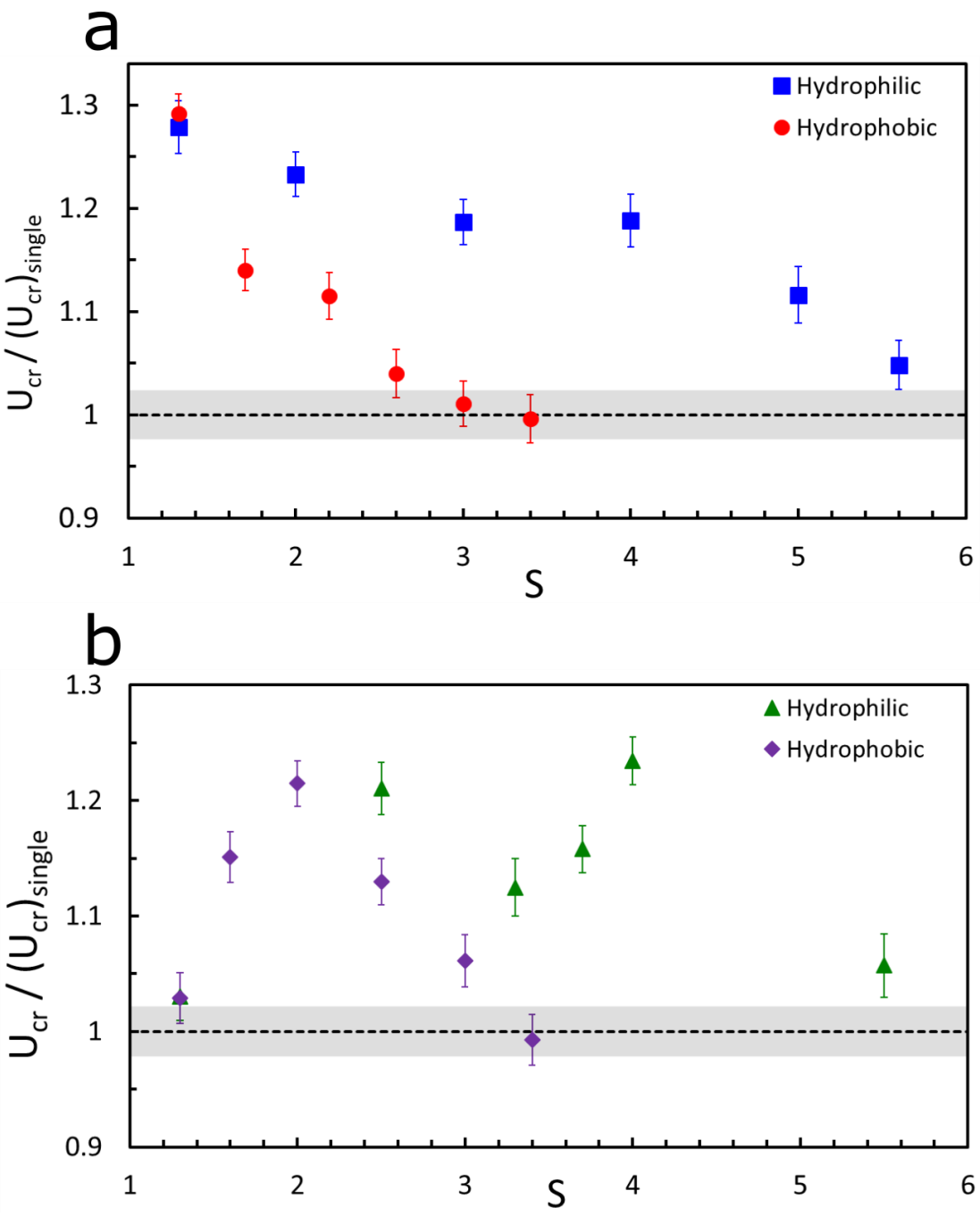

Figure A.3: The ratio of the critical air velocity a) the upstream droplet in tandem arrangement; and b) droplets in the side-by-side arrangement, to that of a single droplet. Data shown are for 5 μl. The error limits for a single drople is shown by the shaded bands.

Figure A.4 shows the " $\cos\theta_{min} - \cos\theta_{max}$ " as a function of airflow velocity for 5 μl droplets on a hydrophilic surface.

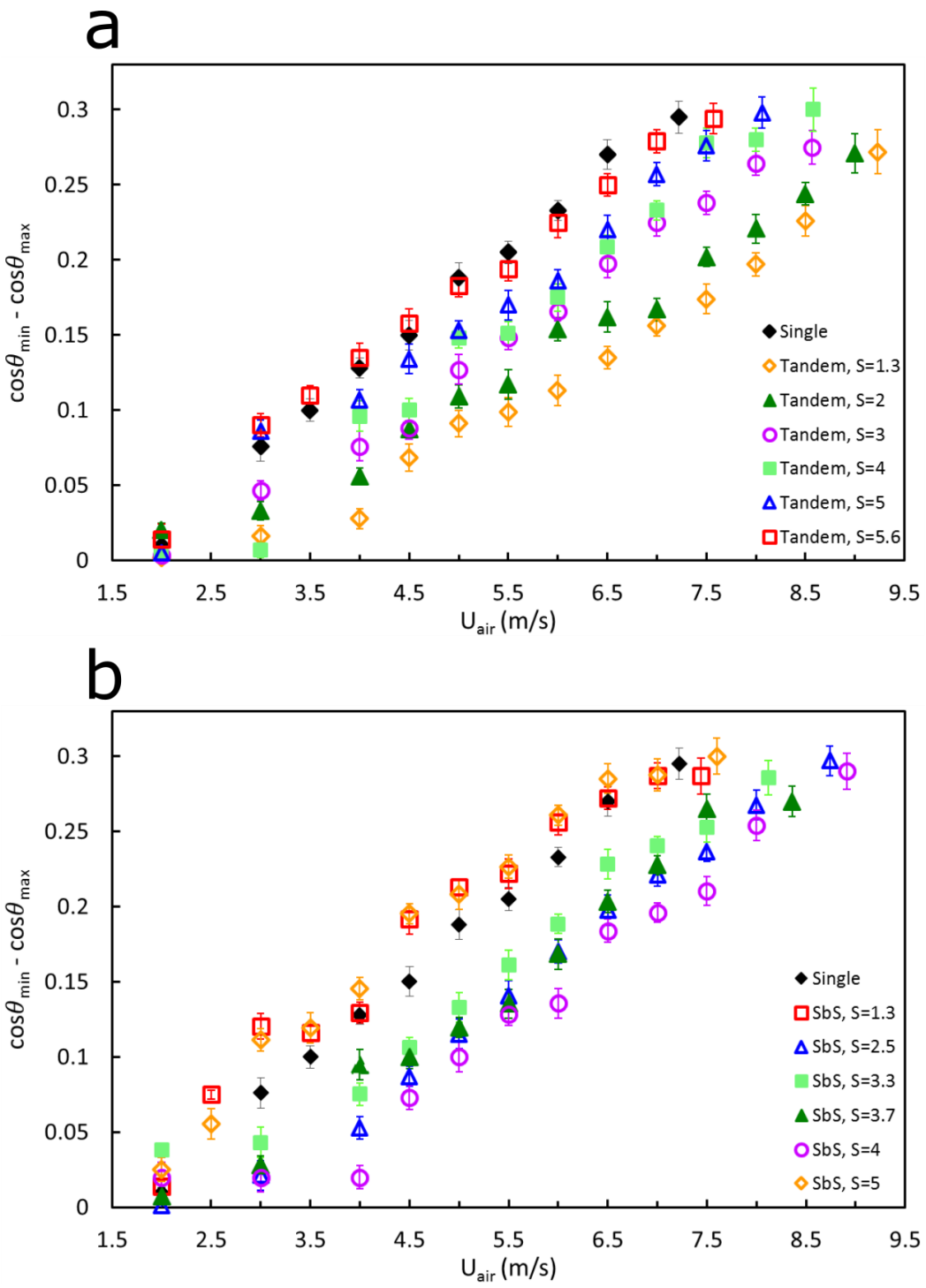

Figure A.4: The trend of $cos\,\theta_{min} - cos\,\theta_{max}$ at different spacings, as a function of air velocity for a) the upstream droplet in a tandem arrangement; and b) droplets in the side-by-side arrangement. The data are for 5 μl droplets on a hydrophilic surface. The air velocity is changing from its minimum value up to the critical air velocity (U_{air}=U_{cr}).

Figures A.5 and A.6 show the "$\cos\theta_{min} - \cos\theta_{max}$" as a function of airflow velocity for 10 and 5 μl droplets on a hydrophobic surface.

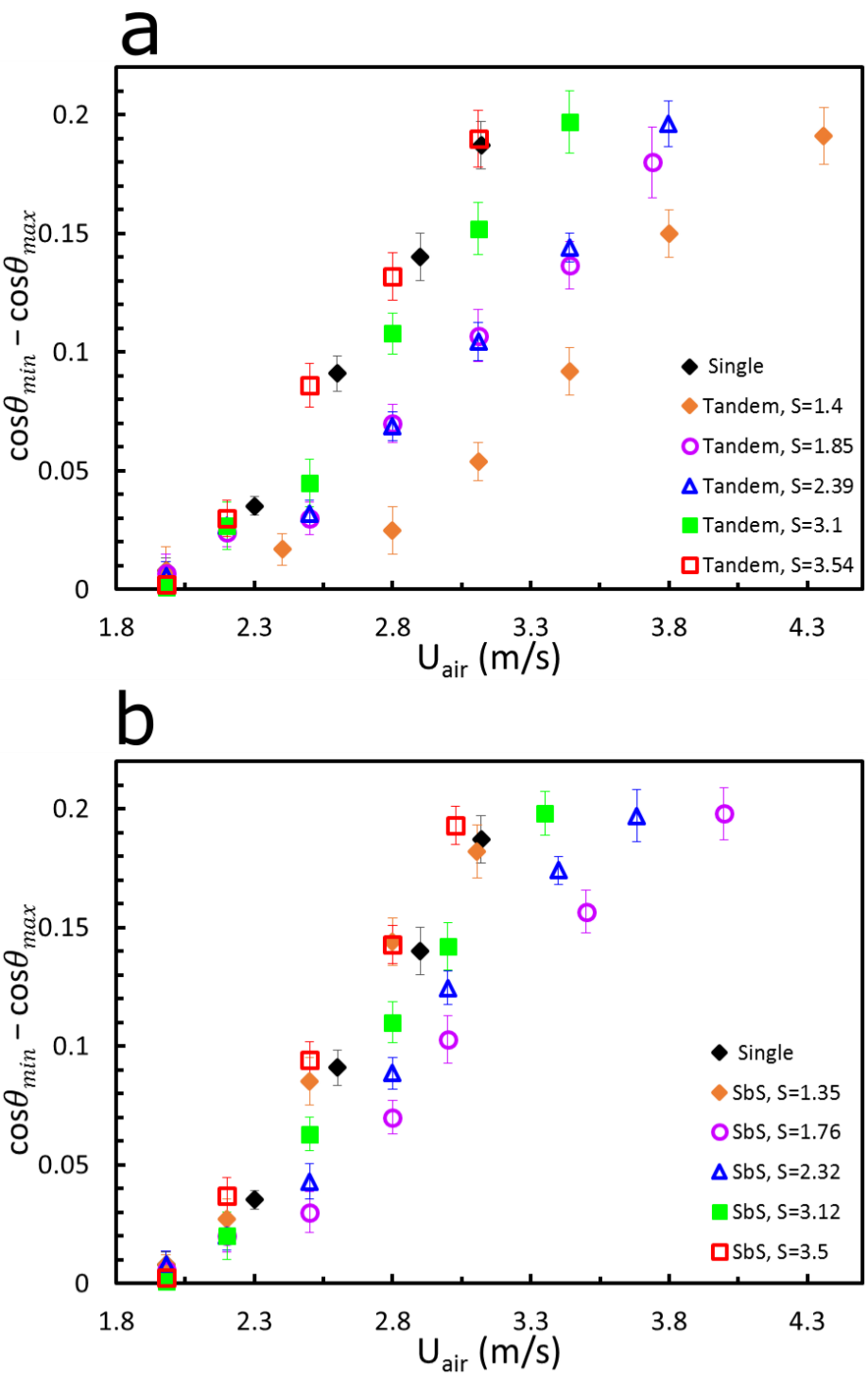

Figure A.5: The trend of $cos\,\theta_{min} - cos\,\theta_{max}$ at different spacings, as a function of air velocity for a) the upstream droplet in a tandem arrangement; and b) droplets in the side-by-side arrangement. The data are for 10 μl droplets on a hydrophobic surface. The air velocity is changing from its minimum value up to the critical air velocity (U_{air}=U_{cr}).

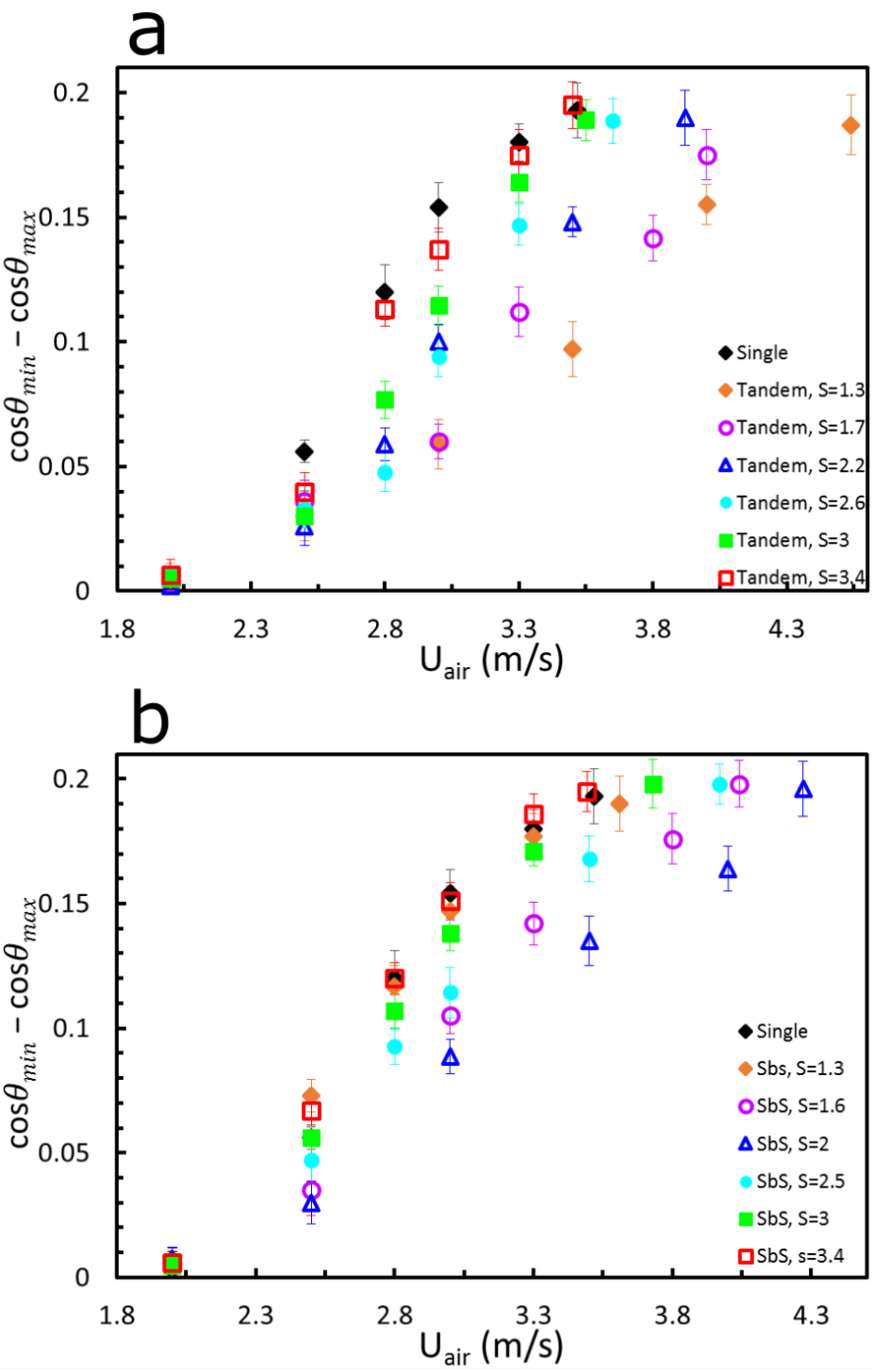

Figure A.6: The trend of $cos\,\theta_{min} - cos\,\theta_{max}$ at different spacings, as a function of air velocity for a) the upstream droplet in a tandem arrangement; and b) droplets in the side-by-side arrangement. The data are for 5 μl droplets on a hydrophobic surface. The air velocity is changing from its minimum value up to the critical air velocity (U_{air}=U_{cr}).

A.3 Spherical cap approximations for a sessile droplet

Based on the spherical cap approximation for a sessile droplet [28], one has:

$$H^2 = A \cdot \frac{(1-\cos\theta_s)^2}{\theta - \sin\theta_s \cos\theta_s} \qquad (A.1)$$

$$H^2 = \frac{(L_b)^2}{4} \cdot \left(\tan {}^{\theta_s}/_{2}\right)^2 \qquad (A.2)$$

where A, H, and L_b are the frontal area, height, and the baseline of a sessile droplet, respectively; θ_s is the average of minimum and maximum contact angle at the incipient motion.

Re-writing A as a function of L_b:

$$A = \frac{L_b^2}{4} \cdot \left(\tan\frac{\theta_s}{2}\right)^2 \cdot \frac{\theta_s - \sin\theta_s\cos\theta_s}{(1-\cos\theta_s)^2} \qquad (A.3)$$

Based on simple trigonometry, one has:

$$\theta_s - \sin\theta_s\cos\theta_s = \frac{2\theta_s - \sin 2\theta_s}{2} \qquad (A.4)$$

$$\tan(\frac{\theta_s}{2}) = \frac{1-\cos\theta_s}{\sin\theta_s} \qquad (A.5)$$

Rewriting Eq. A.3 using Eq. A.4 and Eq. A.5, one has:

$$A = \frac{L_b^2}{4} \cdot \frac{(1-\cos\theta_s)^2}{(\sin\theta_s)^2} \cdot \frac{2\theta_s - \sin 2\theta_s}{2(1-\cos\theta_s)^2} \qquad (A.6)$$

Also:

$$(\sin\theta_s)^2 = \frac{1-\cos 2\theta_s}{2} \qquad (A.7)$$

Substituting Eq. A.7 into Eq. A.6, the relationship between A and L_b is found as:

$$A = \frac{(L_b)^2}{4} \cdot \frac{2\theta_s - \sin 2\theta_s}{1-\cos 2\theta_s} \qquad (A.8)$$

It is shown in Figure A.7 that the parameter $\frac{2\theta_s - \sin 2\theta_s}{1-\cos 2\theta_s}$ (in Eq. A.8), can be estimated as a linear function of θ_s for $5° \le \theta_s \le 120°$ (which covers the values of θ_s in this study). As such, the relation between A, L_b, and θ_s can be further simplified as:

$$A \propto (L_b)^2 \cdot \theta_s$$

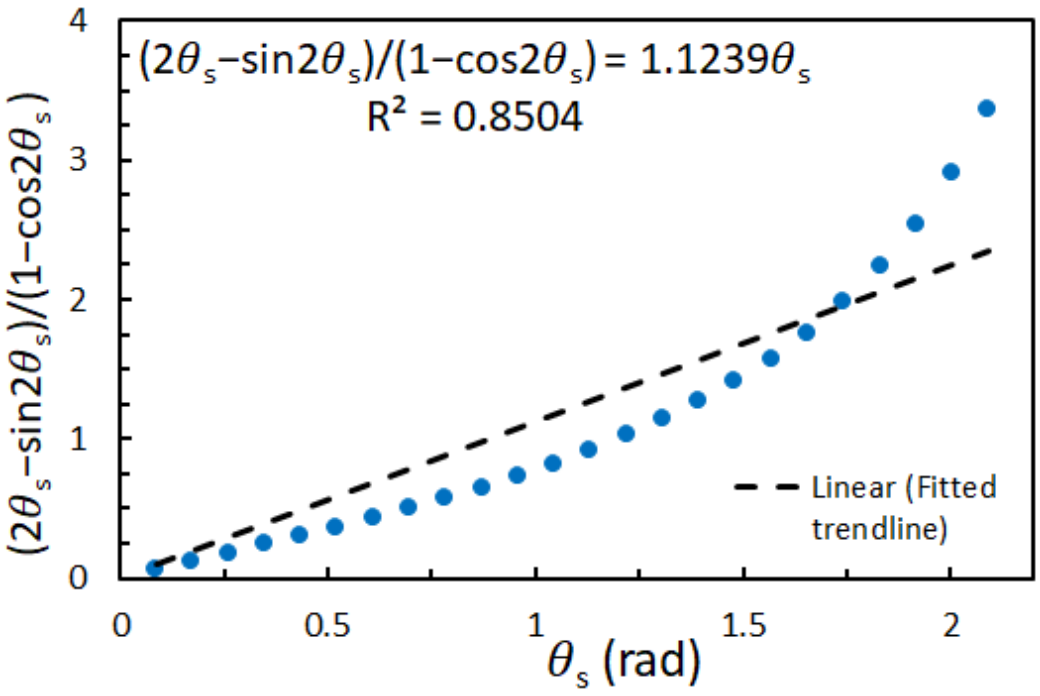

Figure A.7: $\frac{(2\theta_s - \sin 2\theta_s)}{(1-\cos 2\theta_s)}$ as a function of θ_s for 5° ≤ θ_s ≤ 120° (0.087 to 2.094 radian). The linear function which is fitted to the data points is shown by dashed line. The equation of the linear function is also written on the plot.

A.4 Velocity Profile inside the Wind Tunnel

In present thesis, two anemometers were used. An EE75 hot film anemometer (number 5 in Figure A.1) was used for critical air velocity measurements in shedding experiments. To measure the velocity profile at the position of the sessile droplet in the test section (number 8 in Figure A.1), a TSI, T-1.5 hot-wire anemometer was used. The fine sensor of TSI, T-1.5 probe provides the opportunity to measure in situ the air velocity at different heights. Despite the high special precision of the TSI, T-1.5, there was discrepancy between the values of freestream airflow velocities which were measured by TSI, T-1.5, and EE75 anemometers. By testing the EE75 anemometer inside another wind tunnel and hot wire anemometer system, it was revealed that EE75 shows the accurate values of the airflow velocity. As such, the values of air velocity which were measured by TSI, T-1.5 (to find the velocity profile) are calibrated based on EE75

anemometer. Figure A.8 shows the relationship for the calibration. The airflow velocity which is measured by EE75 and TSI, T-1.5 is denoted by U and u_{air}, respectively.

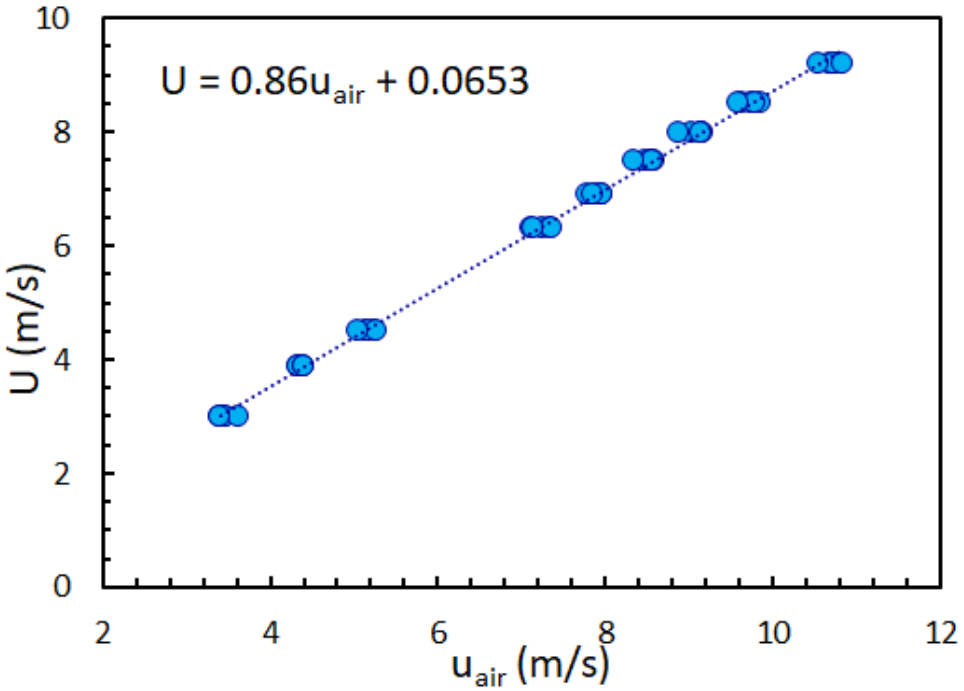

Figure A.8: Calibration of the airflow velocity which is measured by TSI, T-1.5 anemometer (u_{air}), based on the EE 75 (U). The equation for the calibration is shown on the graph.

Figure A.9 shows the schematic view of wind tunnel, the position of the TSI, T-1.5 anemometer, and the position of the solid surface. The origin of the coordinate in the Z direction is 53.6 mm away from the side wall (it is shown on Figure A.9). Five different positions in the Z direction were considered: -12, -6, 0, 6, and 12 mm which mostly encompass the widths of the solid surface inside the tunnel. In the Y direction, 9 points were considered: 1, 2, 3, 4, 5, 7, 9, 12, and 18 mm above the solid surface. As the changes in the air velocity is more critical near the solid surface, the data points in the Y direction are closer to each other near the surface. The origin of the coordinate in the X direction is where the upstream droplet is placed.

The free stream airflow velocity is denoted by U. Nine different U values were considered for the measurements: 3, 3.9, 4.5, 6.3, 6.9, 7.5, 8, 8.5, and 9.2 m/s; this range of the air velocities

included the values which were mostly reported as U_{cr} for droplet shedding experiments. The air velocity which is measured by TSI, T-1.5 anemometer is denoted by u_{air}. The fan blades rotate clockwise. Measurements were repeated three times and the standard deviation is reported as error bars. For most cases, error bars are smaller than the symbols. Figures A.10 and A.11 show the velocity profile at the position of the droplets in the Y and Z directions, respectively.

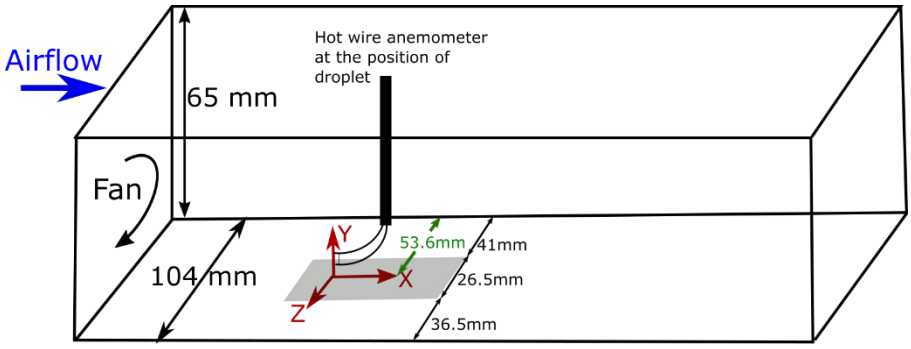

Figure A.9: Schematic view of the wind tunnel as well as the coordinates and the positions of the velocity meter. Not to scale.

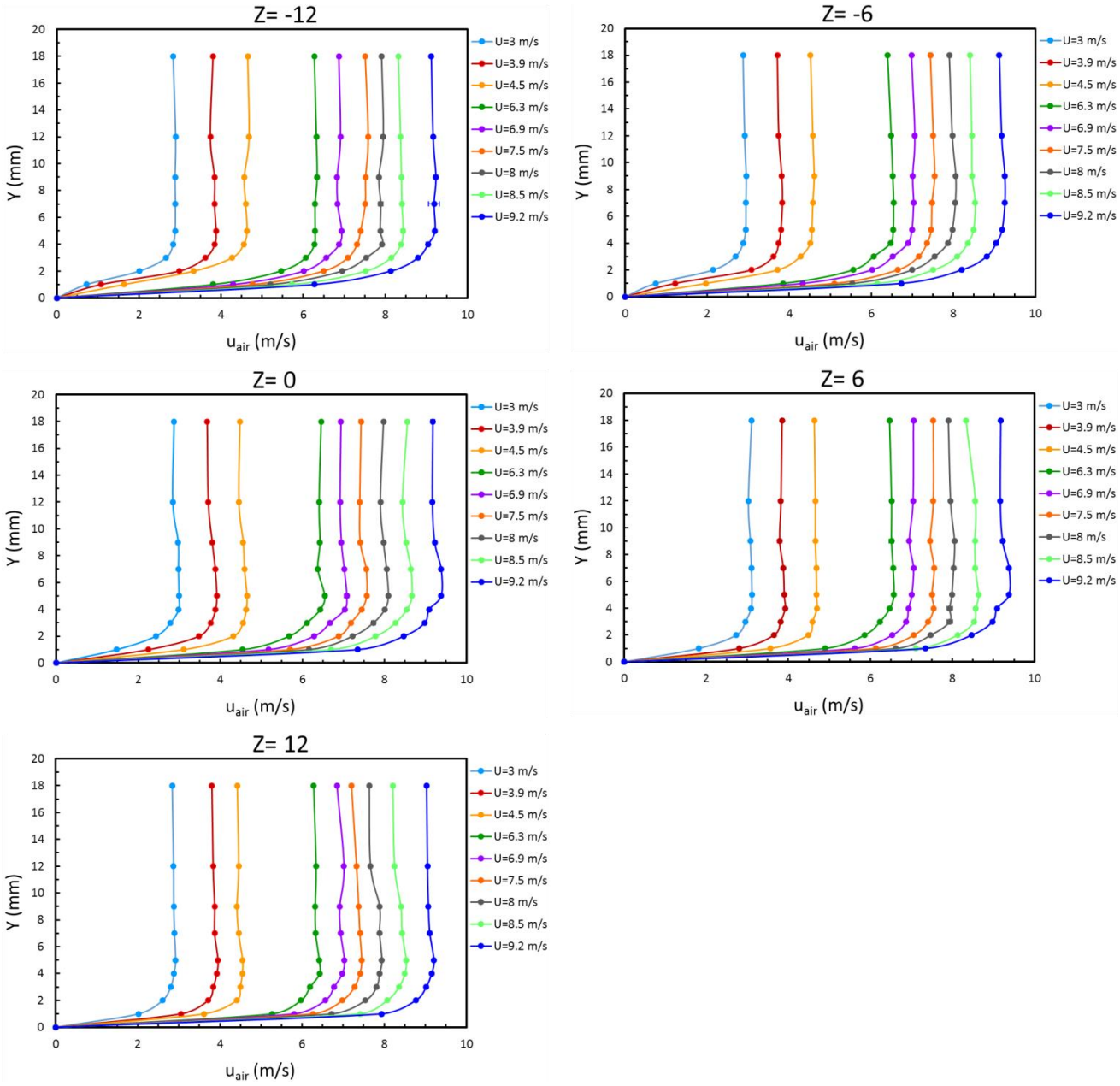

Figure A.10: Air velocity profile in the Y direction at different Z values for different air velocities. The height of the sessile droplets on the hydrophilic surface is 1.02mm and 1.27mm for 5 and 10μl droplets, respectively. The droplet height for 5 and 10 μl droplets on the hydrophobic surface is 1.63mm and 2.03mm, respectively.

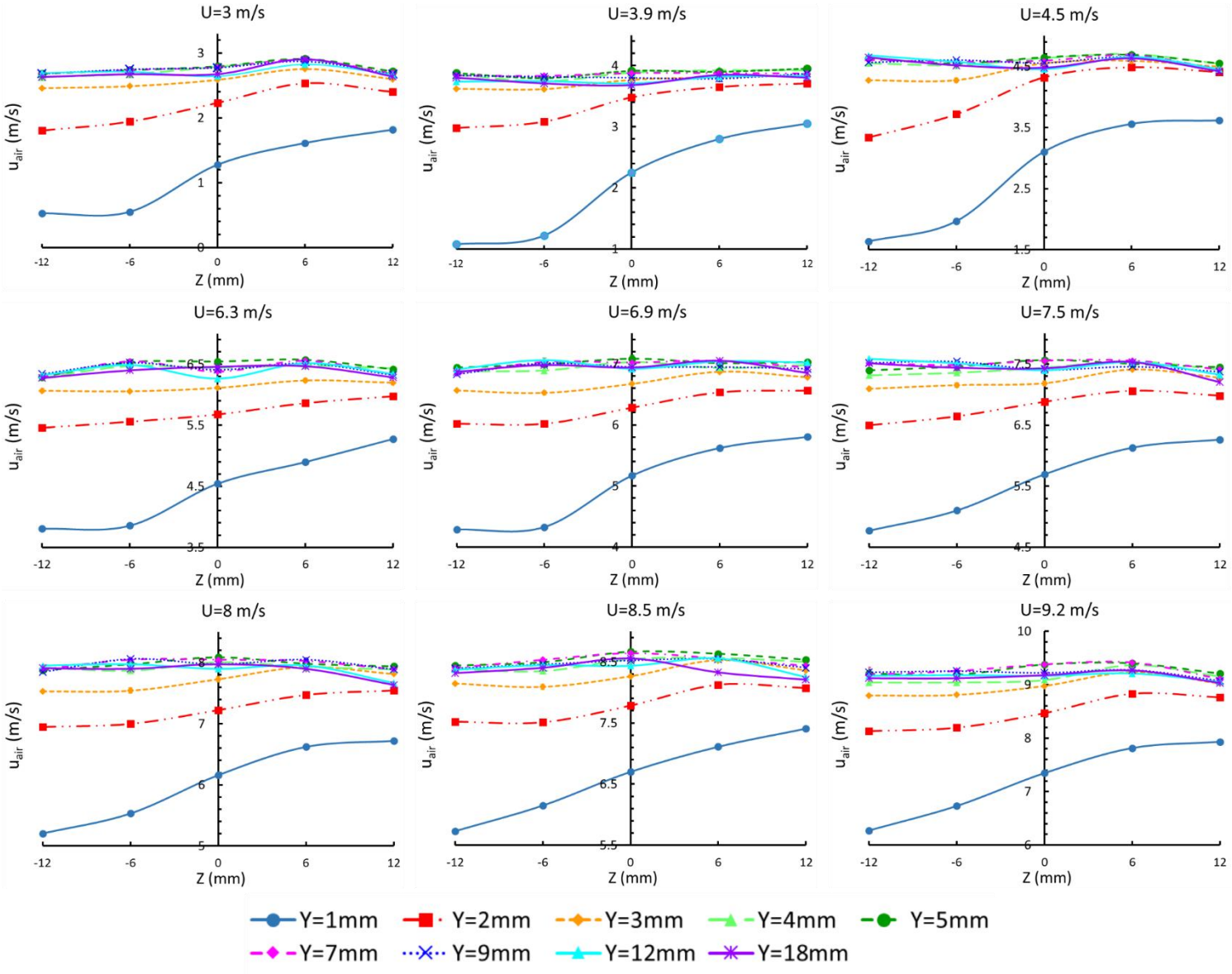

Figure A.11: Air velocity profile in the Z direction at different Y values. The parameter U is the freestream airflow velocity.

Appendix B: Supporting Information for Chapter 3

B.1 Supplemental Plots for the U_{cr}

Figure B.1 shows the $U_{cr}/(U_{cr})_{single}$ for the upstream droplet(s) in various arrangements for 5μl droplets on a hydrophilic surface.

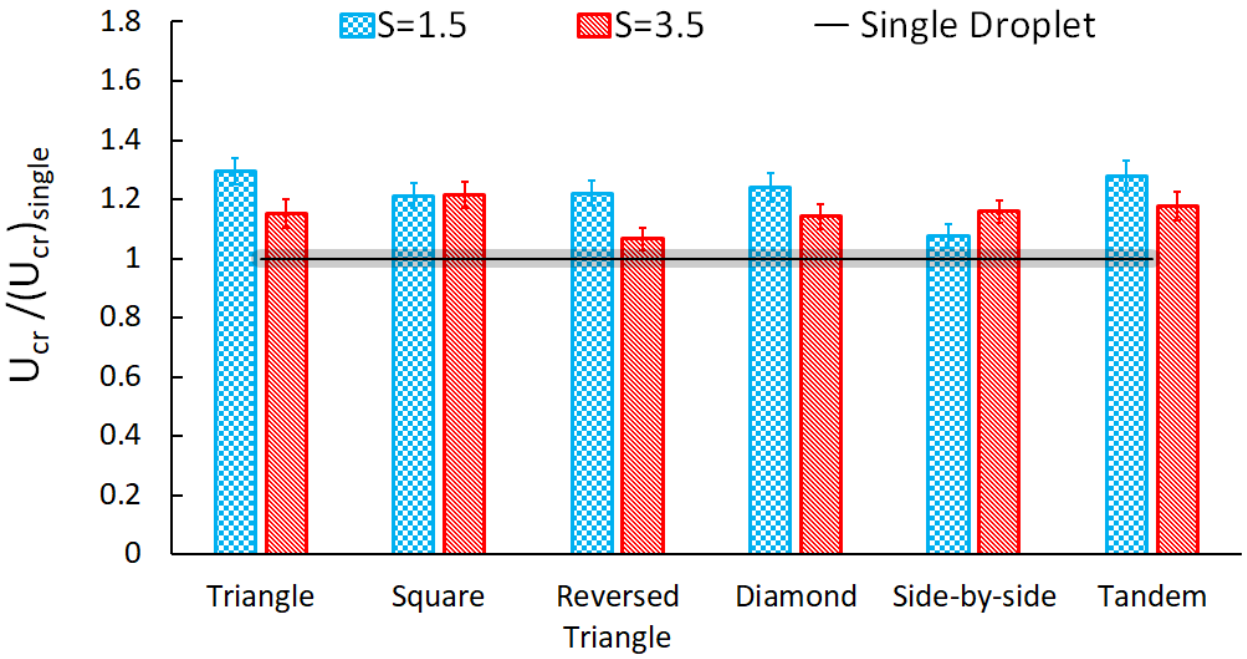

Figure B.1: Critical air velocity for the upstream droplet(s) in different arrangements at two spacing (S) values. The data shown is for 5 μl droplets on a hydrophilic surface. The error of the U_{cr} for the single sessile droplet is denoted by the shaded band.

Figures B.2, and B.3 show the effects of wettability on $U_{cr}/(U_{cr})_{single}$ for 5μl upstream droplet(s) in various arrangements at S=1.5, and an intermediate spacing, respectively.

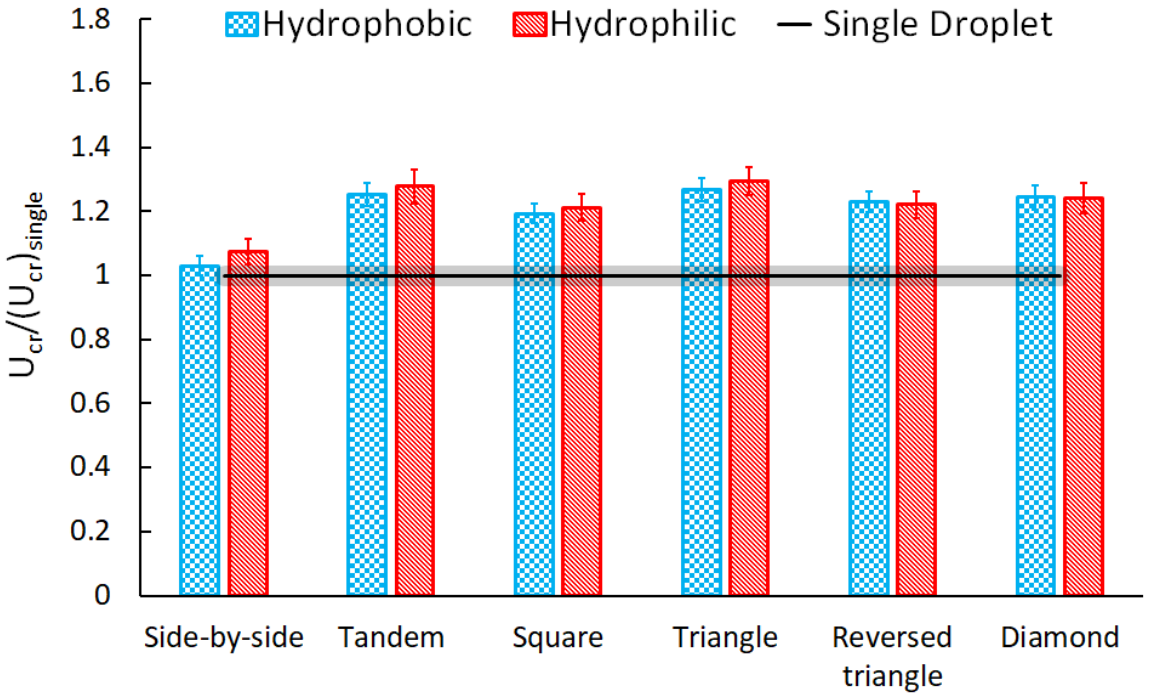

Figure B.2: Critical air velocity for the upstream droplet(s) in different arrangements at S=1.5. The data shown is for 5 μl droplets on both hydrophilic and hydrophobic surfaces. The error of the U_{cr} for the single sessile droplet is denoted by the shaded band.

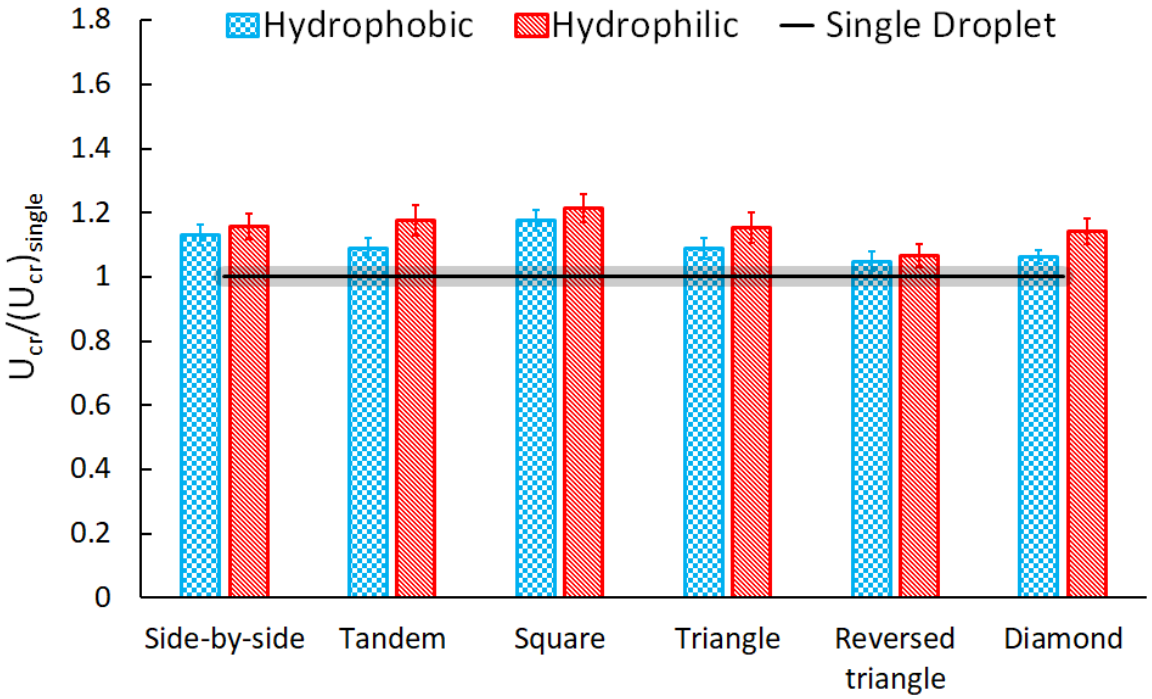

Figure B.3: Critical air velocity for the upstream droplet(s) in different arrangements at S=3.5 (for hydrophilic), and S=2.5 (for hydrophobic) surface. The data shown is for 5 μl droplets; the error of the U_{cr} for the single sessile droplet is denoted by the shaded bands.

Figure B.4 shows the effects of wettability on $U_{cr}/(U_{cr})_{single}$ for 10μl upstream droplet(s) in various arrangements an intermediate spacing.

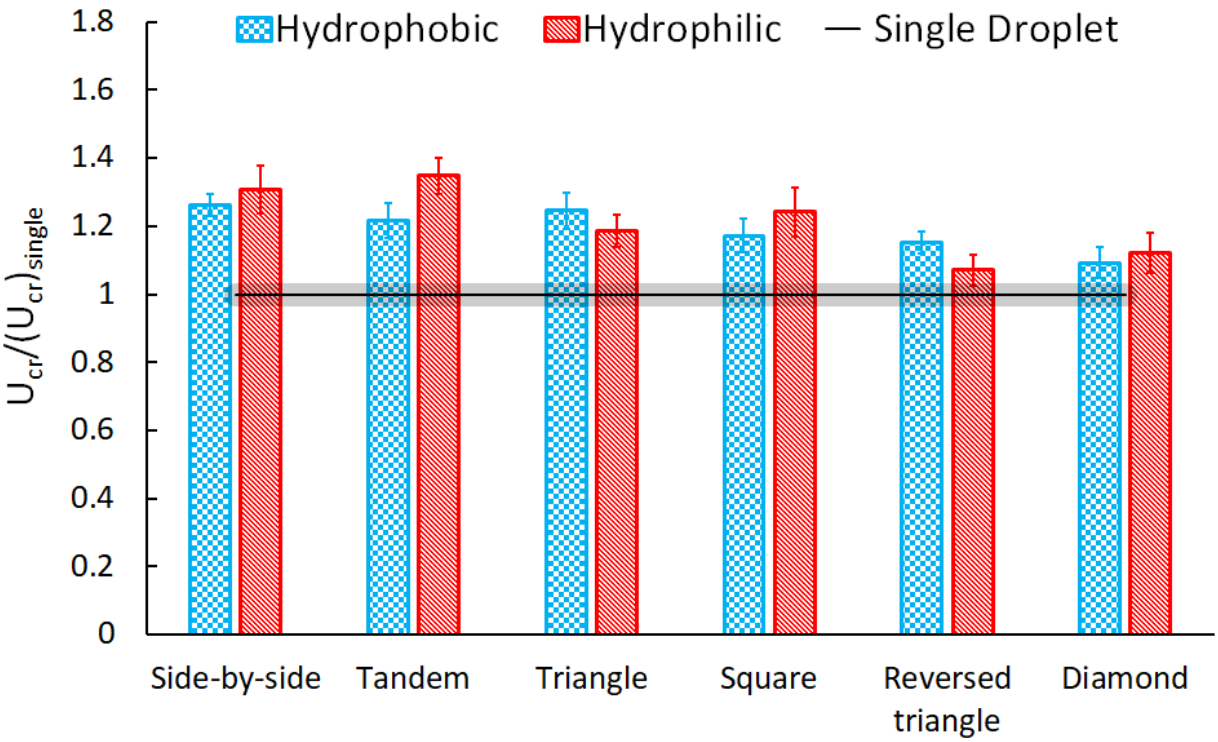

Figure B.4: Critical air velocity for the upstream droplet(s) in different arrangements at S=3.5 (for hydrophilic), and S=2.5 (for hydrophobic) surface. The data shown is for 10 μl droplets; the error of the U_{cr} for the single sessile droplet is denoted by the shaded band.

B.2 Supplemental for Numerical Simulations

Figure B.5 shows the geometry of the simulated droplets. The upstream simulated droplets have a constant θ_{min} and θ_{max} for all cases. As the experimental data shows in Figures 2.4 and 2.6, upstream sessile droplets have the constant (considering error bars) contact angles at the moment of incipient motion. For the downstream droplets, the geometry was fashioned based on the experimental data, which is different for each case.

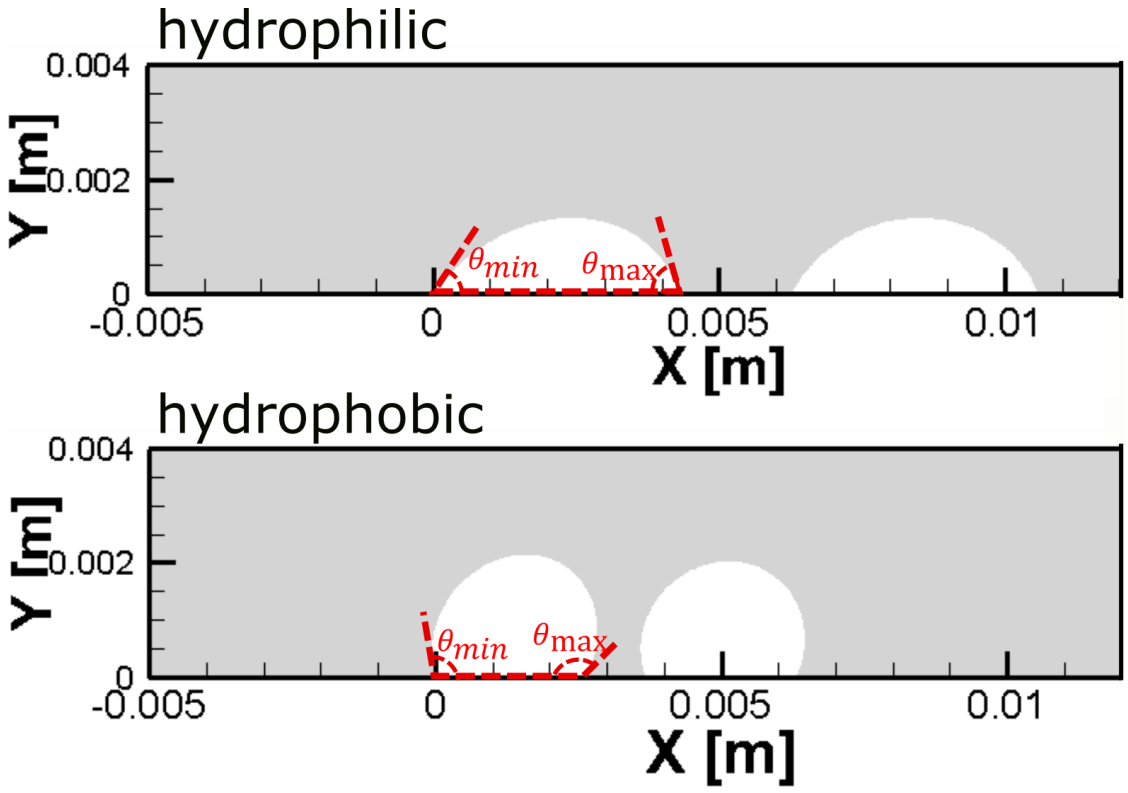

Figure B.5: Geometry of the simulated droplets at the moment of incipient motion. The value of θ_{min} and θ_{max} for hydrophilic surface is 53.5° and 71.5°, respectively. For hydrophobic surface these values are 106.3° and 118.1°, respectively. Data shown is for 10 μl simulated droplets in a square arrangement at S=1.5.

Figure B.6 shows the velocity fields and streamline patterns for a single simulated droplet on a hydrophilic surface at the X-Z plane, at two different Y values: Y=0.5 H and Y=0.75 H. The distance between the dashed lines on Figure B.6 shows the length of the ring-like vortices. As it can be understood from Figure B.6, the length of the ring-like vortices is the same (~3.6 mm) on both planes.

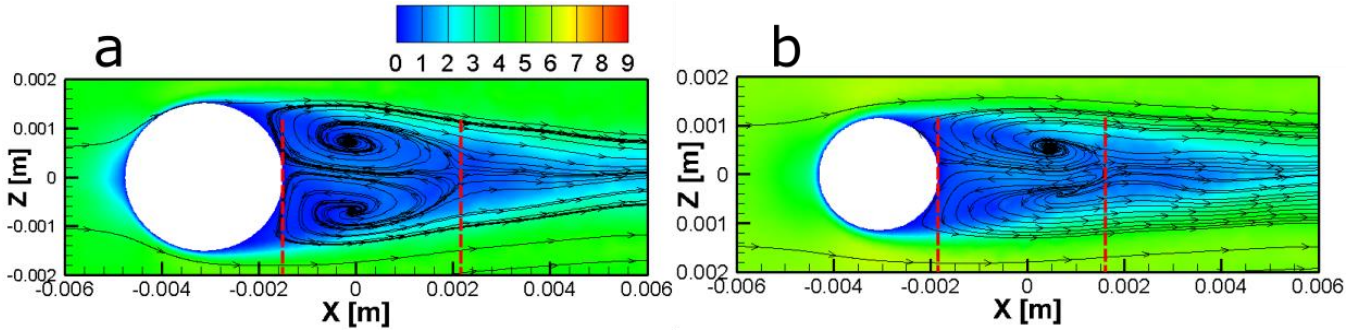

Figure B.6: Velocity fields and streamline patterns for a single simulated droplet at the X-Z plane, at a) Y=0.5 H, and b) Y=0.75 H. Data shown is for 10 μl simulated droplet on a hydrophilic surface, where H is 1.4 mm.

Figure B.7 shows the flow fields for droplets in a triangle arrangement on a hydrophilic surface at the X-Z plane, at two different Y values: Y=0.5 H and Y=0.75 H. The length of the vortices is shown by the distance between the dashed lines in Figure B.7. As it is seen in Figure B.7a and B.7c, the vortices' length is ~1.4 mm on both planes for the upstream droplet at S=1.5. At S=3.5 the vortices' length is ~3mm on both planes (Figure B.7b and b.7d).

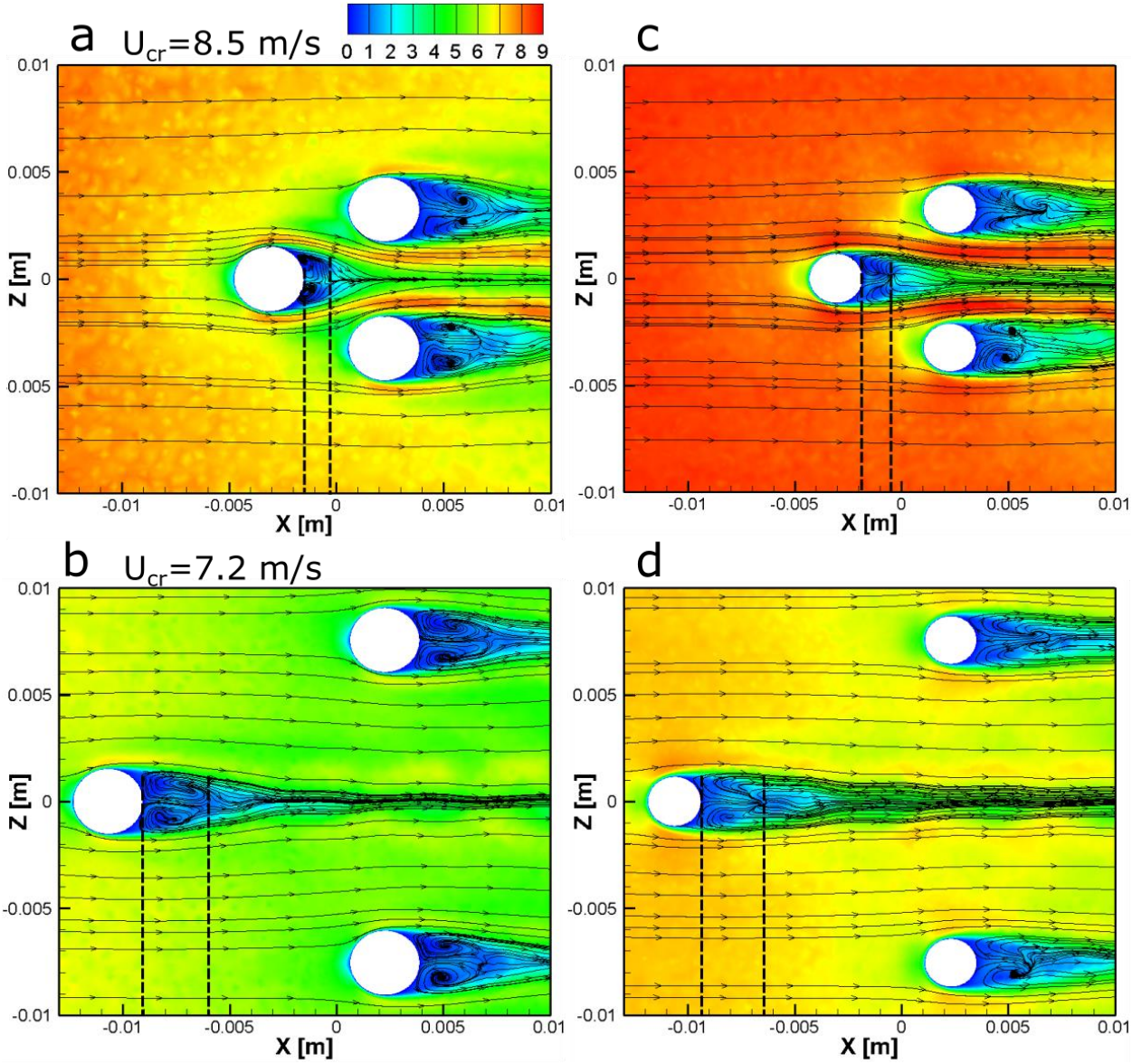

Figure B.7: Velocity fields and streamline patterns for simulated droplets in a triangle arrangement at the X-Z, Y=0.5 H plane at a) S=1.5, and b) S=3.5. At the X-Z, Y=0.75 H plane at c) S=1.5, and d) S=3.5. Data shown is for 10 μl simulated droplets on a hydrophilic surface, where H is 1.4 mm.

Figure B.8 shows the flow fields for droplets in a triangle arrangement on a hydrophobic surface at the X-Z plane, at two Y values: Y=0.5 H and Y=0.75 H, where H is 2mm. As it is seen in Figure B.8, the vortices' length for the upstream droplet is the same (~1mm) on both planes. The length of the ring-like vortices is shown by the distance between the dashed lines in Figure B.8.

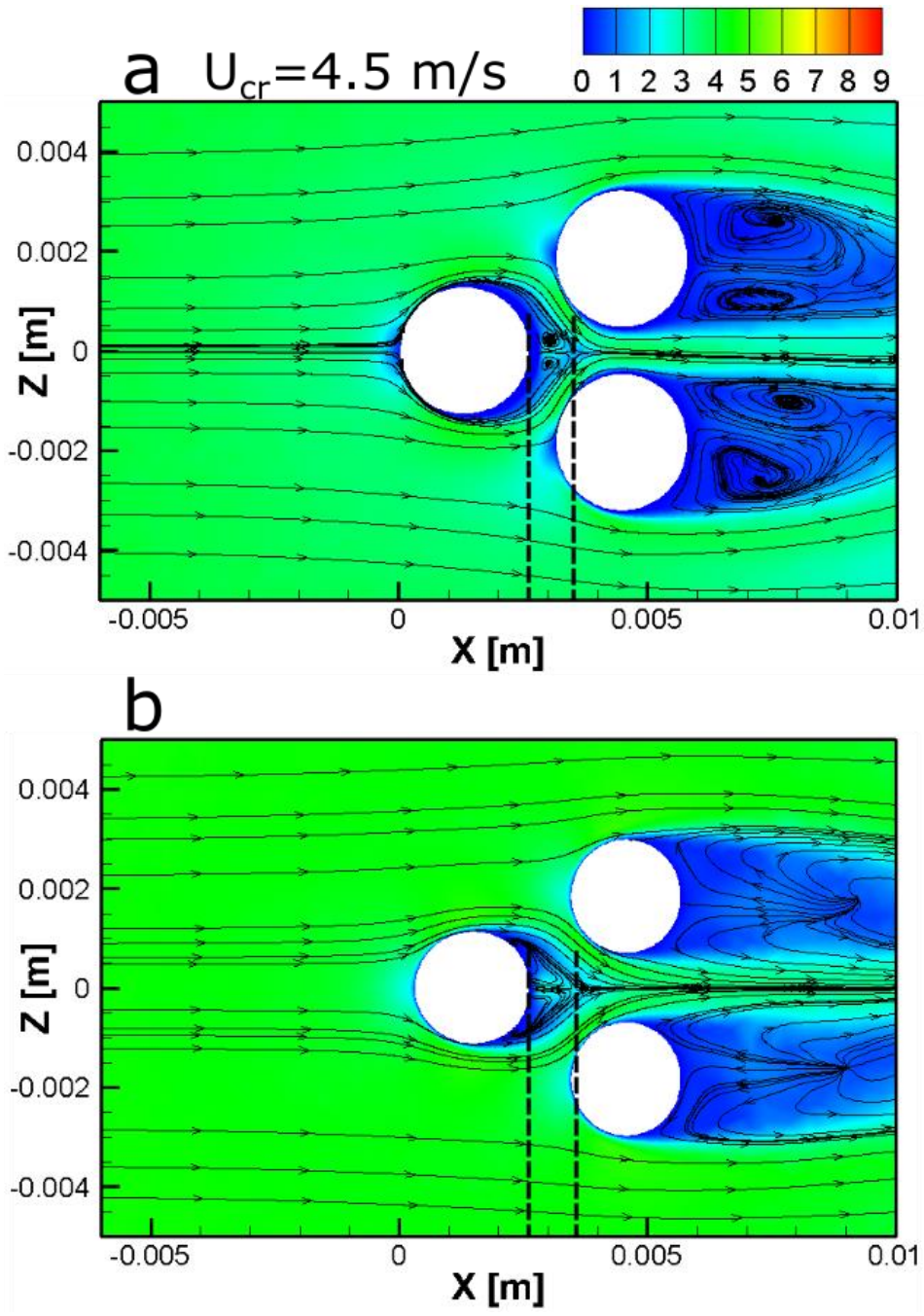

Figure B.8: Velocity fields and streamline patterns for simulated droplets in a triangle arrangement at the X-Z plane, at a) Y=0.5 H, and b) Y=0.75 H. Data shown is for 10 μl simulated droplets on a hydrophobic surface, where H is 2 mm.